



Department of Precision and Microsystems Engineering

Torque Sensing for E-bike Applications

Name:	Marien van Ditten
Report no:	EM 11.008
Coach:	Ir. E.J.H. de Vries
Professor:	Prof. Dr. Ir. E.G.M. Holweg
Specialisation:	Automotive
Type of report:	Master Thesis
Date:	June 27, 2011

TORQUE SENSING FOR E-BIKE APPLICATIONS

MASTER THESIS

Marien van Ditten

June 27, 2011

Delft University of Technology
Faculty of Mechanical, Maritime and Materials Engineering

CONFIDENTIAL

The information in this report is property of SKF ADC-SI.
It cannot be divulged or reproduced without company's authorization.



The work in this thesis was supported by SKF.
Their cooperation is hereby gratefully acknowledged.

Abstract

The Automotive Development Center of SKF was interested in the possibility to develop a torque sensor, either for e-bike or power steering application. A master thesis project was initiated to explore the possibilities. The results of that study are presented in this thesis.

In the first phase of the study, a benchmark was made of the existing technology and the requirements for the product. Market research showed that a sensor for e-bike applications would be the most promising application in the short term. The analysis of the state of the art showed that the prevailing technologies are magnetic field measurement and magnetic phase shift measurement. One of the existing products, a torque sensor integrated in a bottom bracket from Thun, was analyzed. To gain more insight into the requirements of the product, the Quality Function Deployment method was used. To identify the most important needs and functions of the product a paired comparison matrix and a House of Quality were used respectively. The House of Quality showed that, next to torque measurement, price and safety are also important functions.

The second phase concerned the actual design of the sensor. First of all the general concept of the sensor was developed by answering three basic questions: where should the sensor be located, what should it measure and how should it measure. The best concept proved to be a sensor located in the bicycle's bottom bracket (the part that connects the pedals to the frame and contains the pedal spindle). The applied torque will cause a torsion angle between the chain wheel and the spindle. Angled surfaces between the chain wheel and a sleeve fitted around the spindle will cause a translation of that sleeve. On the sleeve an aluminium target ring is fitted, which moves in a time-dependent magnetic field. By measuring the influence on the magnetic field caused by the induced eddy current in the ring, the position of the ring can be determined and thereby the applied torque can be calculated. All relevant parameters of the concept were analyzed by simulations of the

sensor setup in Ansoft Maxwell, a finite element electromagnetic field simulation tool. With the results of these simulations a torque sensing bottom bracket was designed.

In the third phase, the concept was analyzed and tested. To make the Maxwell simulation more usable, an interface was made using MATLAB and Visual Basic scripts. With the interface the user is able to change parameters quickly and perform batch analyses. With the help of this interface, a Design of Experiment analysis was performed in order to identify the most influential parameters and optimize the geometry. It showed there is an important connection between the width of the target ring and the space between the coils. A full size prototype was made and tests were performed on the measurement principle. These test showed a linear relation between the displacement of the target ring and the output of the sensor. The sensor has a sensitivity of 120 mV/mm. The tests also showed that the set-up is sensitive for errors in the position of the target ring. Static tests on the prototype showed that the sensor concept functions. There was no time to perform dynamic tests. These are scheduled in the near future.

The concept torque sensing bottom bracket shows promising first test results. But without sufficient test data, it is not yet possible to give a final verdict. When it is decided to continue the project, several points should be addressed. These are: the design of the intermediate part; the mechanical assembly; the cost price; the sensation to the cyclist and the integration of the electronics.

Contents

Preface	xvii
Introduction	xix
Part I Benchmarking	
1 Market Research	3
1.1 The Market of E-bikes	3
1.2 The Market of Power Steering Systems	6
1.3 Conclusion Market Research	7
2 Competitor Analysis	9
2.1 Magnetic Rotor-Stator Phase Shift Measurement	9
2.2 Magnetic Rings Phase Shift Measurement	10
2.3 Mechanical Phase Shift Measurement	11
2.4 Magnetic Field Measurement	12
2.5 Magnetic Translation Measurement	14
2.6 Optical Phase Shift Measurement	15
2.7 Displacement of Rear Drop Out	16
2.8 Forces on the Bottom Bracket Bearing	17
2.9 Summary of Technologies	18
3 Analysis of Purchased Parts	21
3.1 Thun Bottom Bracket Sensor	21
3.2 Ergomo Bottom Bracket Sensor	26
3.3 Integrative Motor Kit	27

4	Quality Function Deployment	29
4.1	Needs	29
4.2	Paired Comparison Matrix	31
4.3	Functions	32
4.4	House of Quality #1	32
Part II	Sensor Design	
5	Concepts for a Torque Sensor for E-bike Application	39
5.1	Where - Location of Sensor	39
5.2	What - Physical Quantity	40
5.3	How - Measurement Principle	44
6	Design of Sensing Elements	49
6.1	Eddy Current & Variable Reluctance	49
6.2	Concept of Sensor	52
6.3	Modelling of Sensor Using Ansoft Maxwell	53
6.4	Results of Electromagnetic Field Simulations	56
6.5	Conclusions of Simulations	65
7	Detailed Design of Torque Sensing Bottom Bracket	67
7.1	Mechanical Design	67
7.2	Electrical Design	72
Part III	Simulation & Testing	
8	BoB SimControl for Torque Sensing Bottom Bracket	75
8.1	Refining the Mesh	75
8.2	Visual Basic script	76
8.3	Structure of Program	77
8.4	Results	81
9	Design of Experiment Analysis	83
9.1	Design of Experiment	83
9.2	Build Up of Simulation Model	84
9.3	Phase 1: Parameter Screening	85
9.4	Phase 2: Parameter Optimization	86
9.5	Conclusions Design of Experiment Analysis	89
10	Assembly & Test of Prototype Bottom Bracket	91
10.1	Assembly of Prototype	91
10.2	Test of Measurement Principle	93
10.3	Static Tests	95

10.4 Conclusions	97
11 Conclusions and Discussion	99
11.1 Conclusions	99
11.2 Discussion	100
Part IV Appendices	
A Competitor Analysis Matrix	105
B Thun Bottom Bracket Sensor Data Sheet	109
C Paired Comparison Matrix	113
D House of Quality #1	115
E SVP BoB SimControl	117
F Design of Experiment	121
F.1 DoE Screening 1	121
F.2 DoE Screening 2	122
F.3 DoE Full Factorial	122
Bibliography	123

List of Figures

1.1	Products from competitors	5
1.2	ION technology e-bikes	5
2.1	Torque sensor using a magnetic rotor and stator assembly	11
2.2	Drawing of torque sensor using magnetic rings	11
2.3	Drawing of mechanical phase shift torque sensor	12
2.4	Inverse magnetostrictive effect torque sensor	14
2.5	Examples of application of NCTE torque sensor	15
2.6	Honda Accord EPAS system torque sensor	15
2.7	Optical phase shift measurement	16
2.8	Displacement sensor in rear drop out	17
2.9	Force measurement in bottom bracket	18
3.1	Thun bottom bracket sensor	22
3.2	Output of Thun BB sensor during measurement	23
3.3	Exploded view of the disassembled Thun BB sensor	24
3.4	Magnetic ring from the Thun BB sensor	24
3.5	Measurement of the magnetized region on the spindle	25
3.6	PCB from Thun BB sensor	25
3.7	Ergomo bottom bracket sensor	26
3.8	Integrative motor kit	28
4.1	Work flow of Quality Function Deployment	30
4.2	Example of paired comparison matrix	32
4.3	Results of paired comparison matrix analysis for torque sensor	34
4.4	Example of a House of Quality	35
4.5	Results of House of Quality #1 for torque sensor	36
5.1	Schematic mapping of bicycle	41

5.2	Concept Bottom Bracket with flexible connection	42
5.3	Schematic drawing of concept magnetic rings & duty cycle	44
5.4	Schematic drawing of concept variable reluctance	46
6.1	Eddy current proximity sensor.	50
6.2	Magnetic circuit caused by a coil with an air gap	51
6.3	Differential variable reluctance displacement sensor	52
6.4	Cross section of sensing concept	53
6.5	Modelling of sensor in Ansoft Maxwell	54
6.6	External circuit imported in Maxwell simulation	55
6.7	Magnetic Flux density using different materials	57
6.8	Induced eddy current in the target ring in steel and aluminium .	57
6.9	Effect of thickness (axial) of target ring on the sensitivity	58
6.10	Effect of coil spacing on the sensitivity	59
6.11	Magnetic flux density of sensor with ferrite core	59
6.12	Influence of different frame tubes on the sensor	61
6.13	New model of torque sensing bottom bracket	63
6.14	Output of the Wheatstone bridge versus displacement of the sleeve	64
6.15	Target ring and coils with current magnitude and direction	64
7.1	CAD design of the SKF Torque Sensing Bottom Bracket	68
7.2	Connection of chain wheel bracket to the spindle	69
7.3	Intermediate piece connecting spindle and chain wheel bracket .	70
7.4	Mechanism for transforming the rotation to translation	71
7.5	Electronic circuit for the prototype	72
8.1	2-D Maxwell model of torque sensing bottom bracket	76
8.2	Flow chart of the main structure of the program	78
8.3	Example of recorded Visual Basic script	78
8.4	Architecture of the MATLAB program	80
8.5	Screen shot of MATLAB program (BoB SimControl)	81
8.6	Result of a batch simulation	82
9.1	Bold approach of parameter variation in screening phase of DoE	84
9.2	Build up of analysis model showing the four main parts	85
9.3	Result of screening phase of the DoE	87
9.4	Results of the second phase of the DoE, varying two parameters	88
9.5	Results from Minitab of the second phase of the DoE	90
10.1	Mold for fabricating the intermediate part	92
10.2	Complete assembled prototype	92
10.3	Test set-up for static test of measurement principle.	93
10.4	Output of sensor when moved around the center between the coils	95
10.5	Influence of eccentricity of the target ring on the output voltage	96
10.6	Output of sensor during manipulation of the prototype	97

List of Tables

2.1	Summary of technologies	19
4.1	Critical to Satisfaction for torque sensor product	31
4.2	Critical to Quality	33
5.1	Locations and its possible physical quantities	43
5.2	Advantages and disadvantages of different measurement methods	46
5.3	Multi criteria table	47
6.1	Sensitivity of sensor using different materials as target ring . . .	56
6.2	Sensitivity of sensor with ferrite core	58
6.3	Sensitivity of sensor with different kind of frame tubes	60
6.4	Sensitivity of sensor with reduced air gap	60
8.1	Sensitivity of sensor calculated using 3-D and 2-D Maxwell model	77
9.1	Parameters for the screening phase of design of experiment analysis	85
9.2	Parameter range and interval for DoE phase 2	87
10.1	Oscillation of measurement signal caused by mounting of target ring.	94

Preface

When I look back to September of 2010 I did not know what to expect. People said that it would be difficult and tiring to work abroad and speak a different language, and they were right. They also said that all the effort you would invest in the beginning would pay out at the end, and they were right again.

I was going to live and work in France. The country where, at least to the Dutch clichés, everybody is always on strike, nobody speaks English, everybody is lazy and nobody can drive a car. After 10 months I can report that most of it is not true.

But more importantly, it showed me the subtle difference between two cultures which are only a few hundred kilometers apart. A valuable lesson learned in a profession which is more and more global.

I would like to thank Alberto Carlevaris, for giving me the opportunity to come to the ADC-SI team, Olivier Joubert, my Maître de Stage, who had confidence in me and gave me the space to follow my own path, and Mathieu Hubert, my day-to-day mentor, for pointing me in the right direction and answering all my silly questions.

The ‘Torque’ team further consisted of Vincent Sausset (mechanical engineer), Matthieu Rioteau (electrical engineer), Alan Roué (quality) and Alexis Gatesoupe (project manager). I would like to thank them all for their work and help.

And I would like to thank all the other people in ADC-SI, the team within SKF where I spend 10 months on this project. They showed me that the persistent cliché that that French people are lazy is certainly untrue.

Merci à tous, pour votre accueil chaleureux, votre patience quand j'étais aux prises avec la langue française, et tous les jeudis soirs !

I would also like to thank Edward Holweg, who made it possible for me to do my assignment at SKF in France, and Edwin de Vries, who made sure that everything was running smoothly in Delft.

Introduction

Torque Sensing for E-bike Applications

Thousands of people face the same dilemma every day: do I go by car, or do I take the bike? And too often people choose the car. Whether the argument is that there is a strong head wind in the Dutch *polder*, the groceries that have to be carried are too heavy or there is a steep incline on the way to work, it almost always can be attributed to the fact that it takes too much effort. For this reason, a lot of small journeys are made by car, leading to the emission of harmful gases into the atmosphere.

In the last ten years a strong increase in the sales of electrical assisted bicycles has taken place. These e-bikes (sometimes called *pedelec*) will assist the cyclist with an electric motor to overcome the arguments as stated above. People will use the bike more frequent and over longer distances than a traditional bike. Therefore, urban mobility can be increased and emissions can be reduced. Not to mention the advantages to public health.

To be able to control the assistance provided by the electrical motor, it is important to measure the cyclist's effort. One way of doing that is by measuring the torque applied to the pedals. SKF sees opportunities in the e-bike market and has launched a project to investigate the possibilities.

Structure of the Thesis

This master thesis is the result of a nine month project at the Automotive Development Center - Sensor Integration department of SKF. The thesis is split up in three parts: Benchmarking, Sensor Design and Simulation & Testing.

In Part I, the market of e-bikes and torque sensing is investigated. A market research is done in chapter 1. The existing competition is analyzed in chapter 2. Several products that seemed interesting are purchased for analysis in chapter 3. At the end of the benchmarking phase a Quality

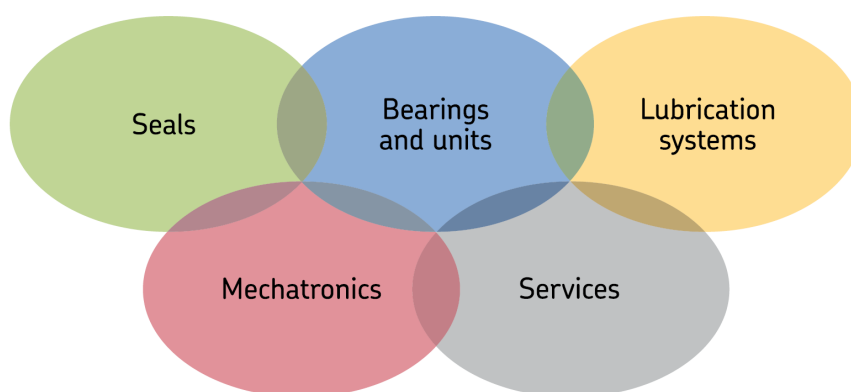
Function Deployment is done in chapter 4 to translate the voice of the customer into clear design requirements.

Part II covers the path from brainstorming to the final concept. First, in chapter 5, several ways of torque sensing are considered, and finally one concept is chosen for further analysis. In the following chapter (chapter 6) this concept is simulated using finite element calculations to investigate the influence of several design parameters in order to determine the optimal geometry. At the end of part II, the final mechanical and electrical concept are presented in chapter 7.

In Part III, the design is evaluated using simulations and testing. Before the simulations, a MATLAB program is written as an interface for the simulations. This program is described in chapter 8. With the help of this program the concept can be analyzed to find the best parameter combination. A Design of Experiment was performed, the analysis can be found in chapter 9. In chapter 10 the prototype of this concept will be tested. After that, the thesis will be concluded with the conclusions and recommendations in chapter 11.

SKF and the Automotive Development Center

SKF Group is the leading global supplier of products, solutions and services within rolling bearings systems. SKF stands for *Svenska Kullagerfabriken* (Swedish ball bearing factory). The company started in 1907 and grew quickly into a global player. Nowadays, the company has over hundred manufacturing sites and is represented in more than 130 countries. The company specialized in more than just bearings. As shown, SKF is built on five platforms: bearings, seals, lubrication, mechatronics and services. SKF employs over 44,000 people worldwide.



The company consists of three main divisions: Industrial, Services and Automotive. The first two focus on servicing industrial original equipment manu-

facturers (OEMs) and aftermarket customers respectively. The automotive division focuses on the automotive OEMs and aftermarket customers.

Part of the automotive division is the Automotive Development Center (ADC). This department develops products, not only bearings, that can be used in the automotive sector. Within the department there is a high level of mechatronics engineering. The unit Sensor Integration (ADC-SI), located at the production facility in Saint-Cyr-sur-Loire, France, mainly focuses on the integration of sensors in bearings and other products. The ADC-SI team consists of 25 people, containing mechatronic engineers, mechanical engineers, electrical engineers and project managers.

Part I

Benchmarking

Market Research

The market research is split in two parts, e-bikes (section 1.1) and EPS systems (section 1.2), because the two fields are very different. Afterwards, in section 1.3, a conclusion is drawn to decide which field has the most possibilities and opportunities for SKF and thus what the focus of the project should be.

1.1 The Market of E-bikes

Trends

With the ban of motorcycles in almost ninety Chinese cities, late 1990s, the annual sales of electric bikes grew from 56,000 in 1998 to 20 million in 2008 [1]. In Europe, with the introduction of inner city congestion charges, growing delay due to city traffic and a growing environmental lobby, the sale of e-bikes is also on the rise. In the Netherlands, for instance, the sales of e-bike has quadrupled to 153,000 between 2006 and 2009. Nowadays one in eight bikes sold is an e-bike, even if these bikes are on average three times as expensive as a normal bike [2].

E-bikes are sold in two ways: as a complete bike, designed from the ground up as an e-bike, or as a retrofit kit. Both consist of the same basic parts:

- **A motor**, either a hub motor in the front or the rear wheel or a frame mounted motor driving the chain;
- **A battery pack**, providing the power for the bike. Most battery packs can be detached from the bike to charge them with a separate charger;

- **A handle bar mounted control panel**, to operate the system, choose assistance mode, etc.;
- **A controller**, to control the operation of the system;
- **A sensor**, to monitor movement of the pedals (in European systems).

Contrary to Asia, where e-bikes are sometimes more like electric scooters than a bike, in Europe e-bikes have to obey some strict rules. One of the most important rules is that the bike is not allowed to be electrically propelled if the cyclist is not pedaling or pedaling backwards.

To control this, a simple cadence sensor could be sufficient. But to deliver a superior mode of electric assistance control, a torque sensor can be used. The sensor measures the effort the cyclist is putting into the bike, and with that information the amount of assistance from the electric motor can be controlled. The market for intelligent e-bikes is not yet mature. There are several systems on the market to measure torque, but there are still opportunities to conquer a part of the market.

At the moment, the prevailing technology used is magnetic field measurement, using the reversed magnetostrictive effect (section 2.4). This technology can be easily integrated into the bottom bracket, and does not require any modification to the bike frame.

Competitors

At the moment most e-bikes are either produced in high volume in China, or by European or North American bike manufacturers as high-end products. The torque sensor is more applicable for the high-end products. The bike manufacturers do not develop the sensor themselves because they lack the know-how or the experience. In the last year, a lot of new companies entered the e-bike market. The German company Schaeffler Technologies introduced through its bearing manufacturer FAG a torque sensing bottom bracket. The same was done by Thun, a bottom bracket manufacturer for more than forty years. Shimano, a global manufacturer of high quality bicycle parts, announced its *Shimano Total Electric Power System* (STEPS, figure 1.1a), containing all the necessary parts to construct an e-bike. During the summer automotive giant Bosch introduced its vision on the e-bike market with their *eBike* system (figure 1.1b). Bike manufacturers themselves are also busy developing technology. The Accell group, which contains bicycle brands like LaPierre, Sparta and Koga Miyata, has its own technology, called *ION* (figure 1.2). These companies can be seen as competitors to SKF.



Figure 1.1: (a) Shimano STEPS [3] (b) Bosch eBike. [4]



Figure 1.2: (a) Example of an e-bike with ION technology from Sparta [Sparta] (b) schematic view of the ION technology with a rear wheel hub motor and battery pack integrated into the frame. [5]

Possible Market Gap

At the moment, the e-bike market is still wide open. Not a lot of products are available. If SKF gets in the market of e-bikes before the market is saturated, there is a chance that SKF can take a leading role.

1.2 The Market of Power Steering Systems

Trends

More and more cars are equipped with electrical power steering systems (EPS). EPS systems have several advantages over traditional hydraulic systems:

- **More efficient:** The hydraulic pump has to run all the time, even when there is no steering action. This drains power from the engine constantly. Eliminating the constant power demand of a hydraulic system will reduce the fuel consumption up to 5%. [7]
- **Less space:** The EPS system is more compact than a traditional system, making packaging easier and also makes it a suitable option for smaller cars.
- **Less weight:** The EPS system is lighter than a traditional system, which will boost efficiency even more.
- **Better steering action:** Because the system is assisted by electric motors, it is able to be tuned to the wishes of the manufacturer and/or consumer.

To control the EPS system, measurement of steering angle and steering effort (torque applied by the driver) should be measured. Most vehicles are already equipped with steering angle sensors. It would be beneficial to integrate the position sensing and torque sensing into one sensor.

The market is in a mature state, as can be seen in chapter 2. Several manufactures offer torque sensors, using various technology. The technologies that are mostly used are contactless and based on magnetics. The two most used technologies are magnetic rotor-stator phase shift measurement (section 2.1) and magnetic field measurement (section 2.4). Both technologies require modifications to the steering shaft. The first technology requires a torsion bar, the second requires a magnetic region applied into or onto the shaft.

Competitors

Most car manufacturers do not produce their steering systems themselves. They buy complete steering racks from automotive suppliers like ZF and

Valeo. These systems contain the torque sensor. Some suppliers develop their sensors themselves, some use sensors from companies like Bosch or Bourns. These companies can be seen as competitors to SKF.

Possible partners in the development of a torque sensor for EPS applications can be companies that develop only the technology. Afterwards they license the patents to other companies. Companies that develop technology for steering sensors are MMT and NCTEngineering. Another possibility is to work together with a manufacturer of steering systems that does not develop its own sensor, like ZF. SKF and ZF already had an earlier project on this subject.

Possible Market Gap

The market for steering sensors is already mature. This means that it will be hard to convince car manufacturers to change their existing sensor for the new sensor from SKF. Unless SKF comes up with a design that is better in either performance or price.

1.3 Conclusion Market Research

Because the two fields of application of the torque sensor are quite different with regards to the specification, a choice has to be made. The duration of the project does not allow to develop a torque sensor for both applications in parallel. Therefore, a strategical decision was made to focus the project on the development of a torque sensor for e-bike applications first. Afterwards, a study can be done to determine whether the technology can be used for EPS applications, if desired.

Competitor Analysis

The competitor analysis was done by using the internet, patent databases and internal knowledge. During the analysis, it turned out that there is a lot of overlap in the technologies used by different companies. Therefore, this section is arranged according to the technologies used. All the specifications (if provided) of the sensors are collected in the competitor analysis matrix in appendix A.

Some sensors are actually not real torque sensors. These sensors measure the phase shift between an input and an output shaft which are connected with a torsion bar. The measured phase shift between the two shafts is equal to the torsion angle of the torsion bar. With the material properties, the dimension of the bar and the torsion angle the applied torque can be calculated. But for the sake of simplicity, these phase shift sensors are also called torque sensors in this report, because they are designed specifically to serve that purpose.

Although the project is now focused on e-bike applications, it is still useful to look at solutions used in the EPS field. Some measurement principals for EPS sensors might be adaptable to use on an e-bike application.

2.1 Magnetic Rotor-Stator Phase Shift Measurement

The first and probably most used measurement principal in power steering applications is the measurement of the phase shift between the input and the output shaft by using a magnetic rotor and a ferro-magnetic stator assembly. The input shaft (connected to the steering wheel) and the output shaft (connected to the steering rack) are connected through a torsion bar. To keep the assembly compact, the torsion bar is usually situated within

either the (hollow) input or output shaft. This way, the ends of the input and output shaft can be situated close to each other, through which a considerable phase shift can occur, as can be seen in figure 2.1a.

On one of the shafts (input or output shaft, there is no difference in application) a multi polar magnetic ring is fitted. This ring contains a plurality of alternating north and south poles. On the other shaft, a stator assembly is fitted. This stator assembly usually contains two rings of ferromagnetic material. Both rings are situated around the shaft and have teeth that cover the magnetic ring. The teeth of both rings lock in to each other, but don not touch, and cover the magnetic rotor. There is the same number of teeth per stator ring as there are pole pairs on the rotor. The teeth of one ring cover the north poles of the rotor, the teeth of the other ring cover the south poles.

In this setup, the magnetic flux of the magnets on the rotor is guided into the stators. If a sensor that is able to measure the magnetic flux, for instance a Hall Effect sensor, is placed between the two stator rings, the magnetic flux can be measured, as is illustrated in figure 2.1b. When a torque is applied between the input and output shaft, the rotor and stator rotate relative to each other and so the positions of the magnets change. Therefore, the magnetic flux between the stator rings changes, and can be measured by the Hall sensor. To amplify the signal at the location of the Hall sensor, flux concentrators are used. These are ferro-magnetic parts which guide the magnetic flux in the stator rings to one specific place, close to the Hall sensor.

This way, the phase shift between the input and output shaft can be determined. If the stiffness of the torsion bar is known, the applied torque can be calculated.

The technology is only used in EPS applications. A possible explanation is that this kind of assembly requires a considerable amount of space in the radial direction. Therefore, it might be hard to implement it on an e-bike application.

Companies that use this technology are: Moving Magnet Technologies (MMT), Bosch, Continental, NSK and Valeo.

2.2 Magnetic Rings Phase Shift Measurement

At the end of the input shaft and the output shaft a ring with a plurality of magnets is fixed (figure 2.2). Both rings have the same number of pole pairs and are aligned in a way that on both rings the north and south poles are parallel. The input and the output shaft are connected with a torque coupling. The torque coupling is designed to flex when torque is applied. This results in a phase shift and a change in direction of the magnetic fields between the two rings. In between the two rings, an AMR sensor is placed

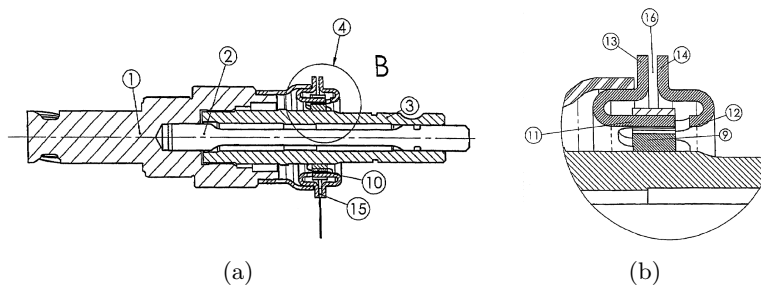


Figure 2.1: Drawing of a torque sensor using a magnetic rotor and stator assembly, (a) with input and output shaft (1,3), torsion bar (2), stator assembly (10) and Hall sensor (15). (b) Detail of sensor with multi polar magnetic ring (9), ferro magnetic stators (11, 12) with flux concentrators (13, 14) and air gap for Hall sensor (16). [8]

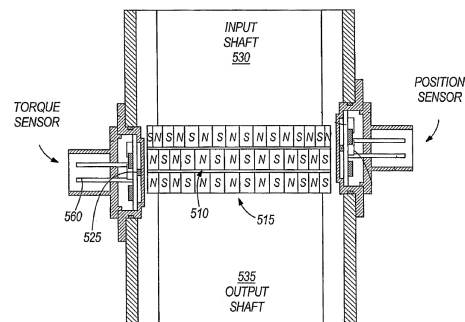


Figure 2.2: Drawing of torque sensor using magnetic rings. Magnetic rings (510, 515) and AMR sensor (525). [9]

which measures this direction. The direction of the magnetic field is thus the measure for the phase shift, which is used to calculate the applied torque.

A patent application for this measurement principle, to be used in a EPS system, was done by SSI Technologies, which was acquired by Bourns inc., an automotive sensor manufacturer. The patent also describes a third magnetic ring, which can be used to measure the rotor position.

2.3 Mechanical Phase Shift Measurement

The phase shift between the input and output shaft can also be measured mechanically with planetary gear sets and the use of rotational sensors. To the end of both input and output shaft a sun gear is fitted. These sun gears are connected to their own planetary gears. These planetary gears are both connected to a common planet carrier. Around the two planetary gears, two separate ring gears are fitted. One of the ring gears is fixed to the sensor housing and is stationary. The other ring gear is also toothed at the external

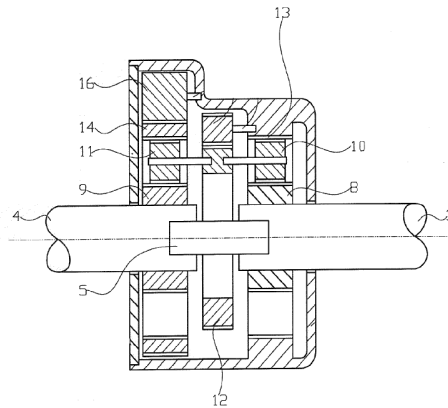


Figure 2.3: Drawing of mechanical phase shift torque sensor with input and output shaft (3, 4), torsion bar (5), sun gear (8, 9), planets (10, 11), common planet carrier (12) stationary ring gear (13), rotating ring gear (14) and rotation sensor (16). [10]

circumference. Their teeth are connected to one or more rotation sensors. This sensor is illustrated in figure 2.3.

When the two shafts rotate without a phase difference (i.e. no torque is applied), the two sun gears will spin, also moving the planets. But because they spin at the same speed, the ring gears remain stationary. When a torque is applied, and thus a phase shift occurs, the sun gears will rotate relative to each other. This will cause the two sets of planets to move differently. Because the planets share the same planet carrier, the ring gear that is not fixed to the body will have to move to compensate the difference of movement of the planets. This rotation is measured by the rotation sensor, and the applied torque can be calculated.

Bourns inc. has a patent application for this technology, but as far as known, this technology is not available commercially.

2.4 Magnetic Field Measurement

Instead of measuring the phase shift of two shafts, the stress induced by the application of torque can also be measured directly. If stress is applied to a magnetic structure, the properties of the magnetic field change, and can be measured.

This truly contactless measurement principal starts with a magnetic shaft. This shaft can be magnetized itself, covered with a magnetic material or fitted with a magnetic sleeve.

The shaft is placed through the sensor body, without causing any friction during the rotation of the shaft. In the vicinity of the shaft one or more measurement coils are placed to pick up the magnetic field emanating from

the magnetic region of the shaft. The change current in the coil can be the measure for torque applied on the shaft. There are two different methods of measurement: fluxgate technology and the inverse magnetostrictive effect.

Fluxgate

The sensing element contains an assembly of two coils, situated circumferentially, with a magnetic saturable material in between. An alternating current is passed through one of the two coils, causing a time-dependent magnetic field in the material between the coils. This time-dependent field induces a current in the second coil, the measurement coil. When no other fields are present, the output of the measurement coil should be the same as the input of the first coil. The magnetic field from the magneto-elastic material of the shaft is superimposed on this magnetic field. The changes in the field emanating from the shaft (caused by stress) will change the induced current in the measurement coil, which is a measure for the applied stress on the shaft.

The Inverse Magnetostrictive Effect

This effect is the change of magnetic susceptibility when the material is subjected to mechanical stress. On the load bearing shaft, a layer of magnetostrictive material is applied. The shaft is placed inside the sensor body, which contains two coils. Between the coils there is no material, unlike the fluxgate sensor where a saturable material is placed between the coils. Through one coil, an alternating current is passed. The coil magnetizes the magnetostrictive material with a time dependent magnetic field. That magnetic field in turn induces a current in the second coil. Again, when no load is applied, the output of the measurement coil should be equal to the input of the first coil. When a torque is applied to the shaft, the susceptibility of the magnetostrictive material changes. This changes the magnetic field in the layer, and therefore also the current induced in the second coil. Hence, the applied torque can be measured.

This technology can be widely used for almost all torque transmitting shafts. Because the torque transmitting shaft is directly the primary sensor part, the only modification that has to be made to the shaft is the application or attachment of a magnetic surface. The company NCTEngineering has patented a method of direct magnetization of a shaft, which is probably used by Thun to create a torque sensor for e-bike applications which is analyzed in section 3.1. The German company Schaeffler also introduced a e-bike torque sensor (figure 2.4), which is also used in the new Bosch eBike product [6]. NCTEngineering also offers torque sensors themselves, for all

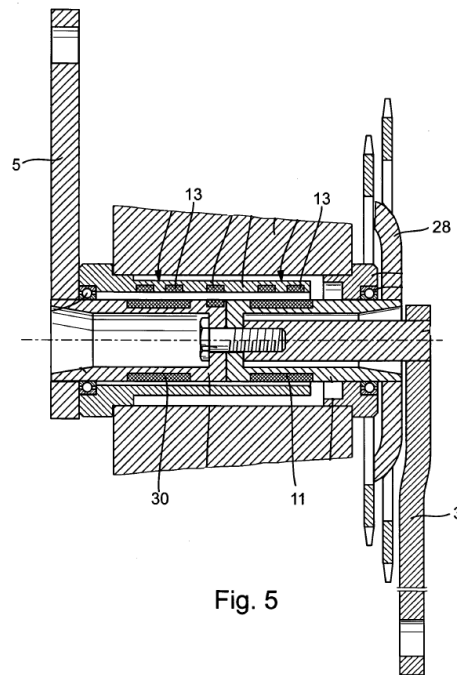


Fig. 5

Figure 2.4: Inverse magnetostrictive effect torque sensor integrated in a bottom bracket from Schaeffler/FAG, used in the Bosch eBike system. With cranks (3, 5), chain wheel (28), magnetic regions (11, 30) and coils (13). [11]

kinds of automotive applications as can be seen in figure 2.5. AAB and Siemens VDO also offer this technology for automotive applications.

2.5 Magnetic Translation Measurement

The input and output shaft are connected through a torsion shaft. At the location where the two ends of the shafts meet, a plastic sleeve is loosely fitted around the shaft. On one shaft-end, the sleeve is connected with a pin and is allowed to translate along the axial direction of the shaft through a slit. The other shaft end has also a pin, but this pin moves through a slit that is tilted 45° with respect to the axis of the shaft. Therefore, when the two shafts rotate compared to each other the tilted slit will cause the rotational movement to be converted to a translation of the plastic sleeve. The sleeve contains an aluminium ring. The housing around the plastic sleeve contains two coils. The input coil causes a magnetic field in the ring. This field in turn will induce a current in the other coil. The magnitude of the current of the output coil depends on the location of the ring, and thus the amount of phase difference between the input and output shaft.



Figure 2.5: Examples of application of NCTEngineering torque sensor (a) in a gearbox and (b) in a drive shaft. [12]

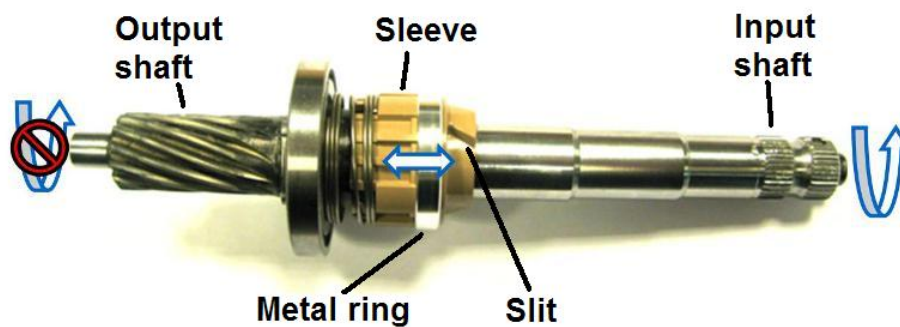


Figure 2.6: Honda Accord EPAS system torque sensor. [13]

This type of torque sensor was found during the analysis of the steering rack of a Honda Accord. A picture of the analysis can be seen in figure 2.6.

2.6 Optical Phase Shift Measurement

A solid shaft runs through the sensor body. At the extremities within the sensor body, two radially slotted disks are fitted. At one side of a disk a light source is placed, on the other side a phototransistor. Upon rotation of the shaft, the phototransistors of both disks give a square wave signal as output, because the slotted disk moves in between the light source and transistor. In unloaded rotation, the two signals have a fixed phase difference. When a torque is applied to the shaft, this phase difference will change due to torsional deformation of the shaft. By measuring this change in phase difference, the applied torque can be calculated, as illustrated in figure 2.7.

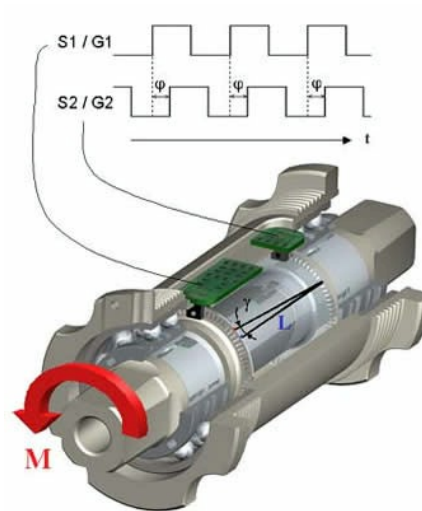


Figure 2.7: Optical phase shift measurement, using two slotted disks with light source and phototransistor. Torque is calculated by measuring the change of phase difference between the two square signals. [14]

Ergomo uses this measurement principle in their bicycle power meter product which is aimed at professional athletes and enthusiastic amateurs to track their training efforts and progress. See also section 3.2 for a detailed analysis of this product.

2.7 Displacement of Rear Drop Out

All the previous measurement principals measure the torque on the shaft it is applied to. But that is not the only place where torque can be measured. When torque is applied through the pedals and crank assembly on a bike, the energy is transmitted through several components to the rear wheel. Everywhere along this route, the torque can be measured one way or another. Sometimes this means that the torque is measured indirectly.

An example of an indirect method is the measurement of the displacement of the rear drop out. The rear drop out is the place on a bicycle frame where the axle of the rear wheel is connected to the frame. This piece of frame is replaced with a sensorized frame attachment. The rear axle is connected to a bracket, which is in turn connected to the frame. The bracket is designed to be less stiff than the frame in the direction of the forces transmitted through the chain.

When a torque is applied to the bike, it will be transmitted through the chain wheel and the chain to the rear sprocket. There, the bracket of the new rear drop out will deflect. This deflection can be measured with a load cell. One side of the load cell is attached to the bracket, the other side is

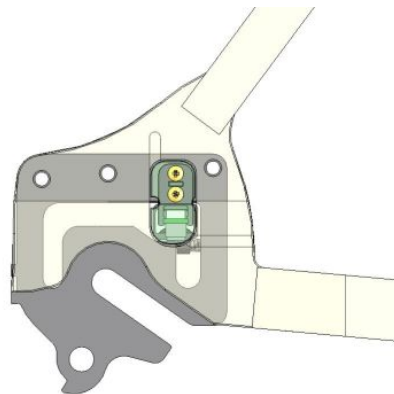


Figure 2.8: Displacement sensor in rear drop out using a load cell between sensor bracket and frame. [15]

connected to the frame with a spring-loaded metal ball. If the rear sprockets radius is known, the torque can be calculated.

The Dutch company IDbike is the inventor of this sensor. It is used by different manufacturers of e-bikes, like Dutch manufacturers Sparta and Gazelle.

2.8 Forces on the Bottom Bracket Bearing

Another example of measurement without a torsion bar is the measurement of the forces on the bottom bracket bearing. While pedaling, the cyclist exerts a force directed mostly downwards. The torsion applied to the chain wheel leads to a tension in the chain, which causes a horizontal force between the frame and the bottom bracket. Both these forces are concentrated in the bearings of the bottom bracket. The chain tension is mostly present in the right hand bearing.

The bearings are placed in a cup which is fastened externally to the bottom bearing tube. An exploded view of such a bottom bracket can be seen in figure 2.9. The right hand bearing cup has a special insert, in which the bearing is fitted. The insert is machined in such a way that all the forces on the bearing are concentrated in a small area. On the surface of this area, a strain gauge is placed. The forces on the bearing will deform the insert, which are measured by the strain gauge. With this measurement, the chain tension can be derived. When the used gear ratio is also known or measured, the applied torque can be calculated. The external placement of the bearings has the additional advantage that bigger bearings can be used, and therefore a bigger spindle. This leads to a stiffer bottom bracket.

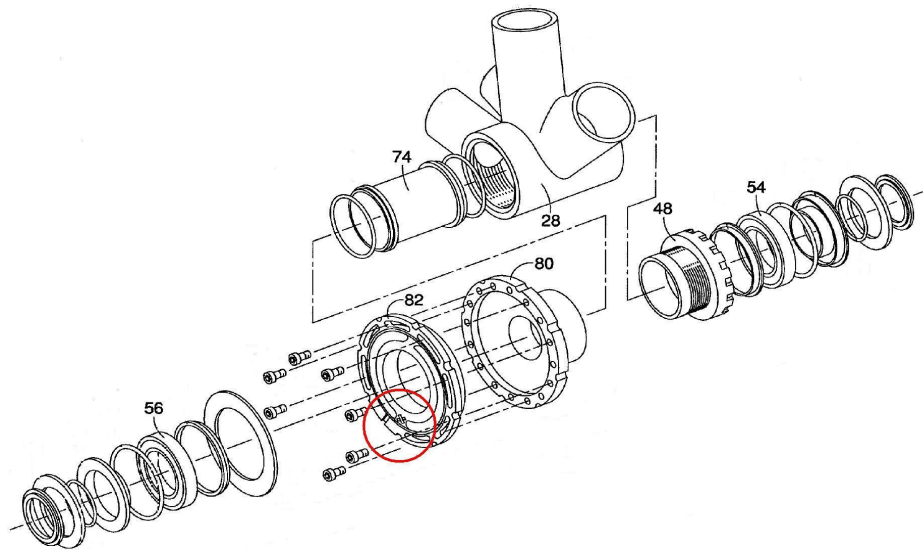


Figure 2.9: Force measurement in bottom bracket, with bearings (54, 56) mounted in cups (48, 80) externally to the bottom bracket tube (74). Right hand bearing mounted in special insert (82) to concentrate forces to area with strain gauge (in circle). [16]

Shimano has applied for a patent on this system, and is using it in their new Shimano Total Electric Power System (STEPS, see figure 1.1a).

2.9 Summary of Technologies

All the technologies that are discussed in this chapter are summarized in table 2.1, together with their advantages and disadvantages. Some technologies use a very accurate method, but rely on magnetic rings, which are made of rare earth materials. These materials are only exported by China. This is not a desirable situation, because it will make the manufacturer dependent of one supplier.

Technology	Section	Advantage	Disadvantage
Magnetic rotor-stator	2.1	High precision	Torsion bar Magnetic ring
Magnetic ring	2.2	Compact construction	Torsion bar Magnetic rings
Mechanical	2.3	Proven sensor technology	Contacting method Mechanical components Torsion bar
Magnetic field	2.4	Non-contacting No torsion bar	Need to magnetize shaft
Magnetic translation	2.5	Simple method No signal post-processing	Mechanical components
Optical	2.6	Cheap components	High mounting precision Requires calculation with microprocessor
Displacement drop out	2.7	Simple method	Needs modification of bicycle frame
Force in bottom bracket	2.8	Simple method	Indirect measurement Needs gear ratio measurement

Table 2.1: Summary of technologies.

Analysis of Purchased Parts

To gain more understanding and get more hands-on experience with some of the available technology, several existing products were purchased. Two of the products were torque sensors integrated in a bottom bracket. The products were both made in Germany and at a price point aimed for the high-end market. The first one is a sensor from the German bottom bracket manufacturer Thun and uses magnetic field measurement as its measurement principal (section 3.1). The second bottom bracket sensor is from Ergomo, a company specialized in training equipment for professional athletes. It uses an optical measurement system (section 3.2).

The last product is made in China and at a considerable lower price point. The interesting part of this product was to analyze its working principal, and to find out how it was possible to produce it for a low cost. The product is a ‘integrative motor kit’, which contains a hub motor with integrated controller and torque sensor (section 3.3).

3.1 Thun Bottom Bracket Sensor

Alfred Thun GmbH & Co. is a German company that specializes in bottom brackets for more than forty years. Therefore, it is interesting to see such a company makes a step towards sensorized products. The products are professionally packaged, and look like quality items. The products are accompanied by detailed documentation about assembly and sensor properties (see appendix B).

The Thun X-Cell RT series consists of two different models. Both models have a torque sensor and a speed sensor. The difference is that one model has an analog measurement signal output for the speed sensor, while the

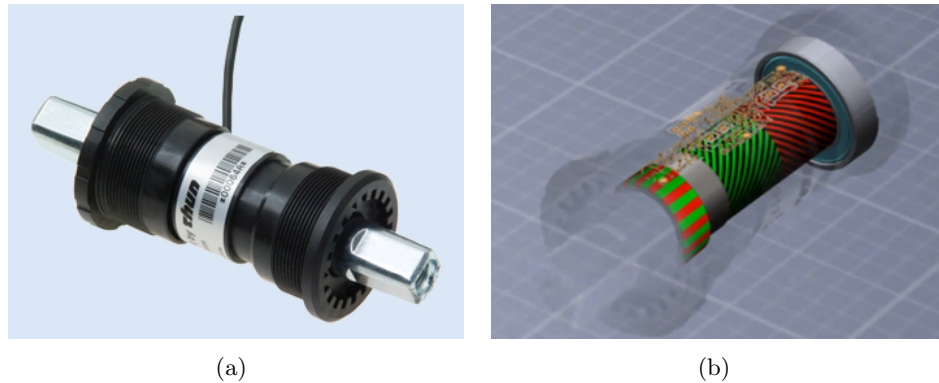
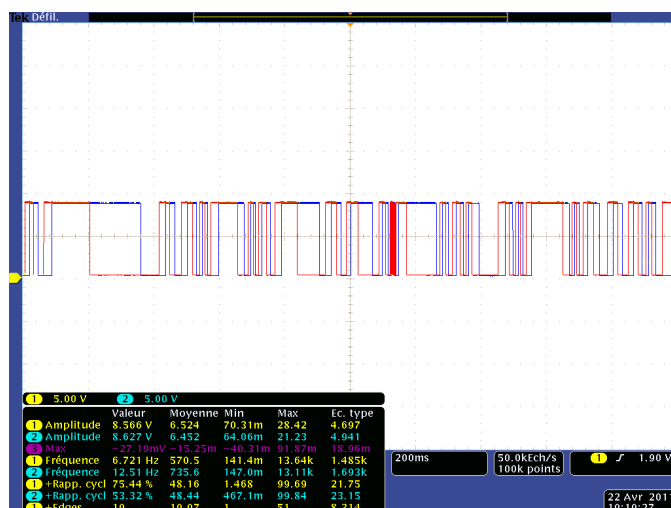


Figure 3.1: Thun bottom bracket sensor (a) product as received [Thun] (b) Illustration from the Thun website showing the magnetization on the shaft. On the left side a 16 pole pair ring and on the right side a magnetized region. [18]

other has a digital output. Both models were purchased for € 100. Documentation on the website of the company reveals the working principle of the sensors, illustrated in figure 3.1b . The speed measurement is done with a 16 pole pair magnetic ring and two Hall effect sensors. The use of two Hall sensors, placed at an electrical phase difference of 90° , provides two outputs. A sine and cosine for the analog output, two square waves for the digital output. Both types signals have a 90° phase difference. This way, the direction of rotation can also be measured. Torque measurement is done using the magnetostrictive principle, as described in section 2.4. The shaft is permanently magnetized using Pulsed Current Modulated Encoding (PCME) technology. This technology is patented by NCTEngineering, another German company [17].

Before disassembly, the product was first connected to an oscilloscope, to analyze the signals. Figure 3.2a shows a screen shot of the oscilloscope showing the speed measurements, while turning the spindle by hand. Two square signals, with a 90° phase difference enable the user to measure the pedaling speed and the direction. The torque signal was also analyzed. One end of the spindle was clamped in a workbench clamp and to the other end a torque was applied, with a wrench. The output, shown in figure 3.2b, shows the response to the applied torsion. A torsion wrench was also used, but because it was too hard to apply a steady torque, no real measurement could be done to determine the linearity or sensitivity.

After this analysis, the sensor was disassembled. Figure 3.3 shows an exploded view of the sensor. From left to right it shows: the end cap used to screw the bottom bracket (BB) into the frame tube; a standard sealed deep groove ball bearing (DGBB) with no manufacturers markings; the sensor body; the spindle (greased) with second DGBB and the second end cap. The assembly also contained a magnetic impulse ring, which was mounted



(a)



(b)

Figure 3.2: Screen shot of oscilloscope of the output of the Thun Bottom Bracket sensor measuring (a) the speed and direction of rotation, (b) the applied torque to the spindle by a wrench.

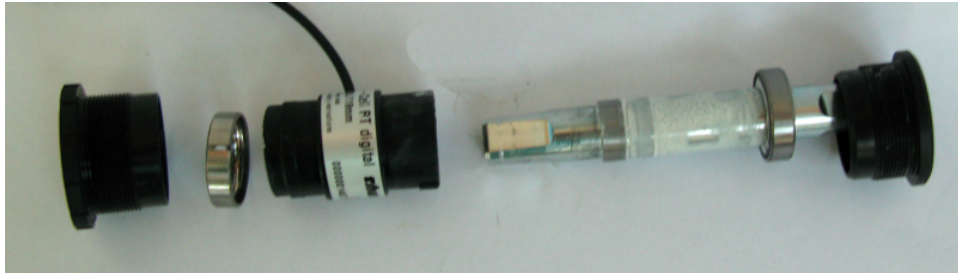


Figure 3.3: Exploded view of the disassembled Thun Bottom Bracket sensor.

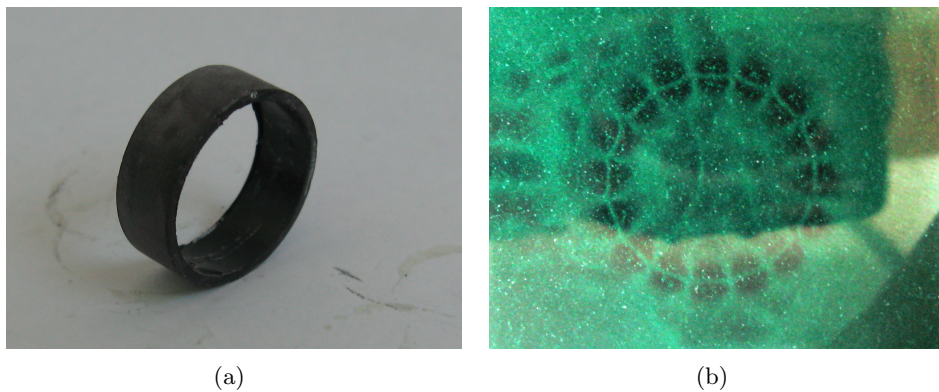


Figure 3.4: (a) Magnetic ring from the Thun BB sensor, used for speed and direction measurement. (b) Magnetic ring under magnetic field foil, showing the magnetization of the ring with 16 pole pairs.

on the spindle.

The impulse ring (figure 3.4a) is made of a flexible magnetic material and had 16 pole pairs (figure 3.4b). The magnetic field of the spindle was very weak, and could not be detected with the foil, and was hardly measurable with a Gauss-meter. The spindle was further analyzed with a Metrolab three-axis Hall effect sensor. This measurement device is able to measure magnetic fields as small as 1 Gauss. The sensing element was held at one end of the magnetized region of the spindle and thereafter moved to the other end of the region. The measurement is plotted in figure 3.5. The plot shows that the magnetic region is very weak and therefore, a lot of noise is disturbing the measurement. But there is an offset visible when the sensor is moved from one side of the region to the other side (approximately half way during the measurement time). It shows that the spindle is indeed magnetized, although very weak.

The sensor body was fitted over the spindle, and contained an over molded PCB as shown in figure 3.6a. The PCB (figure 3.6b) contained two Hall effect sensors for the speed measurement, two coils for the torque measure-

ment and several components for amplification and signal conditioning.

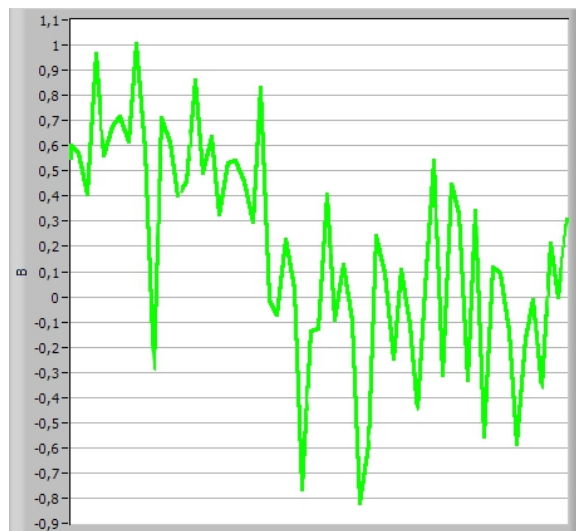
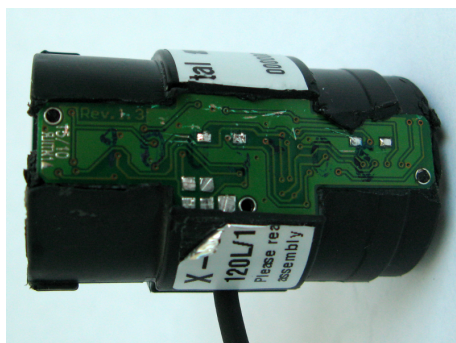
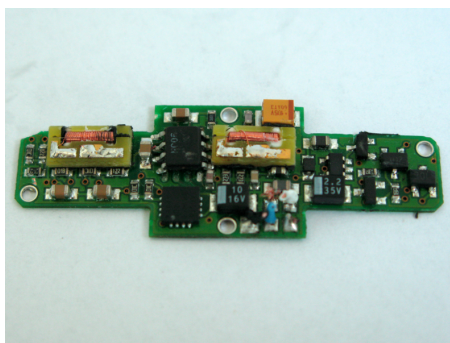


Figure 3.5: Measurement of the magnetized region on the spindle using a Metrolab three-axis Hall magnetometer. The horizontal axis denotes the measurement time, the vertical the magnetic field strength in Gauss.



(a)



(b)

Figure 3.6: PCB from Thun BB sensor. (a) Stripped sensor body showing the overmolded PCB. (b) PCB of the Thun sensor with two Hall effect sensors (far right), two coils for torque measurement (left and center) and several components for amplification and signal conditioning.

3.2 Ergomo Bottom Bracket Sensor

The bottom bracket sensor of Ergomo is supposed to be part of a power measurement setup, targeted on professional athletes and enthusiastic amateur cyclists. It is normally combined with a microcontroller which converts the measured torque signal together with the measured speed to a power value. This measurement is used for training purposes and post race analysis.

The sensor uses the optical phase shift measurement principle as explained in section 2.6. The sensor consists of two radially slotted disks and two optical sensors, as can be seen in figure 3.2. Both sensors give a square wave output. When a torque is applied, the phase shift between the two signals is the measure for the amount of applied torque.

Upon delivery of the sensor, the first impression of the product was that it was somewhere between prototype and production state. This is probably due to the low volume of production of the sensor. The sensor body was sealed on several places with some kind of white putty. The price of the sensor was \$ 700.

The interior of the bottom bracket is visible on figure 3.2. It shows that the sensor uses five roller bearings. Normally there are only two bearings in a bottom bracket. The reason for this construction with five bearings is probably that the optical system used requires a high level of precision, which cannot be obtained with a single bearing on either side.



Figure 3.7: Ergomo bottom bracket sensor with slotted disks for optical measurement. [14]

3.3 Integrative Motor Kit

The integrative motor kit promises to be a complete kit of an electric hub motor, a built-in sensor and controller and a control panel (figure 3.8a). Next to this kit, only a battery pack (24 volt) should be necessary to retrofit a bicycle to make it an e-bike. The price of the purchased product was \$316.

Before disassembly, the product was briefly analyzed. The whole assembly weighted around 4.5 kg. It contained a hub motor with two cables. To one cable a connector was fitted, to connect the system to a battery pack. The other cable was connected, via a rather crude interconnection, to the panel.

As a preliminary analysis, the battery connection of the motor kit was connected to a power supply at 24 volt. When the system was turned on, the low battery light was blinking on the control panel. Increasing the supply voltage to 27 volt solved this problem.

The location of the torque sensor was thought to be at the mounting position of the rear sprocket(s). Manually applying torque to this connection did not yield any result. When the motor was rotated in the forward direction around the axle, a noise was heard. Turning the motor in the other direction did not result in the same noise.

Opening of the hub motor revealed a brushless DC motor (figure 3.8b), with the control electronics in the center of the motor. After the stator was removed from its housing, the torque sensor was visible. It consists of two magnetic rings (both with 20 poles, figure 3.8c), a torsional spring and a PCB with four Hall effect sensors (mounted on the stator, figure 3.8d). When a torque is applied to the pedals of the bicycle, it is transmitted through the chain to the rear sprocket. The sprocket mounting is connected to the motor housing via the torsional spring, which is the rotor of the hub motor. The connection with a torsional spring will cause a phase shift between the sprocket mounting and the rotor. This phase shift can be measured by measuring the phase shift of the output of the Hall cells. Of the four Hall effect cell, probably only two are used. The three cells on the outer ring are probably used for the control of the motor, and only one of these three is used in combination with the cell on the inner ring to measure the applied torque.

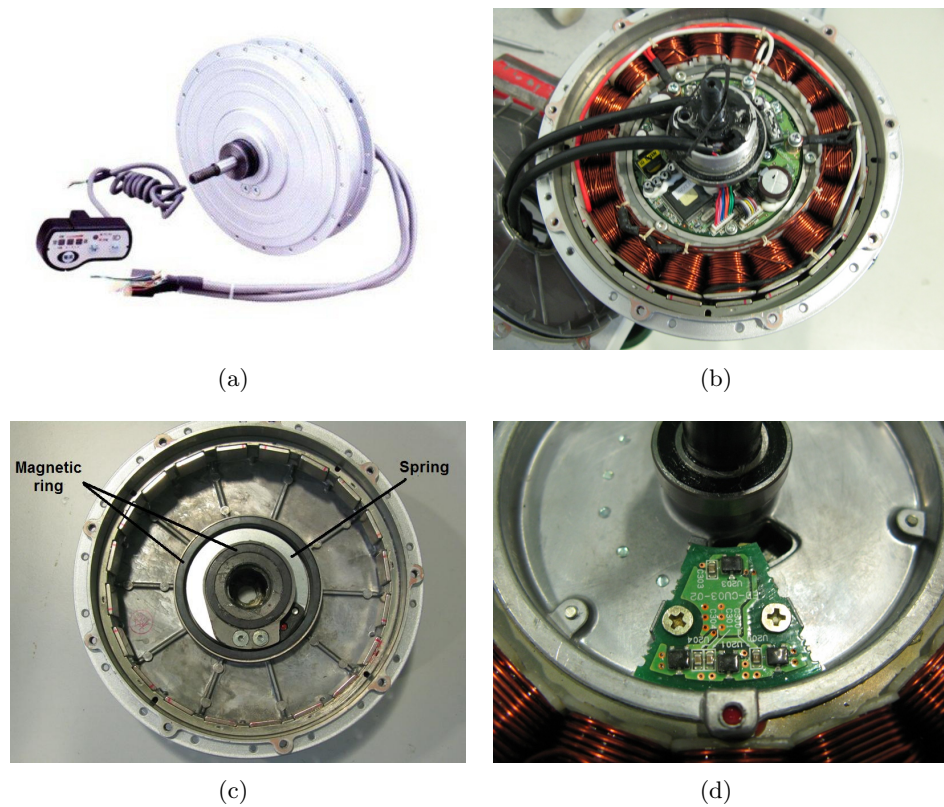


Figure 3.8: Integrative motor kit (a) complete kit with a hub motor with integrated controller and a control panel, (b) brushless DC motor, (c) torque sensor containing two magnetic rings and torsion spring, (d) PCB with four Hall sensors.

Quality Function Deployment

Quality Function Deployment (QFD) is a method used by SKF to translate the fuzzy voice of the customer into a clear list of design requirements of the product that has to be developed. The developer of QFD described it as a

method to transform user demands into design quality, to deploy the functions forming quality, and to deploy methods for achieving the design quality into subsystems and component parts, and ultimately to specific elements of the manufacturing process. [19]

After listening to the voice of the customer, by taking meetings, receiving technical specifications and hearing the customer requirements, all the needs of the customer are formulated. A paired comparison matrix is used to identify the most important needs by comparing all the needs to each other.

When the most important needs are identified, functions are selected that are needed to fulfill these needs. The connection between the needs and the functions is quantified in a House of Quality (HoQ).

After this first House of Quality, a clear view is obtained about which functions are important in the product. With this list, the concept phase can be started. After several concepts are worked out, a Pugh Matrix is used to rate the different concepts in order to select the best. The second House of Quality is used to couple the functions to real quantified design requirements. Because this project ends with a proof of concept prototype, the Pugh matrix and HoQ#2 should be done if the project would be continued.

4.1 Needs

First, all the *needs* are formulated. Needs are aspects of the products that are needed to be present in order to satisfy the customer. Usually the term

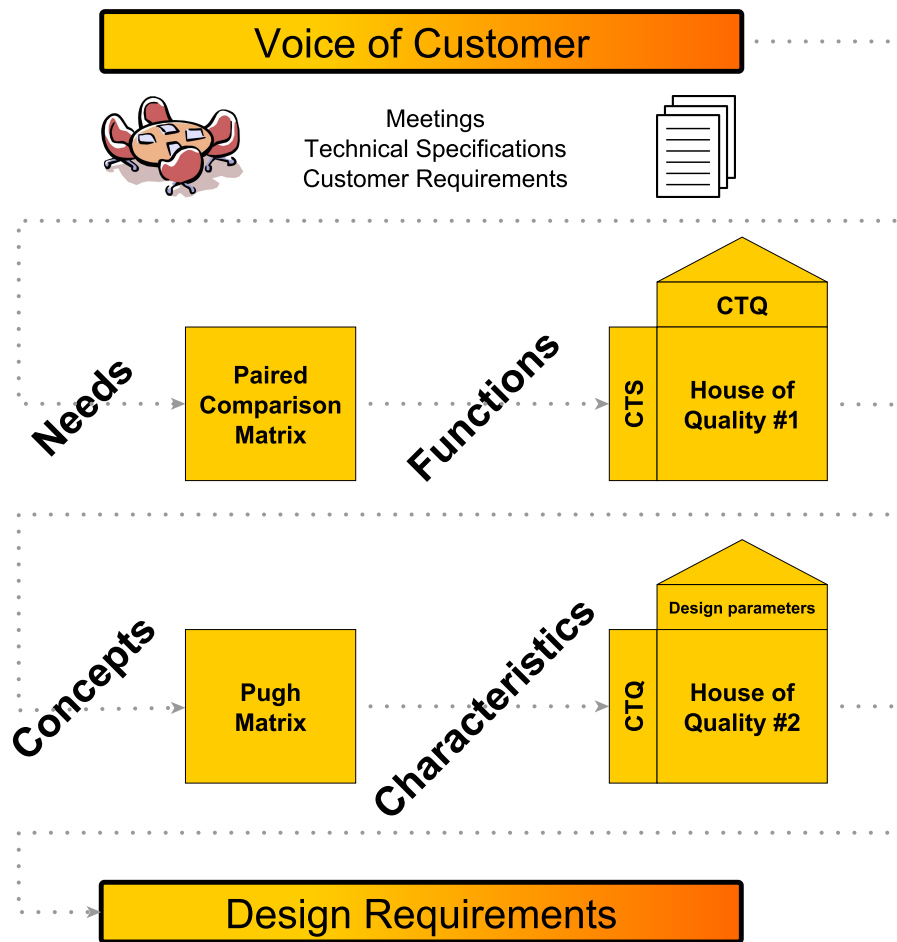


Figure 4.1: Work flow of Quality Function Deployment from voice of customer to design requirements.

critical to satisfaction (CTS) is used. For the torque sensor eleven needs were identified and summarized in table 4.1. They are divided into three categories: three CTSs for the sensing part of the product, four CTSs for the application of the products and four CTSs regarding the life time of the product.

4.2 Paired Comparison Matrix

To determine which needs should be focused on, the Pareto principle is used. The Pareto principle (also known as the 80-20 rule) states that 80% of the result can be obtained by 20% of the work. Or in this case: 80% of the total satisfaction of the customer can be reached by fulfilling 20% of the CTS. But to know which CTS to focus on, the relative importance of the CTS has to be derived. This can be done by using a paired comparison matrix. In this matrix, each CTS is compared to all the other needs and it is determined which need is more important. This rating is done on a scale from 1 to 10, and to avoid long discussions between team members only the grades 1, 4, 7 and 10 are used. So if CTS1 is compared to CTS2 and the rating is 4 it means that CTS1 is 4 times more important than CTS2. When the rating between CTS2 and CTS4 is $\frac{1}{7}$, it means that CTS4 is 7 times more important than CTS2. To aid the process, a matrix is used as pictured in figure 4.2. The fields above the diagonal are filled in the reading direction. The values of the fields under the diagonal are the inverse of the fields above the diagonal. When the complete matrix is filled, the values in each row are summed. These totals are then normalized so that the sum of all CTSs is 100%.

Critical to Satisfaction		
Sensor	Needs to	measure torque measure position measure speed
Application	Needs to	be mechanically integrated in customer application communicate with customer application give no perception of presence to cyclist be safe
Life Time	Needs to	be maintainable withstand disturbances be reliable be of reasonable cost

Table 4.1: Critical to Satisfaction for torque sensor product.

Reading direction
1, 4, 7, 10

	CTS 1	CTS 2	CTS 3	CTS 4	Total	Normalized weight
CTS 1	1	4				
CTS 2	1/4	1		1/7		
CTS 3			1			
CTS 4		7		1		

Figure 4.2: Example of paired comparison matrix.

For the torque sensor, the analysis was done and the results are displayed in figure 4.3. The full matrix can be found in appendix C. The main conclusions are that both the need to be maintainable and the need to measure position are of very little importance for the torque sensor for e-bike application. The former because the product should be designed such that it does not need any maintenance during its life time. The latter because position information is of no interest for the e-bike manufacturer. Therefore, the need for position is dropped in the next steps of the analysis.

4.3 Functions

The next step in the analysis is to formulate the functions that are needed in the product in order to fulfill the needs. These functions are needed to ensure the quality of the product. Therefore, the term *Critical to Quality*, or CTQ, is regularly used. For example to satisfy the need of measuring torque, a certain range of torque measurement is needed. To satisfy the need of communicating with the customer application, it might be useful to use some kind of standardized connector or a certain protocol. For every CTS, several CTQs can be thought of. All these CTQs are summarized in table 4.2.

4.4 House of Quality #1

To identify the importance of a function, one has to look at the connection between a function and the needs. The importance of the needs is already quantified in the previous section. By quantifying the connection between a need and its functions, the importance of the functions can be determined.

Critical to Quality	
CTS	CTQ
Torque & Speed	Range Accuracy Repeatability Amplitude Offset Resolution Input voltage Refresh rate Weight
Communication	Protocol Standardized connector
Integration	Aesthetics Assembly time duration No modification to customer application
Presence	Extra friction Time lag
Safety	Fail safe function Over torque test
Maintenance	No part destroyed during maintenance Time duration to repair
Reliability	Endurance test
Disturbances	Vibration Moisture Temperature Shock
Cost	Price

Table 4.2: Critical to Quality for torque sensor product.

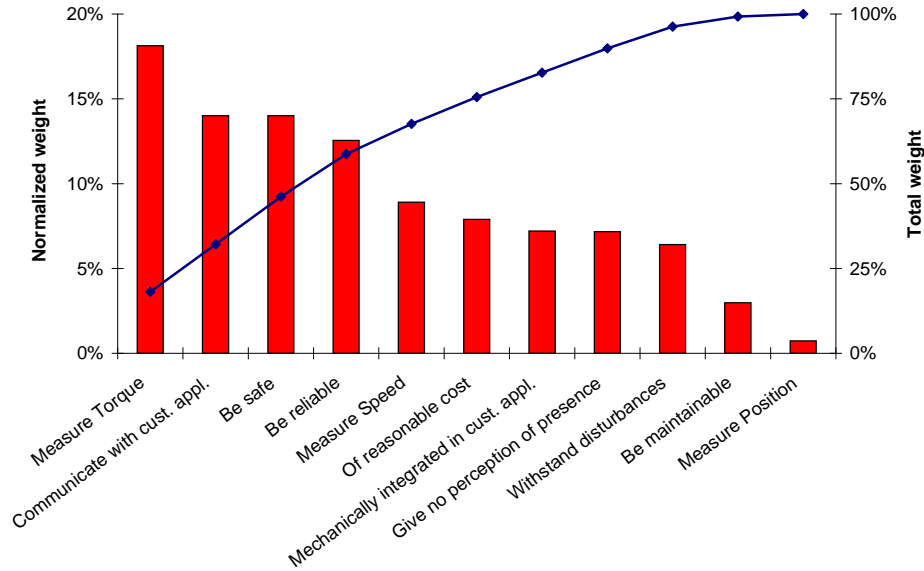


Figure 4.3: Results of paired comparison matrix analysis for torque sensor.

This analysis is done by using a *House of Quality*-diagram (HoQ). A simple example of the HoQ is shown in figure 4.4, to help explain the concept of the diagram.

On the left of the matrix, the CTSs are written, on the top of the matrix the functions. Colors are used to indicate the connections between certain needs and functions, according to table 4.2. But the connections are not limited to these color links. It is quite possible that a function that is thought of by a certain need also has a connection with another need. For example, the CTQ price has a connection with almost all CTSs, not only with the CTS cost.

The functions can be divided into two groups. Quantifiable CTQs and non-quantifiable attributes. The quantification can be done at the bottom of the diagram. Above the CTQs, the desired property of the quantification can be written. An arrow upwards means that a higher value is better, an arrow down indicates that a lower value is desired. An O means that a value closest to the indicated value is desired.

In the body of the matrix, the rating is again done on a scale from 0 to 10, using only 0, 1, 4, 7 and 10 for simplicity. A rating of 10 means that there is a really strong connection between the function and the need, a 1 means that there exists a connection but it is really small. A rating of 0 means that there is no connection. Usually, if the rating is 0, the cell is left blank to aid readability of the diagram.

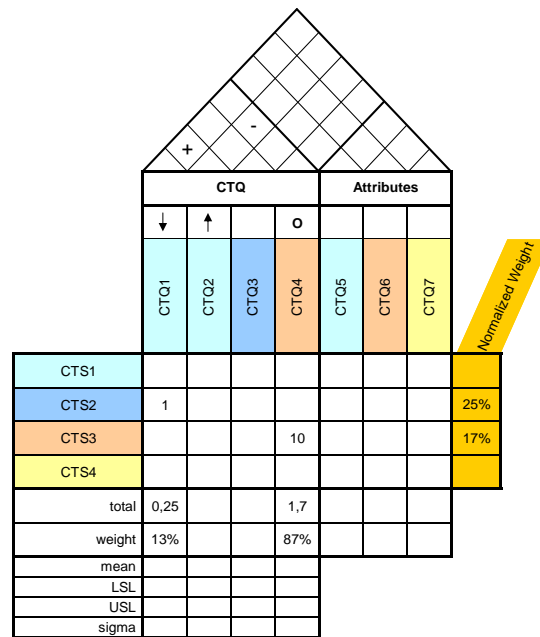


Figure 4.4: Example of a House of Quality.

The rating of every connection is multiplied by the normalized weight of the CTS from the paired comparison matrix and is summed per CTQ. This total is again normalized to a total of 100%. This value indicates the relative importance of the functions for the product.

In the roof of the House of Quality, relations between the different CTQs can be indicated. In the example, there is a positive relation between CTQ1 and CTQ2. This means that by improving CTQ1, CTQ2 will also improve. A minus indicates a negative relation. Most of the time the CTQ cost has a negative relation to a lot of other CTQs, because there is usually a trade-off between cost and quality.

The results of the first House of Quality for the torque sensor for e-bike application are plotted in figure 4.5. The complete HoQ#1 of this project can be found in appendix D. It shows that the most important functions, next to torque measurement, are: cost, safety and reliability.

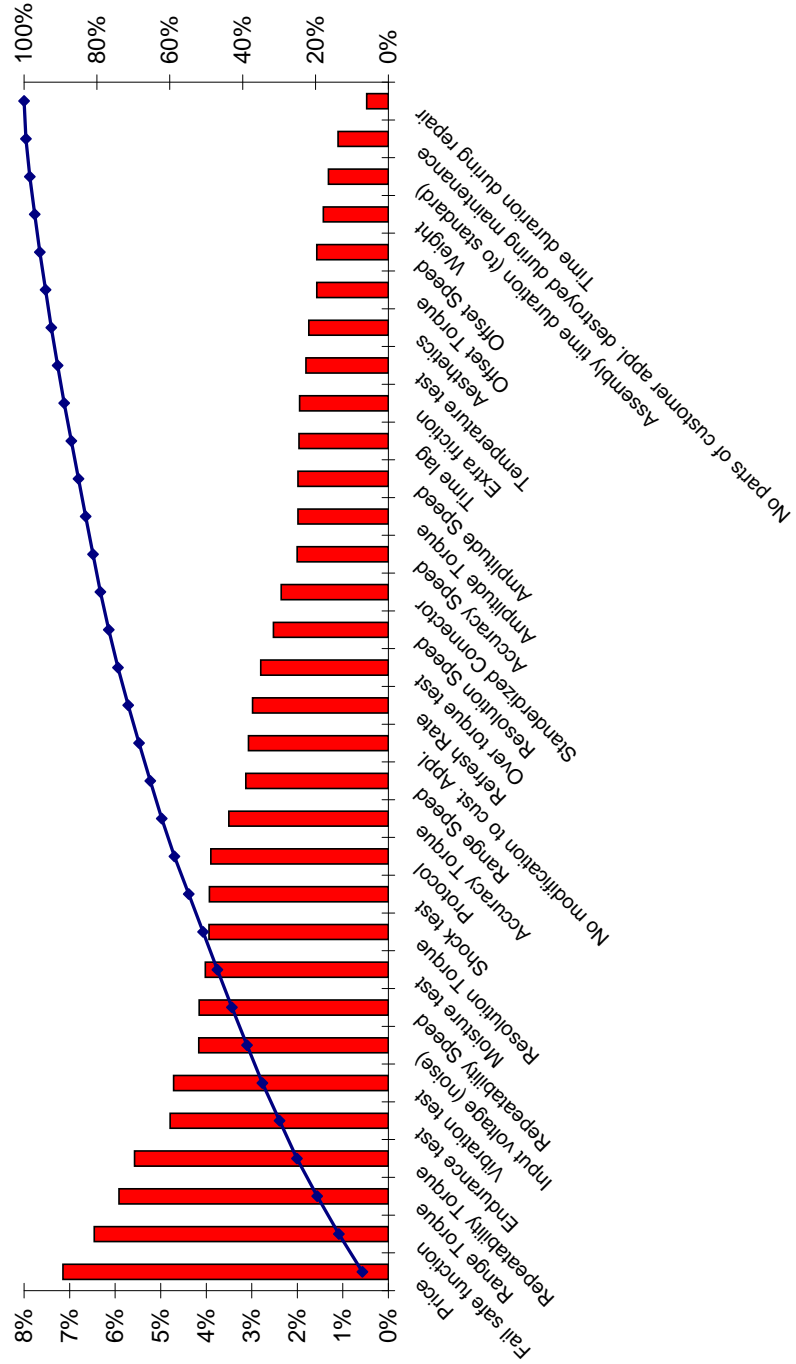


Figure 4.5: Results of House of Quality #1 for torque sensor.

Part II

Sensor Design

Concepts for a Torque Sensor for E-bike Application

The generation of concepts for the torque sensor is done in three phases: *where*, *what* and *how*. The *where* phase (section 5.1) looks at the location on the bike where the sensor should be situated. The *what* phase (section 5.2) determines the physical quantity that is going to be measured. Finally, the objective of the *how* phase (section 5.3) is to find a suitable measurement principle.

5.1 Where - Location of Sensor

The first thing that has to be determined is the location of the sensor. On a bicycle, there are a lot of possible locations for a torque sensor, all with different advantages and disadvantages. Therefore, a schematic mapping is made of a bicycle. In figure 5.1a this mapping is shown. The blue connections indicate the known products, as analyzed in part I.

For SKF, two major requirements are that the sensor can be sold as an individual item and that the sensor is usable on every type of e-bike. Therefore, the sensor should be located on such a location that an individual item can be created. So a torque sensor integrated in a hub motor is not interesting for SKF, because SKF does not produce these motors nor is it certain that every bike is equipped with a rear wheel hub motor.

bike equipped with such a motor. Figure 5.1b shows the same mapping of the bike, but now with all the possible locations of the sensor.

An additional advantage is that there is some prior knowledge available within the company about the product. Therefore, two locations seem interesting: the bottom bracket (SKF produced a bottom bracket, although it

is now discontinued) and the freewheel (SKF produces freewheels for automotive applications).

Looking only at the criteria for the location, the best locations for the torque sensor for SKF are:

- Between the bottom bracket spindle and the chain wheel;
- On the bottom bracket spindle;
- In the bottom bracket bearing;
- In the freewheel.

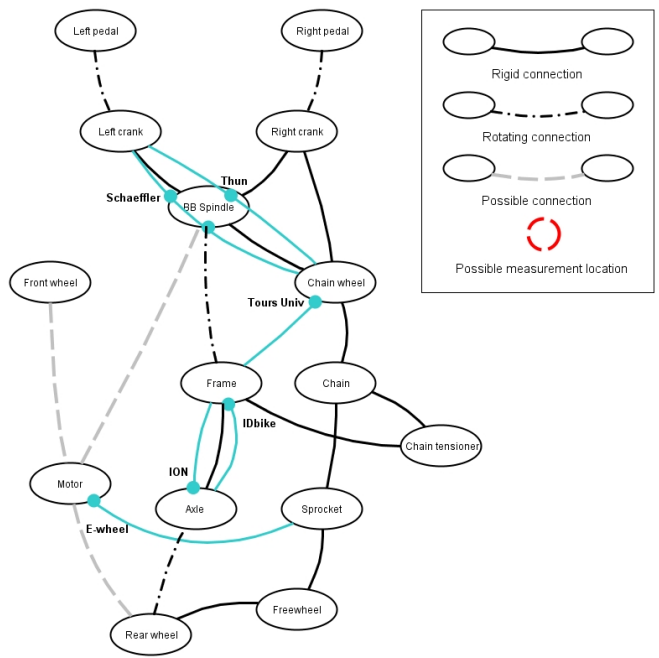
The next step will focus on what physical quantity can be measured on the different locations. The combination of the location and physical quantity that can be measured on that location will determine the final choice.

5.2 What - Physical Quantity

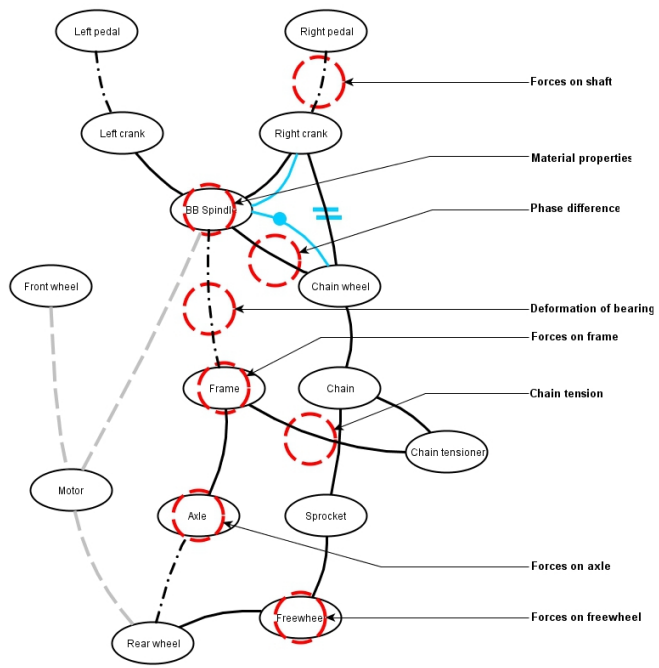
The question what should be measured seems simple: torque. But torque can be measured in many different ways, either direct or indirect. In chapter 2, several technologies were already discussed. The possibilities are (but not limited to):

- Effects of stress on the material
 - Magnetostrictive effect
 - Magnetic susceptibility
 - Resonance frequency (surface acoustic waves)
- Torsion
 - Strain gauge
 - Torsion angle
- Indirect measurement
 - Reaction forces
 - Chain tension

For every identified possible sensor location, as illustrated in figure 5.1b, a measurable physical quantity is thought of. These concepts, with their advantages and disadvantages, are summarized in table 5.1. It shows that the best location for the sensor will be to integrate it in the bottom bracket. This way, a part can be developed that is suitable for retrofitting, is within the scope of existing knowledge and products of SKF and is has enough space for a sensor.



(a)



(b)

Figure 5.1: Schematic mapping of bicycle with (a) location of sensors of competitors and (b) possible locations for torque sensor and final concept.

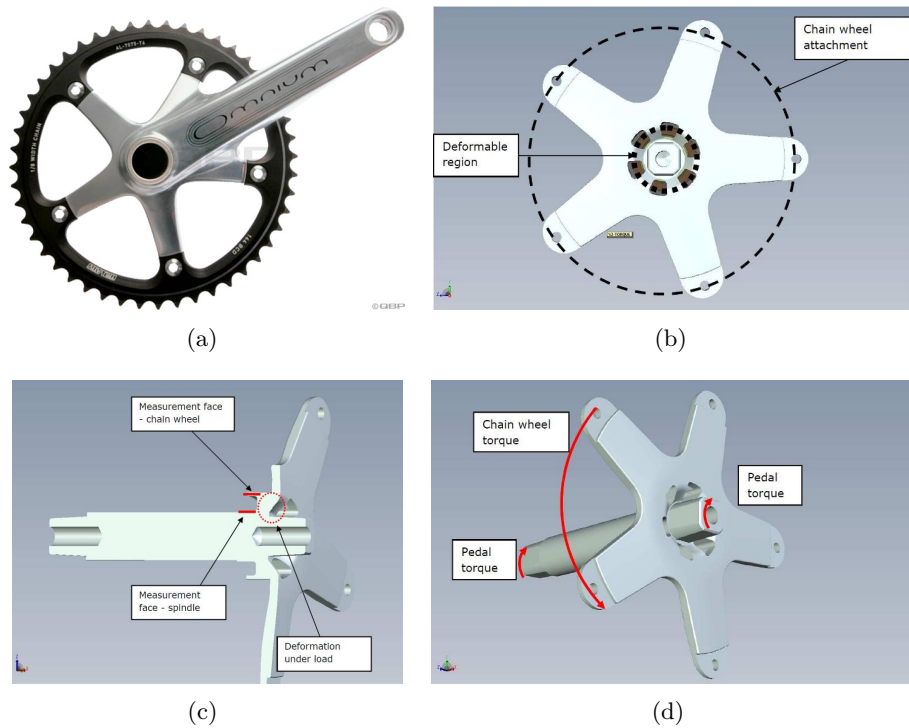


Figure 5.2: (a) A normal right pedal crank, attached rigidly to the chain wheel. (b) Front view of concept geometry with flexible connection between BB spindle and chain wheel. (c) Cross section of concept BB spindle with measurement faces for measurement of torsion angle. (d) Visualization of torques on concept BB spindle with flexible connection between spindle and chain wheel.

The concept is to measure a torsion angle between the BB spindle and the chain wheel. To achieve this, some structural changes have to be made to the assembly. A traditional chain wheel is normally connected to the right pedal crank as illustrated in figure 5.2a. This way, the chain wheel and the crank are connected rigidly to the spindle, and no torsion angle can occur. This concept uses a new geometry, where the pedal cranks are connected rigidly to the spindle and the chain wheel is connected to the spindle through a flexible connection (figure 5.2b). This way, the torque applied to the pedals will be transferred through the spindle to the chain wheel (figure 5.2d). Because the connection between the spindle and the chain wheel is flexible, the applied torque will cause a rotation between the two parts, which can be measured to determine the torque (figure 5.2c).

Where	What	Advantage	Disadvantage
Pedal ↔ crank	Stress on axle	Universal item	Rotating
BB spindle ↔ Chain wheel	Torsion angle	Universal item Space for sensor	Needs modification of right crank
BB spindle	Stresses on spindle	Universal item Space for sensor	Only one side measured
BB bearing	Deformation of inner ring	Direct measure of torsion Technology reusable	Rotating
BB spindle ↔ Frame	Reaction forces	Universal item	Indirect measurement
Frame ↔ Chain tensioner	Chain tension	Simple	Indirect measurement Gear information needed
Axle	Stresses on axle		Not compatible with hub motors
Freewheel	?	Universal item	Complex geometry Small space Rotating

Table 5.1: Locations and its possible physical quantities

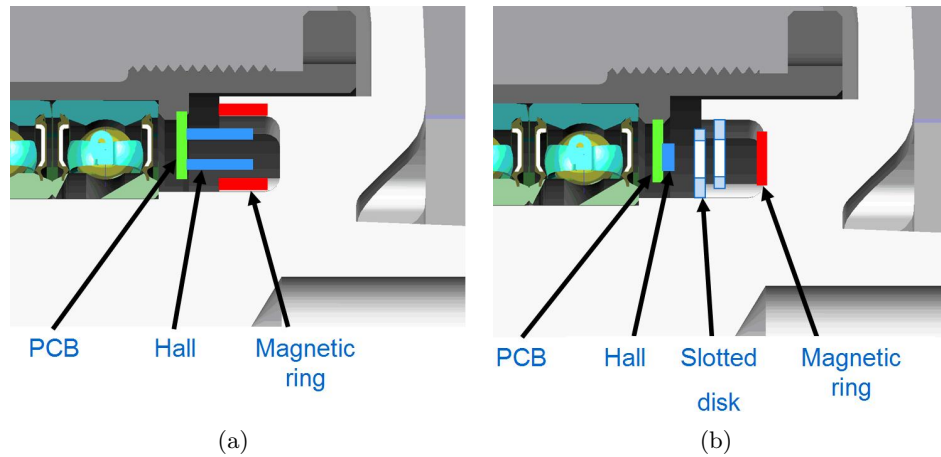


Figure 5.3: (a) Measurement concept with magnetic rings with two Hall sensors which measure the magnetic field of the rings. The phase difference between the two sine waves is the measure for applied torque. (b) Measurement concept with slotted disks. Duty cycle of measurement signal is measured to determine applied torque.

5.3 How - Measurement Principle

Now that is known what is going to be measured, several concepts were made for a measurement principle. These concepts are shortly explained in the following sections (5.3.1 - 5.3.3). Thereafter the best concept is chosen to be further analyzed in section 5.3.4.

5.3.1 Concept Magnetic Rings

The first concept will focus on the measurement of the magnetic field of two magnetic rings. The rings will be fitted to the two measurement faces. The rings will have a plurality of magnetic pole pairs around the perimeter of the ring. The magnetic field will be measured by one Hall sensor per ring. The Hall sensor will measure the amplitude of the magnetic field, thus upon rotation both Hall sensors will output a sine wave. When no load is applied, the two sine waves will have a fixed phase difference. When a torque is applied, the rings will rotate relative to each other. Either embedded or external software will measure this phase difference, and will be able to calculate the torsion angle and therefore the applied torque. A schematic drawing of the concept is shown in figure 5.3a.

5.3.2 Concept Duty Cycle

The second concept has as goal to measure the duty cycle of the measurement signal. Instead of magnetic rings, now two slotted disks are used. The disks are placed perpendicular to the measurement faces. On one side a

source (magnetic ring, LED) is placed, and on the other side a detector (Hall sensor, phototransistor). When no load is applied to the sensor, the slots of the two disks will be in phase. Therefore, when the disks are rotating, 50% of the time the path between the source and the detector is unobstructed. A duty cycle of 50% will be measured. When a load is applied, the disks will rotate relative to each other thereby reducing the opening between the source and sensor. The duty cycle of the measurement signal will decrease. The duty cycle of the measurement signal will be a measure for the applied torque. This measurement principle is illustrated in figure 5.3b.

5.3.3 Concept Rotation to Displacement

The last concept will measure the torsion angle indirectly by measuring the displacement of an intermediate piece that will transform the rotation into a translation. The previous two concepts both are based on the measurement of rotating parts. This can be quite challenging. When the rotation is transformed to a translation, more conventional measurement principles can be used.

A ring will be placed between the two measurement faces. On the inside, the side of the spindle, the ring will be constrained to move only in the axial direction with a key. On the outside, a pin will be fitted in a helical slot. If a rotation occurs between the spindle and the chain wheel, the pin in the helical slot will force the ring to displace axially. The displacement can be measured with several different measurement techniques:

- **Variable reluctance.** By modifying the path of a magnetic circuit (i.e. modifying the air gap between the coil core and the armature), the inductance of a coil will change. By using two coils in a differential, or *push/pull* arrangement, a linear relation can be measured between the displacement and output voltage.
- **Eddy current.** When a magnetic field comes close to a conductor, the magnetic flux will induce eddy currents in the conductor. These currents will produce a magnetic field in the opposite direction. This will lower the inductance of the coil, which again can be measured in a differential set-up.
- **Hall sensing** (with or without bias magnet). When a magnetic field comes close to an electrical conductor with its current perpendicular to the magnetic field, a voltage difference can be measured over the conductor. A bias magnet can be used to enhance the magnetic field. Hall sensors are widely used in the field of speed and position measurement.
- **Capacitive sensing.** When two plates move in relation to each other, the change in capacitive coupling can be measured.

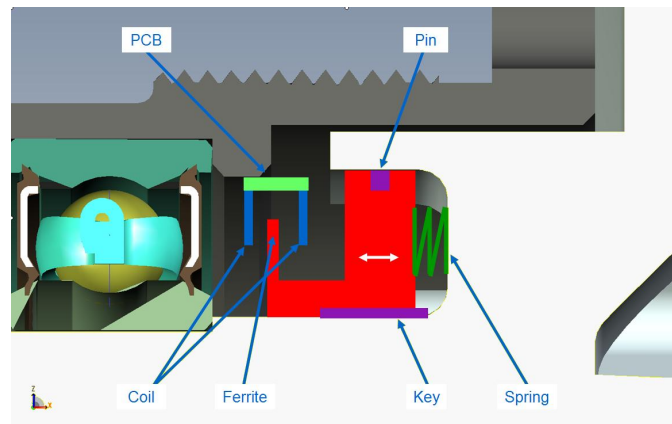


Figure 5.4: Schematic drawing of concept with measurement of variable reluctance. Ring will move in axial direction when torque is applied. The variation of the air gap between the ring will be measured to determine torsion angle.

The concept is illustrated in figure 5.4, with the variable reluctance measurement technique. The other techniques all work in the same way, with a translating sleeve which will have a ring on it and sensing elements (coils, Hall cells, capacitor plates) in the direct neighborhood. The advantages and disadvantages of the different measurement methods are summarized in table 5.2.

Method	Advantage	Disadvantage
Variable reluctance	Linear measurement Concentrated measurement field	Ferrite target material
Eddy current	PCB based coil Aluminium target Contamination no problem	Temperature Range Broad measurement field
Hall sensing	Temperature compensated Small component	Non-linear Magnetic target
Hall + Bias magnet	Temperature compensated Small component	Non-linear Ferromagnetic target
Capacitive	High sensitivity Concentrated measurement field	Temperature sensitive Sensitive to contamination Range

Table 5.2: Advantages and disadvantages of different measurement methods.

5.3.4 Conclusion Measurement Principle

To select a final concept, the three concepts are judged on several criteria. Some of these criteria are based on the analysis during the benchmarking phase in chapter 4. Other criteria came up during the brainstorm sessions. The criteria *accuracy*, *cost of components*, *simplicity of mechanical design* and *necessity for signal post processing* are all related to the measurement quality, price and compatibility of the final product; factors that were identified as *Critical to Satisfy*.

Next to that, during the concept phase it came apparent that some concepts were able to measure *torque at zero rotation speed* while others were not. This was also identified as an important property. Finally, the availability of *available knowledge* would help to speed up the design. In table 5.3, the three concepts are qualitatively rated to gain insight in the viability of the concept. The rating is done on a scale [++, +, o, -, --], where ++ means that there is a positive relation with the criterion (e.g. it would be favorable to choose that concept according to that criterion).

Based on the analysis, the concept Rotation to Displacement was chosen. As measurement principle, both eddy current and variable reluctance based measurement would be applicable. This measurement concept is further worked out in chapter 6.

Criterion	Magnetic Rings	Duty Cycle	Rotation to Displacement
Accuracy	-	+	+
Component Costs	-	-	+
Simplicity of Mechanical Design	+	-	-
Necessity of Post Processing	-	-	+
Zero Speed Measurement	+	--	++
Available Knowledge	++	--	o

Table 5.3: Multi criteria table to compare the three measurement principle concepts.

Design of Sensing Elements

Before a complete sensorized bottom bracket can be designed, first the sensor system has to be developed. First, the principles of eddy current and variable reluctance are further explained (section 6.1). In section 6.2 the geometry of the sensor system is introduced. Thereafter, a model is built and simulated using Ansoft Maxwell in section 6.3. The results are presented in section 6.4. Finally, conclusions were drawn in section 6.5.

6.1 Eddy Current & Variable Reluctance

From the several measurement techniques introduced in section 5.3.3, variable reluctance and eddy current were selected as the most suitable for integration in the torque sensing bottom bracket. Both techniques would require roughly the same design, with two coils with a target ring in between in order to create a differential set-up.

6.1.1 Eddy Current

Eddy currents are currents that are induced in a conductor by a changing magnetic field. This can occur either when a conductive material is moved in a magnetic field, or the conductive material is exposed to a magnetic field that is varying in time. The change in magnetic flux through the conductor will cause a circulating flow of electrons in the material. This current in turn will cause a magnetic field of its own, and opposes the existing magnetic field.

The magnetic field can be created with a coil. When a coil is supplied with an alternating current, the magnetic field will change in time. The induced voltage in a coil, U_{ind} , is dependent on the inductance of the coil,

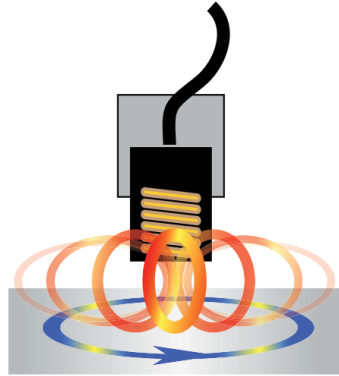


Figure 6.1: Eddy current proximity sensor. Eddy currents are induced in the target when an alternating current is applied to the coil. [20]

L and the change of current I . Or when a magnetic field induces a current in the coil, the induced voltage depends on the number of turns, N , and the change of magnetic flux, Φ_b .

$$U_{ind} = -L \frac{dI}{dt} = -N \frac{d\Phi_b}{dt} \quad (6.1)$$

When a conductor is in the neighborhood, the coil will cause the induction of eddy currents in the conductor. The opposing field caused by the eddy currents will then in turn influence the inductance of the coil. This principle is often used in proximity sensors, as illustrated in figure 6.1. The induced voltage in the coil will be measured and when a conductive target will come into range, this voltage will change.

6.1.2 Variable Reluctance

The working principle of a variable reluctance displacement sensor is to measure the variation of the inductance of a coil by varying the air gap in the magnetic circuit as shown in figure 6.2. The inductance of a coil is described by:

$$L = \frac{N^2}{\mathfrak{R}} \quad (6.2)$$

where N is the number of windings of the coil and \mathfrak{R} the *reluctance* of the magnetic circuit. The reluctance can be seen as a magnetic resistance. It limits the magnetic flux just like the resistance limits the electric current in an electrical circuit. The reluctance is defined as:

$$\mathfrak{R} = \frac{l}{\mu_0 \mu_A} \quad (6.3)$$

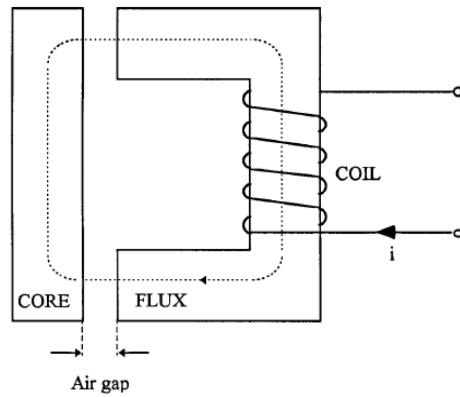


Figure 6.2: Simple representation of a magnetic circuit caused by a coil with an air gap. [21]

where l is the path length of the magnetic circuit, μ_0 the permeability of the free space ($\mu_0 = 4\pi \cdot 10^{-7} \text{ Hm}^{-1}$), μ the permeability of the material and A the surface perpendicular to the magnetic path. To simplify the analysis of displacement sensor it is possible calculate the reluctance of the core, armature and air gap separately.

$$\mathfrak{R}_{tot} = \mathfrak{R}_{core} + \mathfrak{R}_{armature} + \mathfrak{R}_{airgap} \quad (6.4)$$

To obtain a better, and more linear measurement, a differential displacement sensor can be used. Here, the movable armature is placed between two coils, as illustrated in figure 6.3a.

$$\begin{aligned} \mathfrak{R}_{tot} &= \mathfrak{R}_0 + \mathfrak{R}_{airgap} \\ &= \mathfrak{R}_0 + \frac{2(d-x)}{\mu_0 \mu A_{airgap}} \\ &= \mathfrak{R}_0 + k(d-x) \end{aligned} \quad (6.5)$$

Where \mathfrak{R}_0 is the reluctance at zero air gap. The inductance of the coils will be influenced by the size of the air gap.

$$L_1 = \frac{N^2}{\mathfrak{R}_0 + k(d-x)} = \frac{L_0}{1 + \alpha(d-x)} \quad (6.6)$$

$$L_2 = \frac{N^2}{\mathfrak{R}_0 + k(d+x)} = \frac{L_0}{1 + \alpha(d+x)} \quad (6.7)$$

$$\text{With } L_0 = \frac{N^2}{\mathfrak{R}_0}, \text{ and } \alpha = \frac{k}{\mathfrak{R}_0}.$$

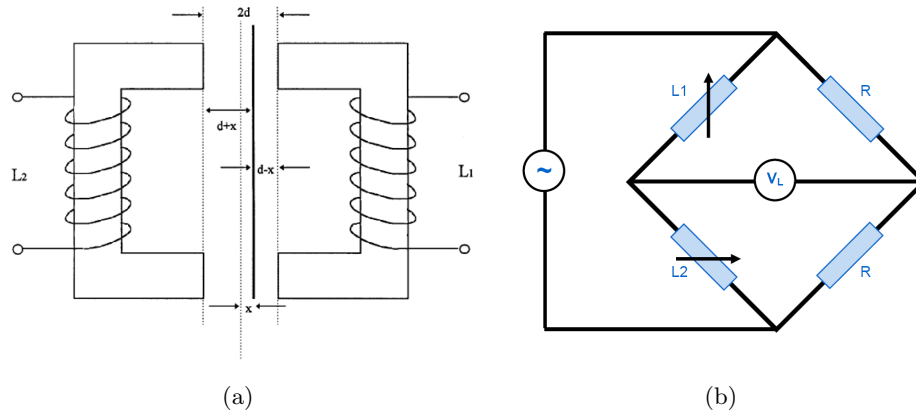


Figure 6.3: (a) Schematic setup of a differential variable reluctance displacement sensor. [21] (b) Wheatstone bridge

So the self-inductance of both coils is a function of the self-inductance at zero air gap, L_0 , and the length of the air gap, $(d - x)$.

The self-inductance that is measured has a non-linear relation to the displacement. This is of course, not desirable for a sensor. To overcome this problem, the two measurement coils are placed in a Wheatstone bridge. The output voltage of the bridge will be

$$\begin{aligned}
 V_L &= V_S \left(\frac{L_1}{L_1 + L_2} - \frac{R_1}{R_1 + R_2} \right) \\
 &= V_S \left(\frac{1}{1 + \frac{L_1}{L_2}} - \frac{1}{2} \right) \\
 &= V_S \frac{\alpha x}{2(1 + \alpha d)}
 \end{aligned} \tag{6.8}$$

So, the output of the bridge will be linear with the displacement of the armature.

6.2 Concept of Sensor

To make sure that manufacturing or machining errors on the target ring would not influence the measurement (errors in thickness would introduce harmonics due to the rotation of the ring) it was decided that the coils should be placed around the full circumference of the target ring. This would also improve the inductance of the coils, which in turn would improve the accuracy of the measurement. This decision has a big influence on the available space inside the bottom bracket. The coils that have to be used

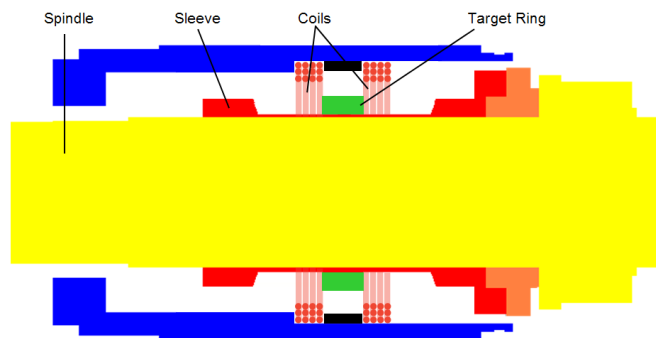


Figure 6.4: Cross-section of sensing concept. A sleeve will move axially according to the applied torque. A target ring is placed on the sleeve. The target ring is centered between coils, which are wound oppositely. The movement of the ring will be measured by measuring the change of the induced voltages of the coils.

when the variable reluctance is chosen need a (ferrite) core surrounding the coils and should face the target ring directly, as in figure 6.3a. The eddy current principle is less demanding on geometry. The only requirement is that the target ring is well within the magnetic field created by the coil.

The following concept geometry was developed: Two coils, wound oppositely, are placed around the spindle. On the spindle, a sleeve is fitted which translates in axial direction according the amount of applied torque. On this sleeve a target ring is fitted. A cross section of the proposed geometry is shown in figure 6.4.

The movement of the target ring will influence the induced voltage of the coils. When there is no load on the bottom bracket, the ring will be in the center of the two coils, and the voltage will be the same for the two coils. When torque is applied, the ring will translate axially and the induced voltages will change. One will go up, while the other will go down. This change can be measured with a Wheatstone bridge.

6.3 Modelling of Sensor Using Ansoft Maxwell

To be able to investigate variations in parameters, a simulation was made using Ansoft Maxwell. This program allows the user to make electromagnetic field simulations using finite element analysis. In this section, the construction of the analysis is described. Results of the analysis are given in the next section. This simulation will be used to investigate the influence of several parameters. It will be hard to validate the results of the simulation before a prototype can be tested. But the trend that will be found by varying a parameter will be presumed to be reliable.

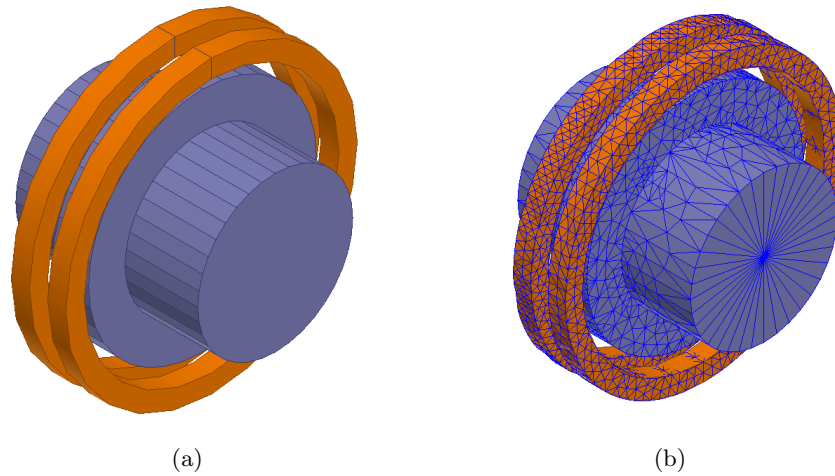


Figure 6.5: Modelling of sensor in Ansoft Maxwell, (a) Simplified geometry of the torque sensing bottom bracket consisting of two coils (wound oppositely) and a body that represents both spindle, sleeve and target ring, (b) Meshed model of the simplified model of the torque sensing bottom bracket.

6.3.1 Modelling & Meshing

In the previous section, a concept geometry was proposed for the sensor. This geometry was built in Maxwell, using estimated sizes for all the components. The goal was to build representative simulation of the torque sensing bottom bracket. This model will be used to evaluate the effect of changes made to the geometry or design parameters on the sensitivity of the sensor. The model used for the simulations is shown in figure 6.5a. The geometry was simplified to reduce calculation time. The spindle, sleeve and target ring were merged into one part. All the parts that would not interfere with the measurement (due to distance or magnetic properties) were left out of the model.

The model was meshed using the standard mesh generator available in Maxwell, and was refined in places which were expected to be important to the analysis. This included the coils and the target ring. In total, the model consisted of 35,374 tetrahedra. The complete geometry was evaluated within a region of air, 200% the size of the model. Later on, the influence of other objects in the vicinity of the sensor is also analyzed. The meshed geometry is shown in figure 6.5b.

6.3.2 External Circuit

The Maxwell software is also able to simulate the electronics used for the sensor in an external circuit. In this model, both the input signal and the output signal were modeled in the external circuit editor. This enabled a

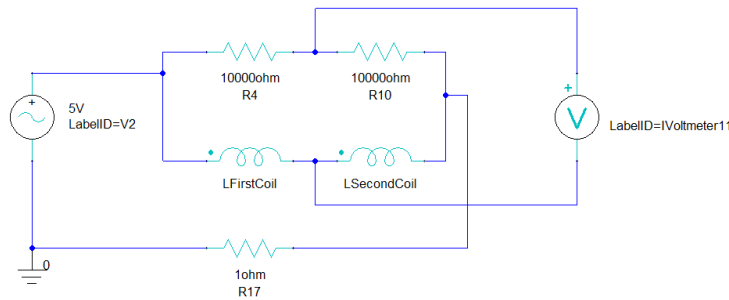


Figure 6.6: External circuit imported in Maxwell simulation used to measure the change of inductance of the coils.

direct read-out of the signal over the Wheatstone bridge. The circuit used is shown in figure 6.6. The circuit consists of a voltage source, with an input of 5 V AC at 20 kHz. The two coils from the model, called *FirstCoil* and *SecondCoil* respectively, are placed in a bridge circuit. The two resistors of the bridge circuit were chosen arbitrary and have a resistance of 10 k Ω . An additional resistor of 1 Ω was included in the circuit to avoid a short circuit through the branch of the bridge with the coils, because Maxwell treats the coils as ideal inductances and have therefore no resistance. A voltmeter was placed over the bridge to measure the change in inductance. The output of the voltmeter can be accessed directly from the Maxwell interface.

6.3.3 Analysis Parameters

Because the input signal is an AC voltage, a transient analysis type is chosen. This type of analysis will also be able to simulate movement of the spindle in a later stage. The output of interest will be the output of the Wheatstone bridge. This will be a sinusoidal signal with the same frequency as the input voltage. For each parameter, two simulations will be done: the first with the target ring centered between the coils, the second with the target ring axially displaced by 1 mm. The output signal will be demodulated and the magnitude will be used to calculate the sensitivity.

To obtain a good read-out of the Wheatstone bridge, two full periods of the input are simulated, to eliminate errors caused by initial overshoot of the signal caused by the initial current (0 Ampere) in the coils. For a supply voltage with a 20 kHz frequency, this leads to a simulation time of $1 \cdot 10^{-4}$ seconds. For each period, ten simulation steps are taken to make sure the output sine wave has sufficient detail. Therefore, the time step is $5 \cdot 10^{-6}$ seconds. Each simulation took about 6 minutes on a single 3.2 GHz processor.

6.4 Results of Electromagnetic Field Simulations

In total, more than forty variations in parameters were done. The most significant results are shown in this section.

6.4.1 Materials

First subject of investigation was the material of the target ring. Four possible materials were used: steel (1008), ferrite, aluminium and copper. Figure 6.7 shows the magnetic flux density on the YZ-plane of the model. The calculated sensitivity is shown in table 6.1. It shows a significant difference between the two magnetic materials (steel and ferrite) and the two non-magnetic materials (aluminium and copper). But figure 6.7b and 6.7d show little to no flux density in the two materials (as can be expected with these materials). Therefore, it was assumed that not variable reluctance, but eddy current would be the dominating physical property in these two materials. Figure 6.8 shows the induced current in the target ring. It is clear that in the aluminium substantially more current is induced than in the steel ring. These eddy currents are in the opposite direction of the current direction in the coils. They influence the inductance of the coils, which can be measured in the Wheatstone bridge circuit. To verify this hypothesis, the simulation with the aluminium target ring was done again, but now the option which takes into account the eddy current was disabled. The sensitivity dropped with nearly 95%.

Material	Sensitivity [mV/mm]	Improvement [%]
Steel 1008	90	-
Aluminium	150	67
Ferrite	100	11
Copper	160	78

Table 6.1: Sensitivity of sensor using different materials as target ring.

6.4.2 Target Ring Thickness

The second parameter that was investigated was the thickness (in axial direction) of the target ring. The effect on the sensitivity was investigated in both steel and aluminium target rings. The results are summarized in figure 6.9. It shows that the thickness of the target ring has different effects on the two materials. It is presumed that this is caused by the fact that the prevailing physical phenomenon is different in the two materials, as explained in the previous section.

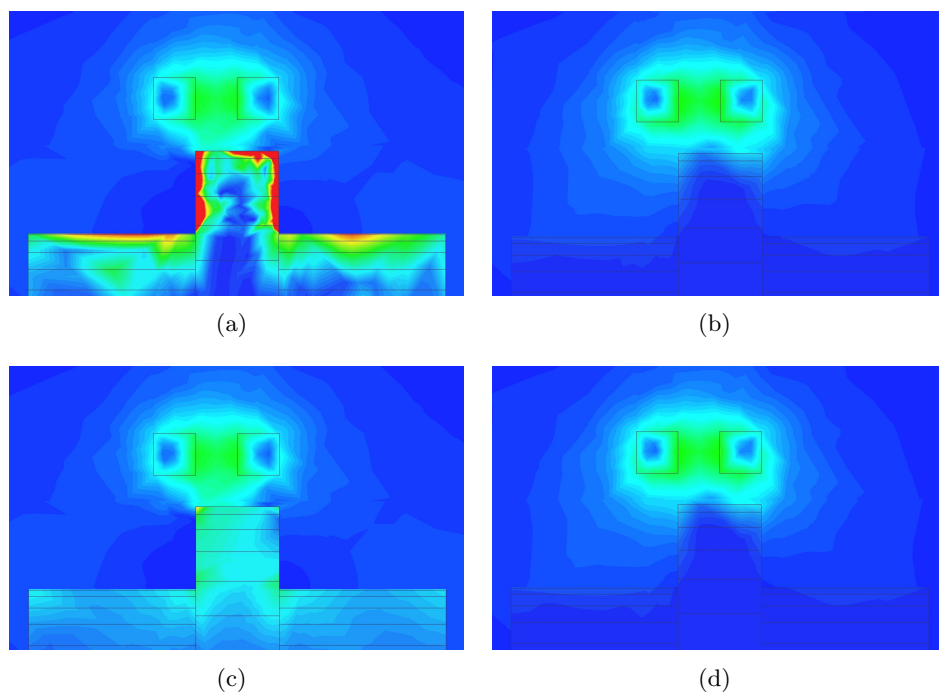


Figure 6.7: Magnetic Flux density using different materials, (a) steel 1008, (b) aluminium, (c) ferrite and (d) copper. All surface plots are scaled on a color scale from 0 to $2.5 \cdot 10^{-3}$ Tesla (blue to red).

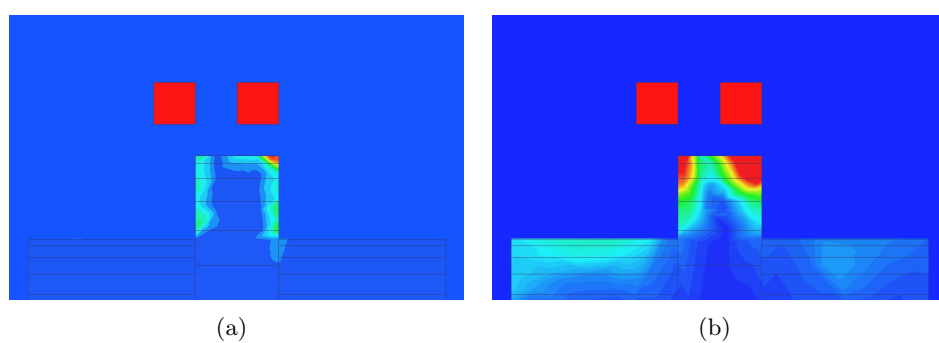


Figure 6.8: Induced eddy current in the target ring from the same simulations as above (a) in a steel target ring (scale $2.5 \cdot 10^4$ A/m²), and (b) an aluminium target ring (scale $2.5 \cdot 10^5$ A/m²). In the (non magnetic) aluminium ring, the induced eddy currents are more than 10 times stronger.

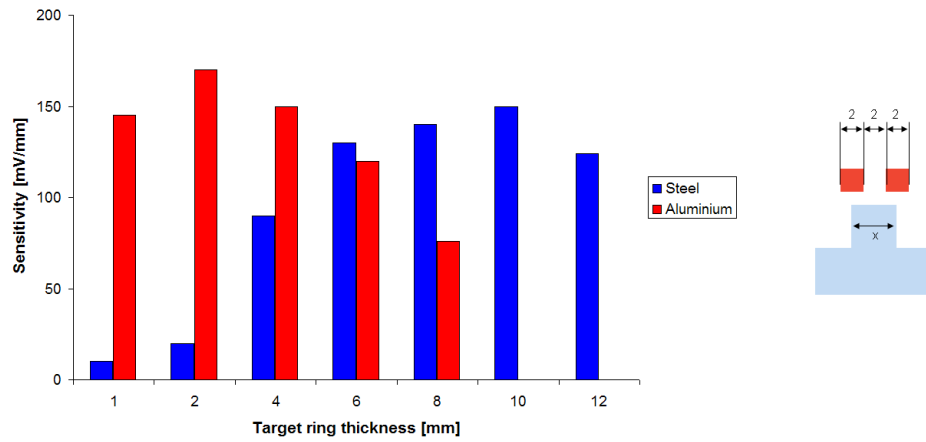


Figure 6.9: Effect of thickness (axial) of target ring on the sensitivity for both metal and aluminium rings.

6.4.3 Coil Spacing

The next parameter that was tested was the space between the coils. In the initial design, the coils were arbitrarily spaced 2 mm apart. This distance was varied, again for both the steel and aluminium target ring. The results of these simulations are shown in figure 6.10. It shows that for both target rings, the sensitivity increases when the coils are closer together.

6.4.4 Ferrite Core

Another method to improve the sensitivity might be to use a ferrite core to guide the magnetic field. Two L-shaped and one I-shaped ferrite rings are placed in between and around the coils. The resulting magnetic field is shown in figure 6.11. When used with a steel target ring, the sensitivity increased 26%. With an aluminium target ring it improved around 3%, as shown in table 6.2.

Target Ring	Sensitivity [mV/mm]	Improvement [%]
Steel 1008	113	26
Aluminium	155	3

Table 6.2: Sensitivity of sensor with ferrite core and improvement over sensor without the core (table 6.1).

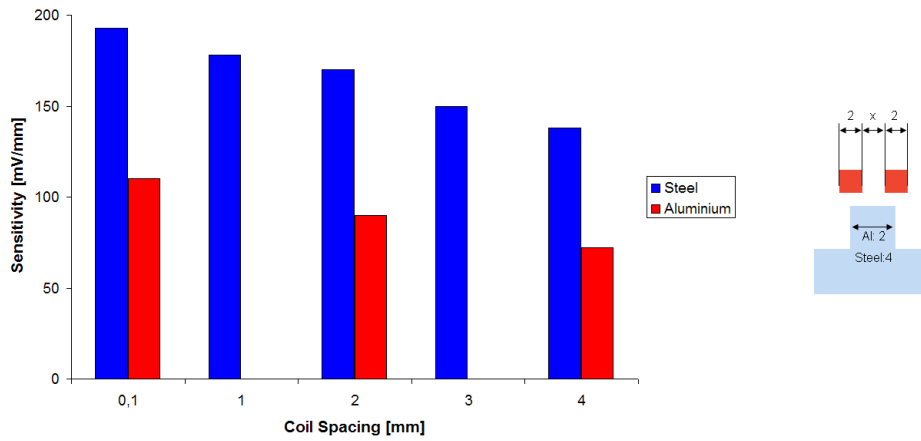


Figure 6.10: Effect of coil spacing on the sensitivity for both metal and aluminium rings.

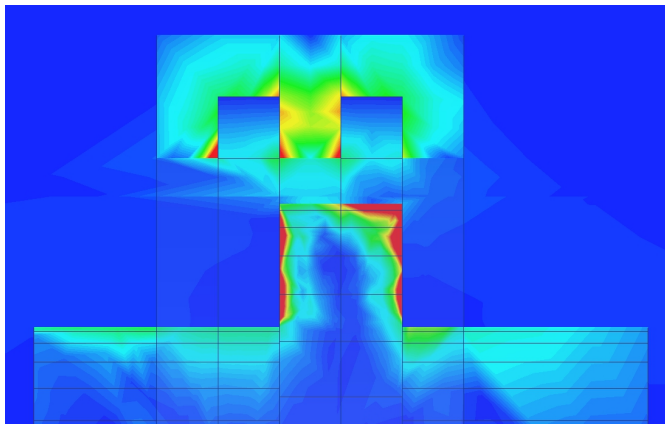


Figure 6.11: Magnetic flux density of sensor with ferrite core. This result shows that the magnetic flux is guided by the ferrite core towards the target ring, thereby improving the sensitivity.

6.4.5 Frame Tube

The last parameter that was tested was the influence of the surroundings, especially the frame tube the bottom bracket will be placed in. Therefore, an optimized geometry (2 mm aluminium target ring, 0.1 mm coil spacing) was used as a reference. Three simulations were done. One with a steel frame tube, one with an aluminium frame tube and a last one with an aluminium frame tube and ferrite shielding in between the coils and the tube. In figure 6.12 the results of these four simulations are plotted. The illustrations show the current density on the YZ-plane cross-section. The resulting sensitivities are summarized in table 6.3. It is clear that the use of an aluminium frame tube will deteriorate the sensitivity and shielding should be used.

Frame Tube	Sensitivity [mV/mm]	Improvement [%]
None	193	-
Steel 1008	218	+13
Aluminium	103	-47
Al. with shield	180	-7

Table 6.3: Sensitivity of sensor with different kind of frame tubes.

6.4.6 Air Gap

An additional parameter that was tested was the influence of the air gap between the target ring and the coils. These simulations were in some way trivial, because the impact of reducing the air gap could be predicted with a great amount of certainty. The simulation was done for both steel and aluminium target ring as the air gap was reduced from 1.5 mm to 0.5 mm. As expected, the sensitivity increased significantly. The results are summarized in table 6.4.

Target Ring	Air Gap [mm]	Sensitivity [mV/mm]	Improvement [%]
Steel 1008	1.5	90	-
Steel 1008	0.5	145	61
Aluminium	1.5	150	-
Aluminium	0.5	295	97

Table 6.4: Sensitivity of sensor with reduced air gap.

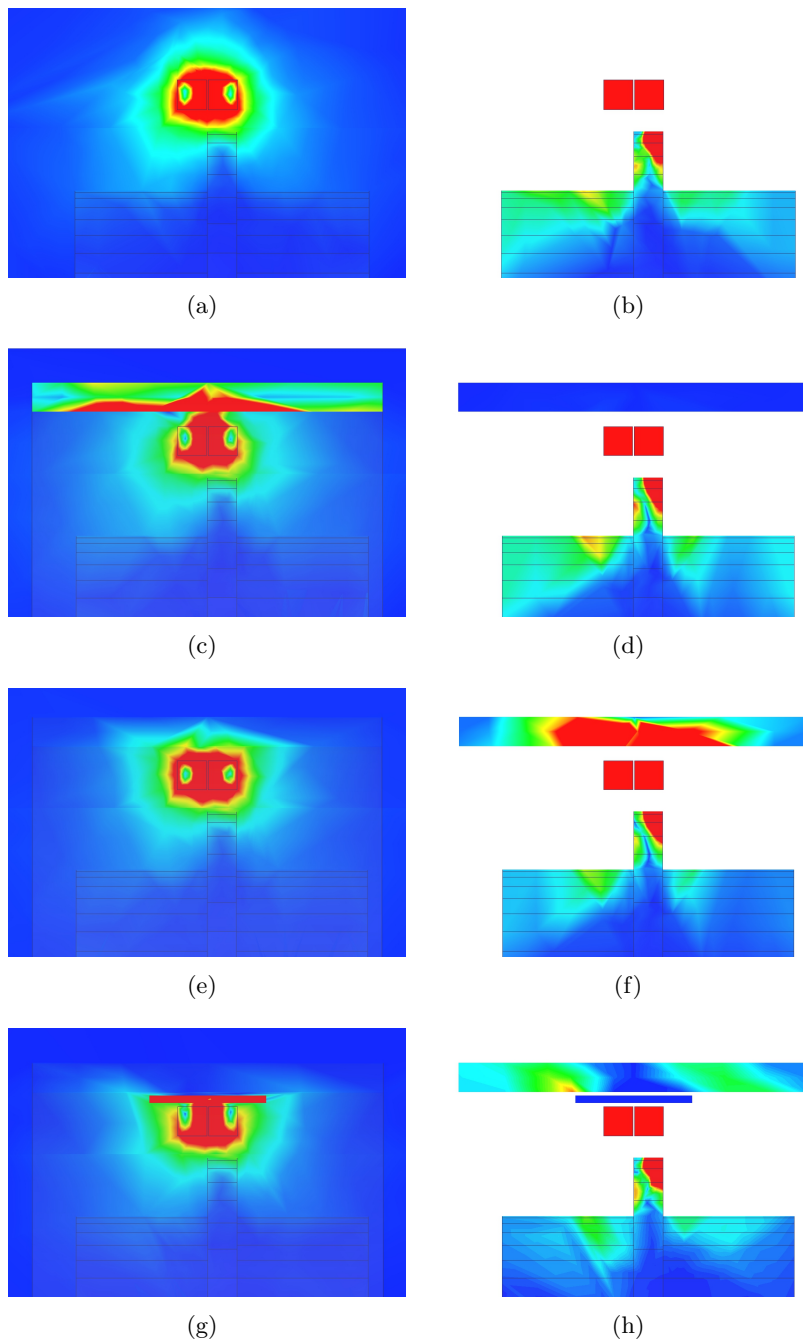


Figure 6.12: Influence of different frame tubes on the sensor. Magnetic flux (left) and current density (right) on YZ plane of different frame tubes. (a),(b) optimized geometry of the model without a frame tube present, (c),(d) a steel frame tube, (e),(f) an aluminium frame tube and (g),(h) an aluminium frame tube with a thin ferrite ring for shielding. All flux plots are scaled to $1 \cdot 10^{-3}$ Tesla, all current plots are scaled to $1 \cdot 10^5$ A/m².

6.4.7 Preliminary Conclusions

From the results of these simulations, conclusions can be drawn which can be used as guidelines and goals in the mechanical design. The following list of conclusions is compiled in descending order of importance.

- **Air gap.** The air gap is by far the most important parameter in the sensor setup. Reducing the air gap will have the greatest impact on the sensitivity. However, the mechanical design will constrain this reduction.
- **Target ring material.** The material that is chosen for the target ring defines the dominating physical principle. When a magnetic material is used, variable reluctance is dominating. Eddy current is dominating when a highly conductive material is used. The simulation showed that eddy currents lead to the highest sensitivity. Therefore aluminium or copper should be used. The difference in sensitivity is only around 7%.
- **Target ring thickness.** As shown in figure 6.9, there is an optimum in the axial thickness of the target ring. When an aluminium ring is used, the thickness should be 2 mm.
- **Coil spacing.** The sensitivity of the sensor increases when the coils get closer together. Therefore, the coils should be placed as close as possible to each other.
- **Ferrite core.** Section 6.4.4 showed that the use of a ferrite core around the coils could increase the sensitivity. However, the effect is small, when used in combination with an aluminium target ring. Also, because space within the bottom bracket is limited, the incorporation of a core will be problematic.
- **Frame tube.** Although not of influence on the mechanical design, attention should be paid to the possible influences of the immediate surroundings of the bottom bracket. It should be noted that an aluminium frame tube will deteriorate the sensitivity of the sensor and therefore some shielding should be included.

6.4.8 Simulation of Moving Spindle

With the conclusions from the simulations as described in the previous section, a more detailed mechanical design was made. In this design, all the important constraints (i.e. spindle diameter, maximum bottom bracket diameter, etc.) were taken into account. Also factors as producibility and possible ways to assemble the product were considered. This led to the

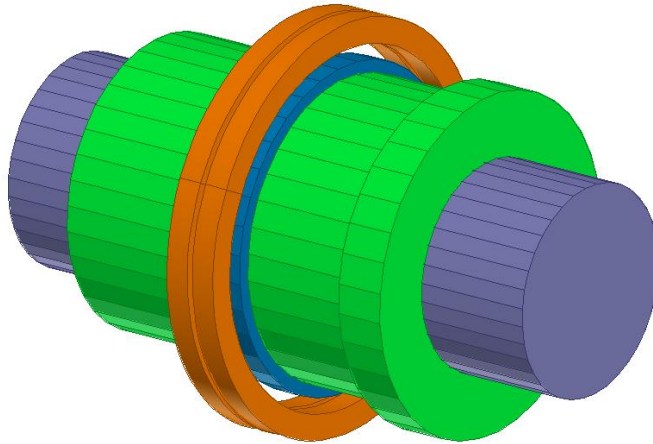


Figure 6.13: New model of torque sensing bottom bracket designed according to the design constraints of the bottom bracket and the guidelines laid out in the preliminary conclusions.

design shown in figure 6.13. With this model a transient simulation was done, in which the sleeve with the target ring was moving. The model was meshed the same way as the earlier model and contained 37,819 tetrahedra.

To control the simulation time, the spindle moved with a speed of 200 m/s through the sensor, from -1 mm to +1 mm. This led to a simulation time of 0.01 seconds. This equates to 200 periods of the supply voltage. The time step was chosen to be $5 \cdot 10^{-6}$ seconds again. These parameters resulted in 2,000 data points. The simulation lasted around 39 hours, again on a single 3.2 GHz processor.

The resulting output of the voltmeter over the bridge circuit is shown in figure 6.14. After demodulation, it would give a linear relation between the displacement and the output of the bridge. A small offset of the minimum output was observed. Theoretically the minimum should be at zero displacement, but in this simulation it was at 0.05 mm. This small offset is presumed to be caused by the fact that the sleeve is not completely symmetrical, and therefore will influence the magnetic field. It functions like a core.

Figure 6.15 shows a close up of the target ring and the coils. The arrows represent the magnitude and direction of the induced current in the coils and the target ring in the YZ-plane. It shows that the induced eddy currents in the target ring are in opposite direction to the coil currents.

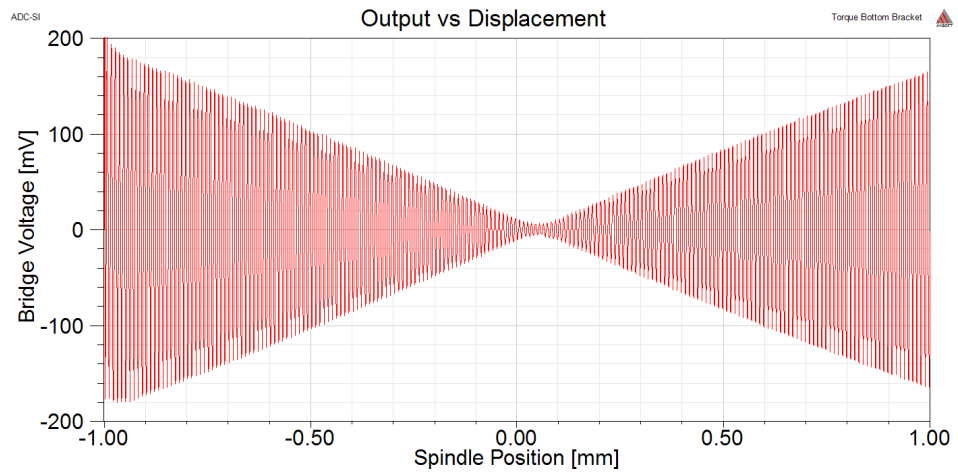


Figure 6.14: Output voltage of the Wheatstone bridge versus the displacement of the sleeve.

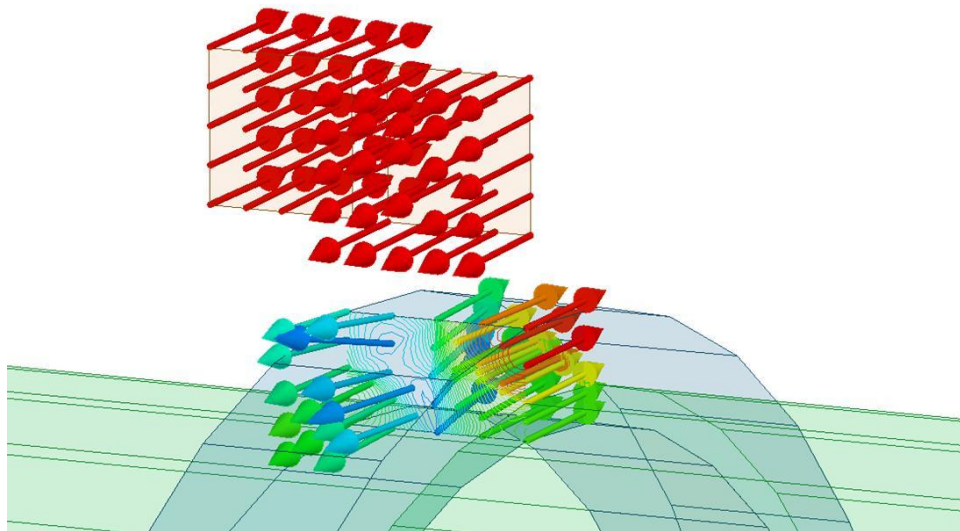


Figure 6.15: Close-up of target ring and coils with current magnitude and direction. It shows the induced eddy currents are opposing the direction of the current in the coils. Coils are represented as cross-sectional planes only for clarity.

6.5 Conclusions of Simulations

The simulations of the sensor concept in Ansoft Maxwell showed that the concept is feasible, and will produce a linear output. Clear design requirements are presented which can be used as design guidance. The next step will be to build a functional prototype to proof the concept and validate the simulations done in Maxwell.

Detailed Design of Torque Sensing Bottom Bracket

After defining the critical parameters for the sensor setup in the previous chapter, both the mechanical and the electrical design could be completed. This work was done by the mechanical engineer and the electrical engineer respectively, both member of the project team. Their work is included in this report for the sake of completeness and clarity.

7.1 Mechanical Design

To be able to comply with the CTS that were defined in chapter 4, several guidelines should be followed during the detailed design of the bottom bracket.

- **Maxwell simulations.** The results of the simulations that were done in Maxwell were used as guidelines for the final design of the torque sensing bottom bracket. These guidelines were already presented in section 6.4.7.
- **ISO standards for the bottom bracket.** For the design of bottom brackets, there are two ISO standards. The first, ISO 6695:1991, describes the size and shape of the square ends of the bottom bracket spindle, in order to be compatible with pedal cranks which are designed following the same standard. The second standard, ISO 6696:1989, describes the size (diameter and width) and the screw thread of the frame tube in which the bottom bracket will be fitted.
- **Standard bearings.** The last constraint of the design is the size of bearings. The goal is to use standard deep groove ball bearings (DGBBs).

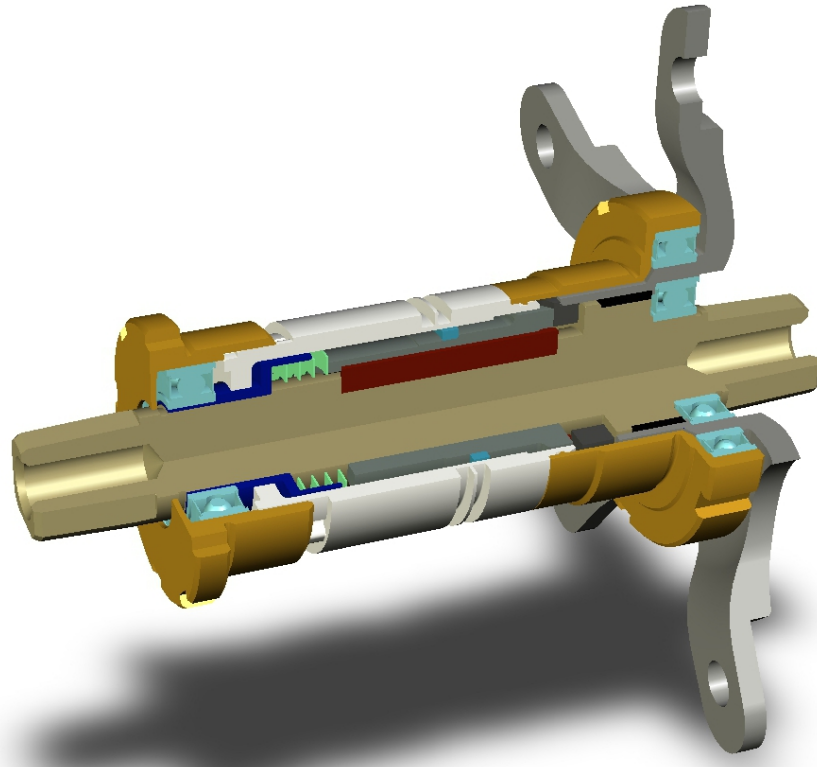


Figure 7.1: CAD design of the SKF Torque Sensing Bottom Bracket.

Following these constraints, the mechanical designer designed a torque sensing bottom bracket with the sensor concept as described in the previous chapters as shown in figure 7.1. All the important design details will be explained in the following sections.

7.1.1 Interface Spindle and Chain Wheel Bracket

As described in previous chapters, the chain wheel bracket will be integrated in the bottom bracket assembly. The bracket will be connected to the spindle through an intermediate piece, as shown in figure 7.2. The intermediate piece will transfer the torque from the spindle to the chain wheel bracket. Because the intermediate piece will be made of flexible material (either a rubber or a plastic), a torsion angle between the spindle and the chain wheel bracket will occur. The shape of the piece can be modified, for example by adding holes (figure 7.3a), to obtain a better relationship between the applied torque and the deformation of the piece. The deformation of the piece was only analyzed

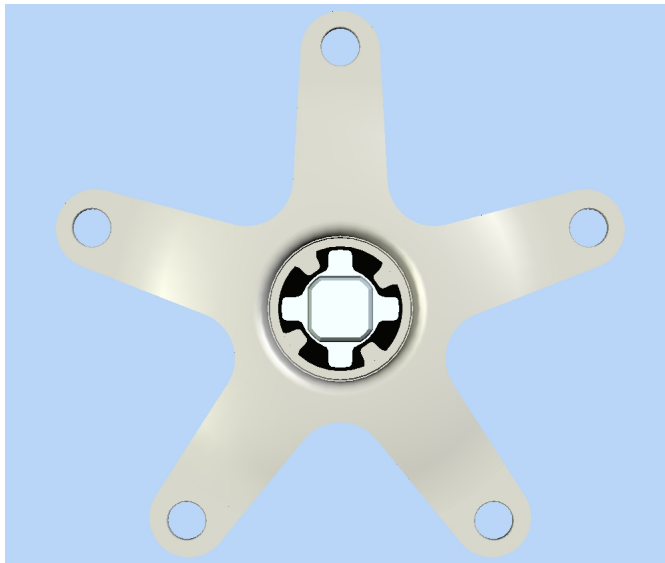


Figure 7.2: Connection of chain wheel bracket to the spindle through a flexible intermediate piece, which will cause a torsion angle between the bracket and the spindle when torque is applied.

with a preliminary finite element analysis, as shown in figure 7.3b. Because the material behavior of plastics is very hard to model, the analysis of such a piece can be a complete separate project. Therefore, for the first (proof-of-concept) prototype, an injection mold will be fabricated to make several pieces. When the proof-of-concept phase will turn out to be successful, a more in-depth analysis will be necessary. This does however mean that the relation between the applied torque and the translation of the sleeve will remain a question until the proof-of-concept prototype will be tested.

7.1.2 Bearings

The torque sensing bottom bracket uses three deep groove ball bearings, as shown in figure 7.1 in light blue. A normal bottom bracket uses only two DGBBs (or sometimes needle bearings). Because the chain wheel bracket is integrated into the bottom bracket, a third DGBB is needed to transfer the vertical forces from the right pedal to the frame. When the design is further improved, the inner of the two right DGBBs could be replaced by a thinner needle bearing or a bushing. The outer of the two right DGBBs is fitted outside the frame tube (so called external bearing), to be able to accommodate a spindle of sufficient diameter.

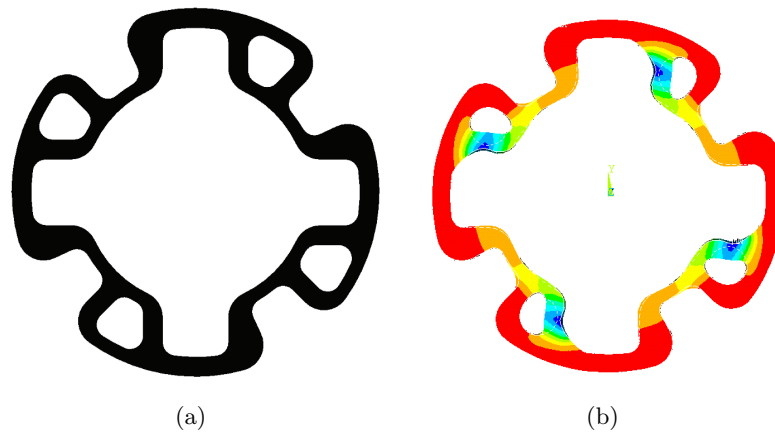


Figure 7.3: Intermediate piece connecting spindle and chain wheel bracket (a) with holes to influence the behavior of deformation, (b) preliminary finite element analysis using ANSYS, showing displacement under load.

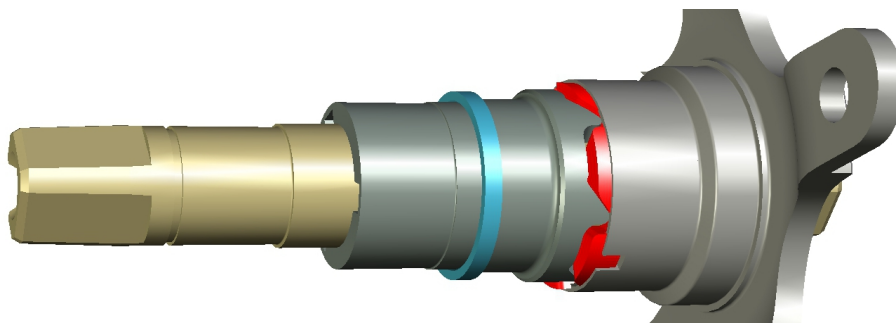
7.1.3 Transformation from Rotation to Translation

After the applied torque has created a torsion angle, this torsion angle has to be transformed into a displacement. A transformation ring is fitted around the spindle and attached to the chain wheel bracket. This transformation ring is shown in figure 7.4 in red. The transformation ring is connected to the chain wheel through several slots (figure 7.4a). The transformation ring and the sleeve (dark grey) have interlocking teeth with helical interlocking surfaces. Because the sleeve is fitted around the spindle with three key-way connections (figure 7.4b), the sleeve is blocked in the rotational direction. When the transformation ring rotates, the sleeve will translate away from the ring. A spring (light green, figure 7.1) will ensure that the sleeve will return to its initial position when the applied torque is reduced. The stiffness of this spring should be taken into account when calculating the applied torque together with the material properties of the intermediate part.

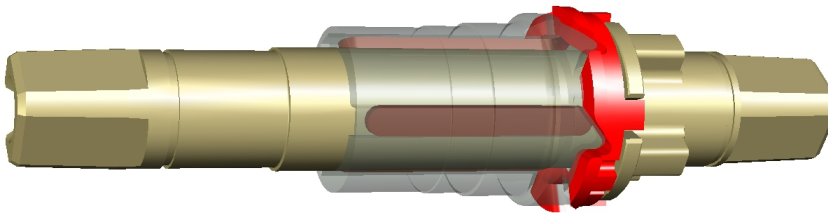
To protect the intermediate piece from a deformation beyond its elastic limits, the transformation ring is also limited in rotation to an angle of 5 degrees, by using a notch, interlocking in a recess on the flange of the spindle.

7.1.4 Target Ring and Coils

The target ring will be fitted on the sleeve (light blue, figure 7.4a). For the first prototype, the exact location of the ring will not be determined mechanically, but the ring will be glued into place after measurement of the complete assembly to account for fabrication and mounting tolerances. The



(a)



(b)

Figure 7.4: Mechanism for transforming the rotation to translation with (a) transformation ring (red) fitted between sleeve (dark gray, left) and chain wheel bracket (right), connected to chain wheel bracket through several slots and interlocking teeth between transformation ring and sleeve with helical sliding surfaces. (b) The rotation of the transformation ring is limited to 5 degrees with notches interlocking in a recess of the flange of the spindle. The sleeve is blocked in the rotational direction with three key-key way connections.

coils will be wound into the two trenches in the outer body (see figure 7.1). The coils will be wound manually for the first prototype.

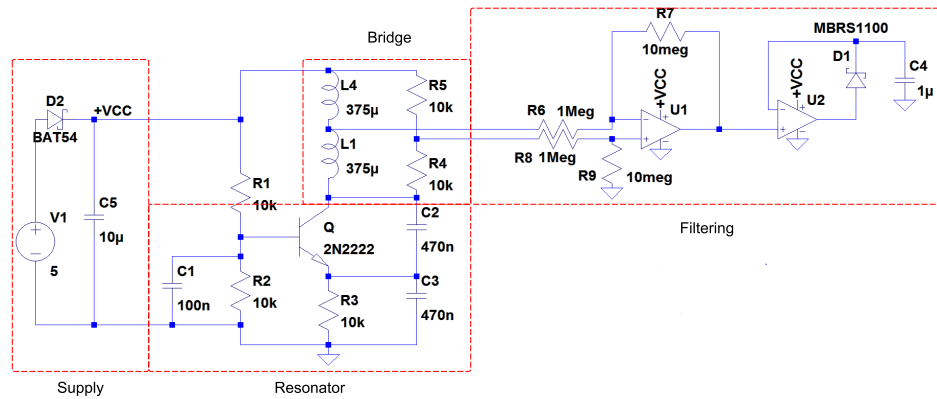


Figure 7.5: Electronic circuit for the prototype, containing the power supply, resonator circuit, Wheatstone bridge and filtering.

7.2 Electrical Design

The electronics for the prototype will be located outside of the prototype on a normal circuit board. When the proof-of-concept prototype turns out to be successful, the electronics can be integrated into the product in a new design iteration. The electronics can be miniaturized into a PCB. The PCB will be located inside the housing or over molded in the housing.

The electronic circuit that will be used is shown in figure 7.5. The circuit consists of four major parts.

- **The power supply:** supplying the circuit with 5 volt DC.
- **A resonator circuit:** to transform the direct current into an alternating current with a frequency of 12 kHz.
- **The Wheatstone bridge:** here, the coils will be connected to the circuit board.
- **Filtering:** the sinusoidal output from the Wheatstone bridge will be demodulated in order to get a single voltage as output.

Part III

Simulation & Testing

BoB SimControl for Torque Sensing Bottom Bracket

This chapter will describe the BoB SimControl program. It is a MATLAB interface to control the Maxwell simulation. All relevant parameters can be changed in a simple graphical user interface (GUI). Batch simulations can be made, and results are automatically generated and plotted.

8.1 Refining the Mesh

Because the measurement principle of the sensor is based on inducing alternating eddy currents into a metallic target ring, special care should be taken when applying a mesh to the finite element analysis model. The current density will be greatest at the surface of the conductor and will decrease deeper into the material. This is called the *skin effect*. The *skin depth*, a measure used to describe the distribution of the current density, will decrease with increasing frequency. The equation for the skin depth is

$$\delta = \sqrt{\frac{2\rho}{\omega\mu}} \quad (8.1)$$

With ρ being the resistivity of the conductor, ω the angular frequency and μ the absolute magnetic permeability of the conductor. For the aluminium target ring, at a sensor frequency of 12 kHz, the skin depth will be 0.7 mm. That means that the meshing used in the simulation should be at least as detailed to be able to simulate this effect correctly.

The simulations that were presented in chapter 6 were done on a three dimensional model. A single simulation took around six minutes to calculate the results. But to account for the skin effect, the meshing should be refined. This would have a dramatic effect on the simulation time. Therefore, the

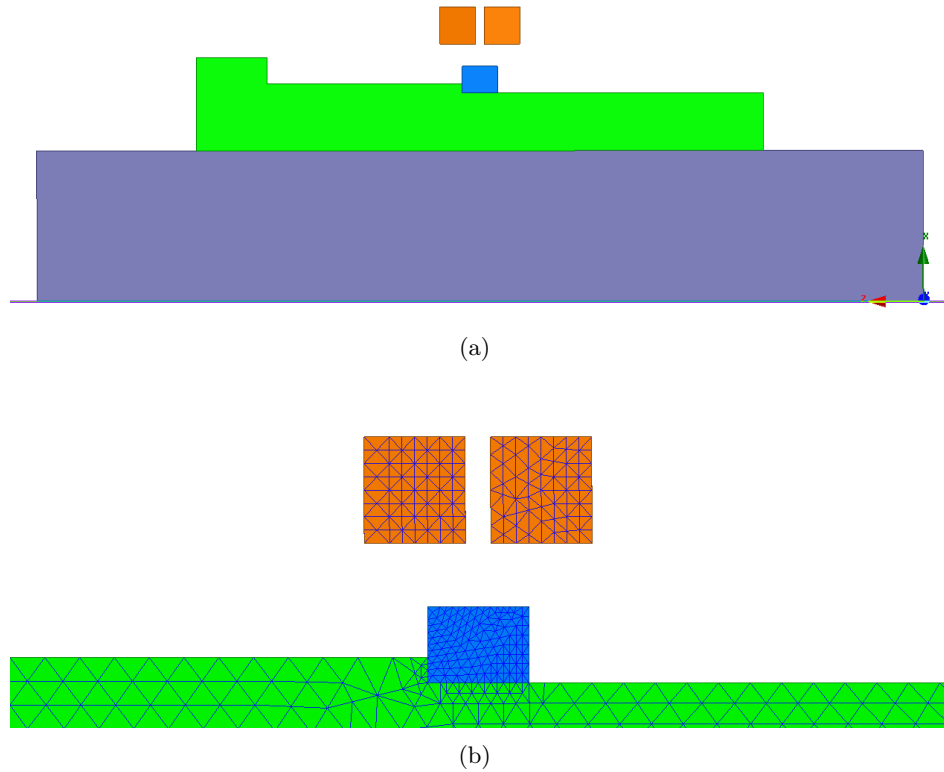


Figure 8.1: (a) 2-D Maxwell model of torque sensing bottom bracket, (b) close up view of the refined meshing of the target ring and the coils.

Maxwell model was changed from a 3-D model to an axisymmetrical 2-D model. To make sure the simulation was not excessively meshed in areas that are less important, several mesh parameters were used. For the target ring, a maximum element length of 0.25 mm was used. The coils were meshed with a maximum element length of 0.5 mm and the sleeve with a maximum element length of 0.9 mm. The spindle was meshed with the default parameters. In this 2-D model, the simulation time was cut to a mere twenty seconds. The results from the 3-D and the 2-D model, using the same parameters (except for meshing) differed by 4.0 % (table 8.1), and therefore it was concluded that the 2-D model could replace the 3-D model. Figure 8.1 shows the 2-D model and the new meshing.

8.2 Visual Basic script

Up until this point, all modifications to the model, like changing of design parameters as done in chapter 6, were done manually. This requires an extensive knowledge of the Maxwell software and the way the model is con-

Model	Sensitivity [mV/mm]	Difference [%]
3-D	177	-
2-D	184	4.0

Table 8.1: Sensitivity of torque sensor calculated using 3-D and 2-D Maxwell model.

structured. Sometimes the change of one parameter would mean that parameters of several parts should be changed. It is possible to parameterize the model in Maxwell, but this still needs knowledge of the complete program and model. A dedicated program was created in MATLAB to function as an interface for this simulation.

Maxwell permits the use of dedicated Visual Basic (VB) scripts to control the build of the model, the execution of the analysis and the post-processing of the results. Almost all actions possible in the graphical user interface (GUI) of Maxwell can be scripted to be executed automatically [22]. Because writing a complete VB code can be a long and difficult process, it is also possible to record a script. This way, all actions that are done in the GUI are recorded in a VB script.

This option was used to create the VB script to create the model of the torque sensing bottom bracket. The script should be modified to be able to read the script in MATLAB, change the parameters and create a new VB script. Figure 8.2 shows how this is done. A (default) model of the sensor is built in Maxwell and all the actions are recorded in a VB script. This script is then modified by hand once, so that MATLAB can work with it. This new, parametrized script will be used as an input for the MATLAB program. The other input will be the list of parameters of the analysis the user wants to run next. The user will input these parameters into the GUI of the MATLAB program. When the user executes the program, the parameters will be inserted into the modified script to write a new VB script. This new VB script will then be executed in Maxwell.

To read the code in MATLAB, the values of the parameters in the script should be replaced by variables corresponding with the variables in the MATLAB program. Figure 8.3a shows an example of VB code to create a rectangle in Maxwell. Figure 8.3b shows the modifications necessary to the script to be able to use it as an input for the MATLAB program.

8.3 Structure of Program

The program will use, as explained in figure 8.2, two inputs: the modified script and all relevant parameters. Using the GUI (shown in figure 8.5), the user will be able to change all the parameters concerning the dimensions of

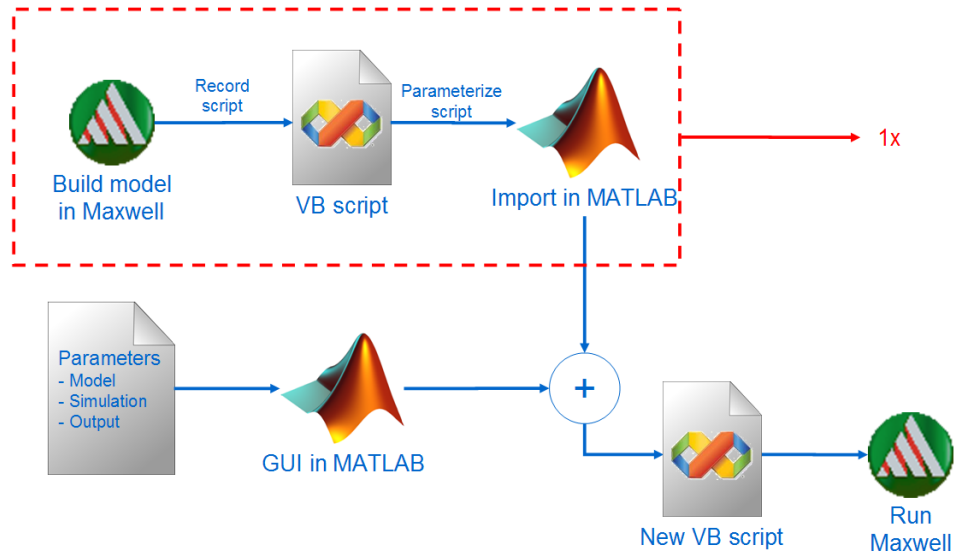


Figure 8.2: Flow chart of the main structure of the program. A VB script is recorded in Maxwell and modified to be used as input for the program. Together with the new parameters a new VB script will be written and executed in Maxwell.

```
oEditor.CreateRectangle Array("NAME:RectangleParameters", "IsCovered:=", true, "XStart:=", _
"8.5mm", "YStart:=", "0mm", "ZStart:=", "9mm", "Width:=", "32mm", "Height:=", _
"3.25mm", "WhichAxis:=", "Y"), Array("NAME:Attributes", "Name:=", "Rectangle1", "Flags:=", _
"", "Color:=", "(132 132 193)", "Transparency:=", 0, "PartCoordinateSystem:=", _
"Global", "UDMId:=", "", "MaterialValue:=", "" & Chr(34) & "vacuum" & Chr(34) & "", "SolveInside:=", _
true)
```

(a)

```
oEditor.CreateRectangle Array("NAME:RectangleParameters", "IsCovered:=", true, "XStart:=", _
"", num2str(SleeveAoX), unit, "", "YStart:=", "0mm", "ZStart:=", "", num2str(SleeveAoZ), unit, "", "Width:=", _
"", num2str(SleeveAZ), unit, "", "Height:=", _
"", num2str(SleeveAX), unit, "", "WhichAxis:=", "Y"), Array("NAME:Attributes", "Name:=", "Rectangle1", "Flags:=", _
"", "Color:=", "(132 132 193)", "Transparency:=", 0, "PartCoordinateSystem:=", _
"Global", "UDMId:=", "", "MaterialValue:=", "" & Chr(34) & "vacuum" & Chr(34) & "", "SolveInside:=", _
true)
```

(b)

Figure 8.3: Example of recorded Visual Basic script for creating a rectangle (a) as recorded in Maxwell, (b) modified to use as input in MATLAB.

the model, the mesh-settings and the parameters for the analysis. There are two main ways to execute the program.

- **Execute a single run.** This option enables the user to run a single analysis of a certain parameter-set. This can be used for quick analysis of a certain configuration. When the single run is finished, Maxwell will remain open so that the user can directly analyze the results.
- **Execute a batch of analyses.** When the influence of a certain parameter has to be analyzed, a batch can be run. This batch will contain a plurality of analyses. The number of analyses will depend on the range of the parameters. The user can choose to vary one or two parameters. Next to these chosen parameters, the offset of the sleeve and target ring will always be varied, in order to calculate the sensitivity. The sensitivity will be calculated between the two outer positions of offset per parameter variation. After all runs of the batch are done, the program will process the results:
 - It will plot and save the output of the sensor for each parameter combination;
 - It will calculate the sensitivity of the sensor for each parameter combination;
 - It will plot and save the sensitivity of the sensor versus the range of the chosen parameter(s) in a 2-D or 3-D plot (for when 1 or 2 parameters are chosen to be varied respectively).

Figure 8.4 shows the architecture of the program as programmed in MATLAB. It uses several (sub)GUIs and m-files which will be briefly explained.

- **Maxwell_Interface_GUI.** Main GUI, used to input necessary parameters and launch single run analysis.
- **GUI AnalysisSettings** Sub GUI for changing the parameters associated with the analysis.
- **GUI_Batch_Settings.** Sub GUI for running a batch of analyses.
- **RetrieveParameters.m.** Script to recalculate parameters that are dependent on other parameters. After a change of a parameter, all dependent parameters are recalculated.
- **WriteNewVBScript.m.** Writes Visual Basic script according to syntax used by Maxwell to build the model and run the analysis in Maxwell.
- **RunScriptInMaxwell.m.** Executes the script in Maxwell by executing a command in the Linux command line.

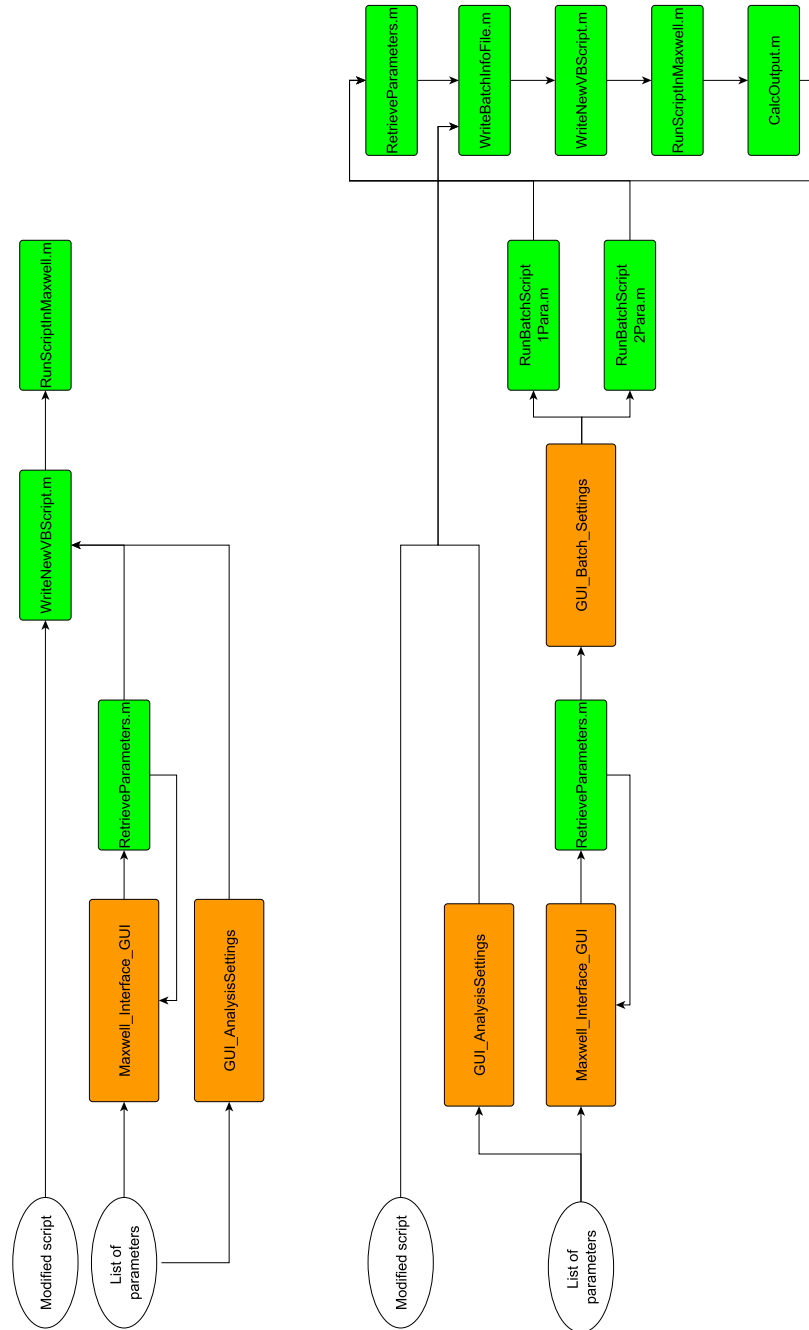


Figure 8.4: Architecture of the MATLAB program. (top) The architecture of the single run mode, and (bottom) the architecture of the batch mode. Orange boxes represent (sub)GUIs, green boxes represent m-files.

- **RunBatchScript1Para.m** Runs batch of analyses with one changing parameter (+ parameter offset to be able to calculate the sensitivity). Afterwards, the results will be plotted and saved.
- **RunBatchScript2Para.m** Runs batch of analyses with two changing parameters (+ parameter offset to be able to calculate the sensitivity). Afterwards, the results will be plotted and saved.
- **WriteBatchInfoFile.m.** Writes a .txt file with the parameters for each run of the batch.
- **CalcOutput.m.** Calculates output using the results from the Maxwell simulation (results are exported from Maxwell in .csv format and imported in MATLAB).

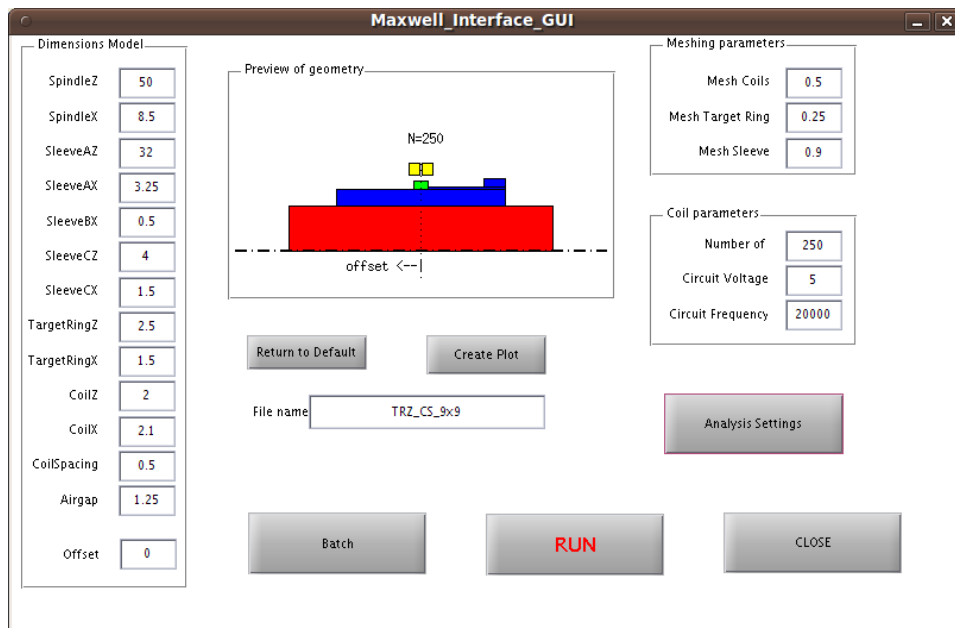


Figure 8.5: Screen shot of MATLAB program (BoB SimControl) to control simulation in Maxwell.

8.4 Results

After all the code was written, a design validation plan (SVP) was written and used to validate all separate functions. For each function, step by step its functioning and correctness was checked, to make sure the program was running correctly. The main document of the SVP can be found in appendix E.

When a batch was executed, the time per run was around forty seconds. Figure 8.6 shows the result of a batch analysis with two parameters: coil spacing and the axial thickness of the target ring. The coil spacing was varied between 0.5 and 4.5 mm, with 0.5 mm intervals. The target ring thickness was varied between 1 and 5 mm, also with 0.5 mm intervals. So there were $9 \cdot 9 = 81$ parameter combinations. To calculate the sensitivity, there are at least two points needed. All parameter combinations were simulated with an offset of 0 and 1 mm. Therefore, a total of 162 runs were analyzed, with a total run time of 74 minutes.

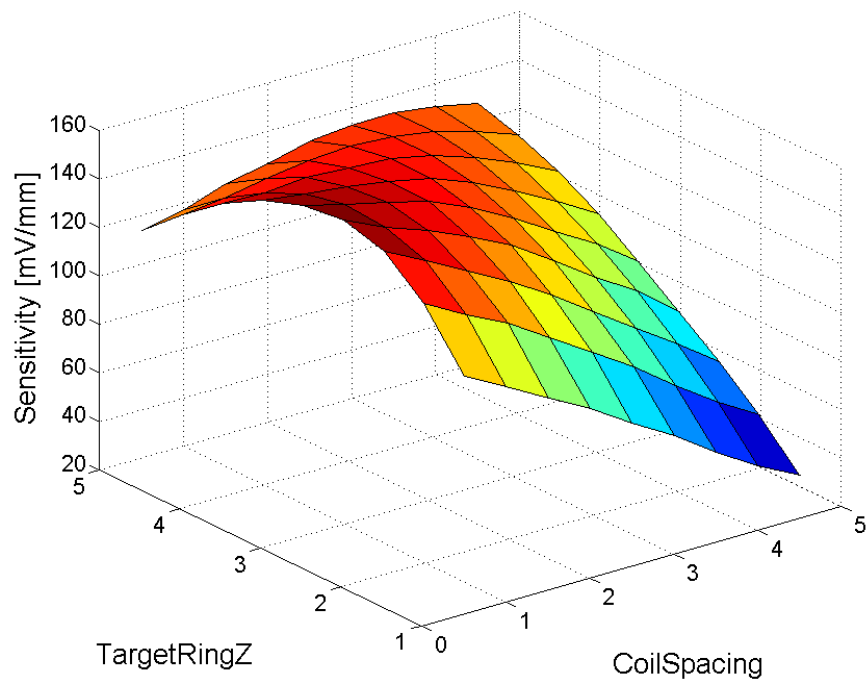


Figure 8.6: Result of a batch simulation with coil spacing and axial target ring thickness as chosen parameters.

Design of Experiment Analysis

In chapter 6 the influence of several parameters was investigated on a preliminary simulation model. The selection of the parameters that were varied was mostly based on estimated guesswork. Also, the influence of several parameters varying at the same time was not investigated. Therefore, it was not possible to discover correlations between parameters. An example of such a correlation can be seen in figure 8.6 in the previous chapter. It shows that the combination of the coil spacing and the target ring thickness has a specific effect on the sensitivity of the sensor.

9.1 Design of Experiment

Now that the final geometry of the concept is known, it is interesting to analyze possible modifications of the concept. This is done by simulating all possible design variations. However, with over ten variable parameters, there will be hundreds of possible designs.

So, a more structured way of analyzing is the Design of Experiment (DoE) method. This method has as goal to reach a conclusion with a small but carefully planned set of experiments. The method consists of two phases: screening and optimization.

9.1.1 Screening

Before one begins with the DoE analysis, there is probably little knowledge of the system. Some influential parameters might be known (in this concept the air gap will probably be of major importance), but there might be some major effect present in the system that is not as easy to see. There are also a lot of parameters to consider.

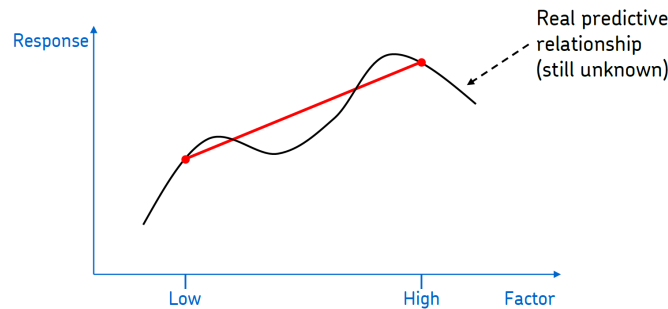


Figure 9.1: Bold approach of parameter variation in screening phase of DoE. [24]

The goal is to identify parameters and low order interactions that have a significant effect on the response of the system. This way, all the other parameters that are not significant can be eliminated.

To make this first selection, a bold approach is taken. The effects of the variation of the parameters is presumed to be linear, as illustrated in figure 9.1. Therefore, only the outer edges of the range of the parameter have to be taken into account. But when there are ten parameters, all with two levels, to be analyzed, a full analysis would still consist of $2^{10} = 1,024$ tests.

To reduce the number of tests, a fractional factorial experiment is designed. This means that several parameters are grouped into one, reducing the number of experiments. By careful planning of these groups, the analysis can still yield a reliable result. The outcome of the analysis will not have a sufficient resolution to directly select the optimal configuration, but is detailed enough to separate the influential parameters. This planning can be done using standardized tables. In this project, the program Minitab was used to perform all data processing. [23]

9.1.2 Optimization

In the optimization phase, another DoE is done, but now limited to the parameters that were found to be of great influence on the output, in this case the sensitivity of the sensor. The goal of the optimization phase is to gain more understanding of the mathematical relationship between the parameters, and so be able to select the optimal combination of parameters.

9.2 Build Up of Simulation Model

To minimize the calculation time, the Maxwell model of the torque sensing bottom bracket as described in chapter 7 is simplified into a 2-D model, as explained in chapter 8. The model consists of four main parts: the spindle, the sleeve, the target ring and the coils. The sleeve is initially modeled as three parts, and thereafter merged into one. The schematic build up of the

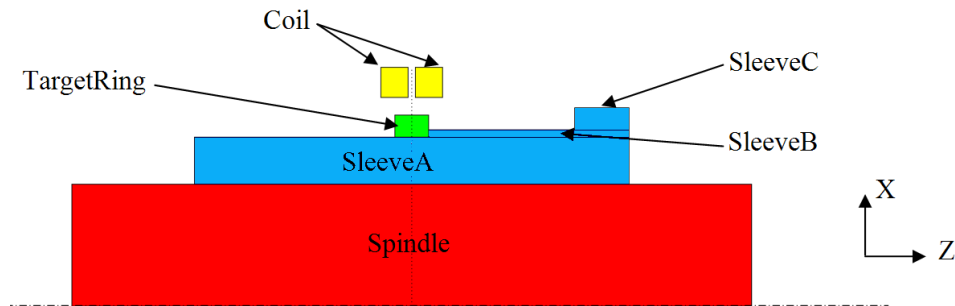


Figure 9.2: Build up of analysis model showing the four main parts. The sleeve part is built with three parts and merged thereafter.

model is shown in figure 9.2. All parts are modeled with a measurement in the Z (axial) and X (radial) direction. Next to the physical measurement, there are some other parameters that can be varied. All the parameters that will be used in this DoE are summarized in table 9.1.

Parameter	unit	Default	Min	Max
Air Gap	mm	1.25	0.5	5
Coil spacing	mm	0.5	0.5	10
Spindle X	mm	8.5	5	10
Sleeve A X	mm	3.25	1	5
Sleeve A Z	mm	32	15	35
Sleeve B X	mm	0.5	0.5	5
Target ring X	mm	1.5	0.5	5
Target ring Z	mm	2.5	0.5	10
Coil X	mm	2	0.5	2
Coil Z	mm	2.1	0.5	5
Number of turns	-	80	10	500
Supply voltage	V	5	1	10
Supply frequency	Hz	12k	10k	1M

Table 9.1: Parameters, with range, for the screening phase of Design of Experiment analysis.

9.3 Phase 1: Parameter Screening

At first, all the variables from table 9.1 were used for the first phase of the DoE. Minitab designed an experiment with sixteen simulations. Some simulations had the problem that they were not possible to run due to interference problems. Two parts in the model would overlap, making the geometry not possible. These simulations were then modified to make the

runs possible. The results of the experiment can be found in appendix F.1. After this first screening phase, it could be concluded that five parameters were depended on other parameters:

- Spindle X
- SleeveA X
- SleeveA Z
- Coil X
- Coil Z

It was decided to redo the screening phase only with the independent parameters. The data of the second screening phase can be found in appendix F.2. The Pareto diagram of the second screening phase is shown in figure 9.3. The first thing that can be noticed is that a lot of parameters are influential when combined with the supply voltage. But it is presumed that the supply voltage will influence the output just on a global scale: increasing the supply voltage will always increase the output. Therefore, it is decided to limit the second phase only to mechanical parameters. The four most influential parameters are:

- Air gap
- SleeveB X
- Coil spacing
- Target ring Z

9.4 Phase 2: Parameter Optimization

The goal of the optimization phase is to find the optimal combination of the four parameters mentioned above. In order to limit the number of simulations, the air gap parameter is omitted in the simulations, because the effect of this parameter is already clear. Reducing the air gap will always improve the sensitivity of the sensor. For the other three parameters, three batches of simulations are done, varying two parameters while keeping one on its default value. The range and interval of the parameters is summarized in table 9.2. The results of these simulations can be found in figure 9.4.

Figure 9.4a shows that when the coil spacing is kept constant, there is a clear optimum in the target ring thickness, at 2.5 mm. The influence of sleeveB is far less important but has its optimum at 0.5 mm.

Figure 9.4b shows that when the target ring thickness is kept constant, the coil spacing shows an optimum at its minimum value of 0.5 mm. The

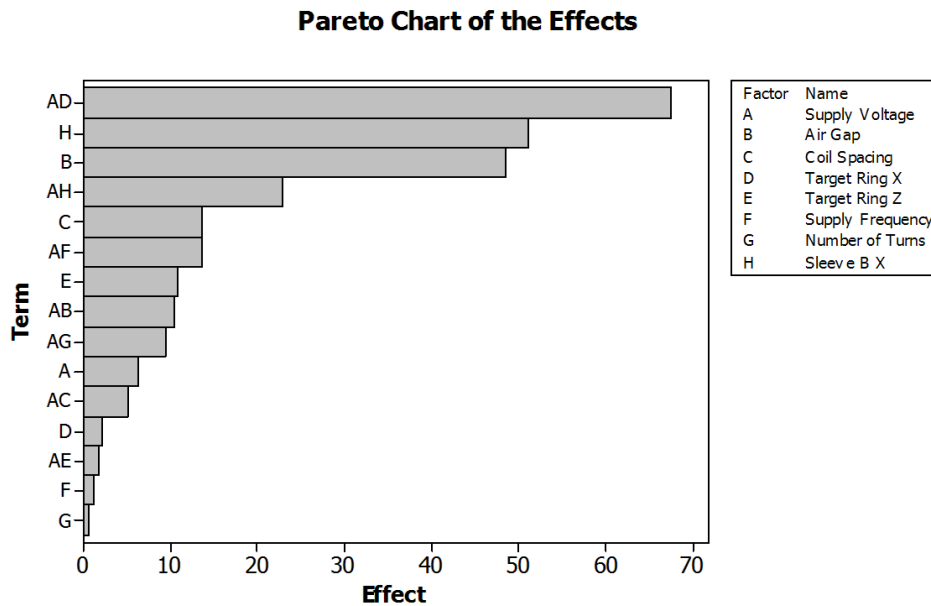


Figure 9.3: Result of screening phase of the DoE, showing that the parameters air gap, sleeveB X, the coil spacing and target ring Z are the most influential mechanical parameters.

Parameter	Min [mm]	Max [mm]	Interval [mm]	Default [mm]
SleeveB X	0.5	1.5	0.2	0.5
Target ring Z	0.5	9.5	1	2.5
Coil spacing	0.5	9.5	1	0.5

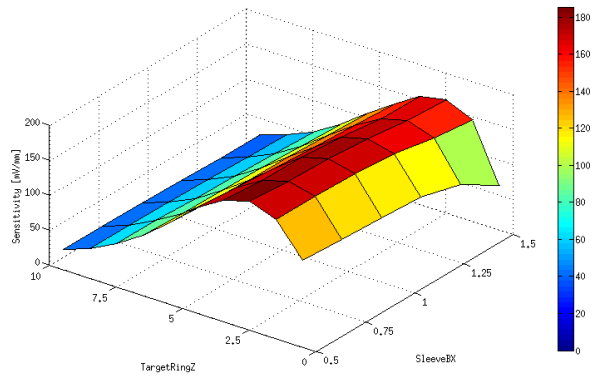
Table 9.2: Parameter range and interval for DoE phase 2.

influence on the sensitivity of the thickness of sleeveB is the same as in the previous figure.

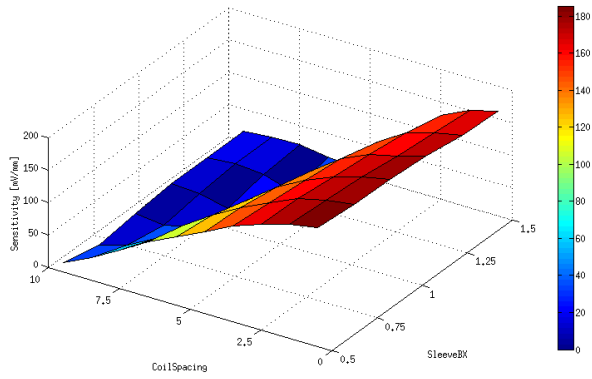
Figure 9.4c shows a clear coupling between the target ring thickness and the coil spacing. The optimal combination is with a target ring thickness of 2.5 mm and a coil spacing of 0.5 mm. But when one parameter is changed, the other parameter should be changed as well, in order to keep the optimal configuration.

These results show that the concept geometry as presented in chapter 7 was already close to the optimal geometry. When designing a new iteration of the sensor, reducing the air gap should be of the utmost importance. Thereafter, care should be taken when changing either the target ring thickness or the coil spacing, because these parameters show a clear coupling.

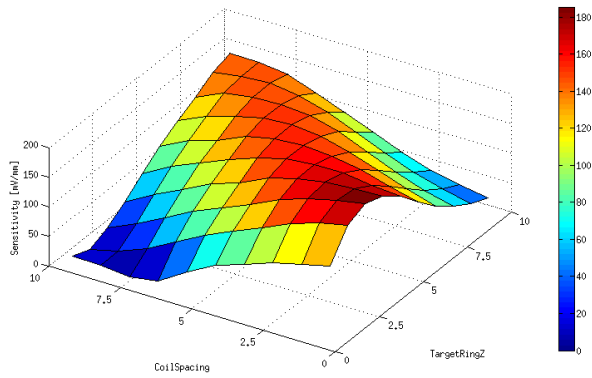
This analysis with fixing one parameter while varying the other two



(a)



(b)



(c)

Figure 9.4: Results of the second phase of the DoE, varying two parameters while keeping the third fixed on its default value (see table 9.2), (a) sleeveB X vs. target ring Z, (b) sleeveB X vs. coil spacing, (c) target ring Z vs. coil spacing

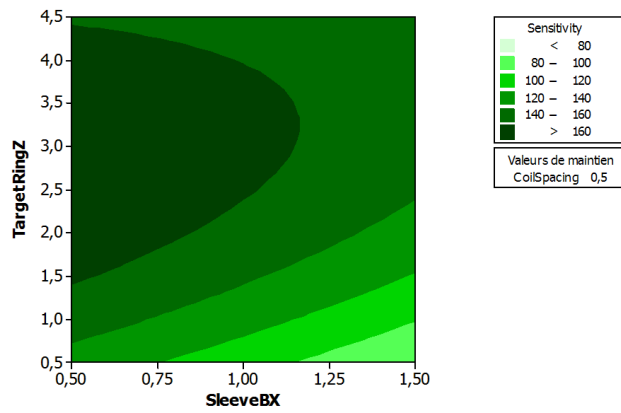
can be dangerous, because it will exclude a possible influence of the third parameter. To make sure that this was not the case, a full factorial analysis was done on these three parameters. To limit the number of simulations, the step size of the parameters coil spacing and target ring Z was increased to 2 mm, instead of 1 mm. The step of parameter sleeve X was increased to 0.5 mm. The parameters coil spacing and target ring Z had five levels and the third parameter, sleeve X , three. The full factorial analysis consisted thus of $5 \cdot 5 \cdot 3 = 75$ simulations. The results of these simulations can be found in appendix F.3. On first inspection, these results point also to a maximum around sleeve $X = 0.5$ mm; coil spacing = 0.5 mm; target ring $Z = 2.5$ mm.

The results were also put into the Minitab software. The mathematical model modeled the results in such a way that its conclusion was that the optimum configuration was at: sleeve $X = 0.5$ mm; coil spacing = 0.5 mm; target ring $Z = 4.5$ mm. As seen in figure 9.4 and in the results of the full factorial, this seems not likely. In order to force Minitab to find the maximum around a target ring thickness of 2.5 mm, the range of the full factorial was reduced to a range between 0.5 and 4.5 mm for both coil spacing and target ring Z . The results of the Minitab analysis can be seen in figure 9.5. Minitab advises an optimum at: sleeve $X = 0.5$ mm; coil spacing = 0.5 mm; target ring $Z = 2.88$ mm. This result is more in line with the empirical conclusions.

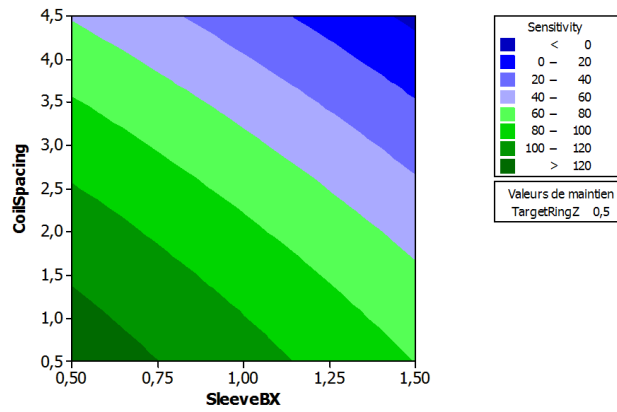
9.5 Conclusions Design of Experiment Analysis

The DoE analysis shows that it is dangerous to rely solely on one analysis, either empirical or using software like Minitab. When only the results of Minitab would have been followed, the advised optimal geometry would not reflect the true optimal geometry. In order to optimize the geometry, the knowledge gained by empirical analyses helped to guide the analysis into the right direction. Why the initial result from Minitab was so far from the empirical result is unknown, but it is suspected that the mathematical fitting used in Minitab did not recognize the shape of the data, and therefore fitted the data wrong.

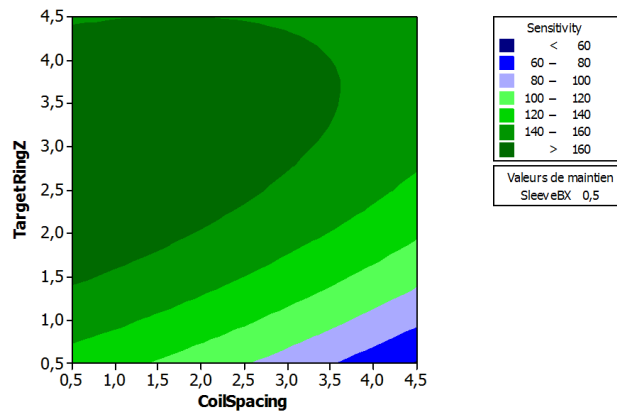
The parameter sleeve X was presumed to be of significant influence at the end of the first phase of the DoE analysis. But the results shown in the previous section indicate that the parameter has less influence than expected. This is probably caused by the interference problems encountered in the simulations. In the first phase, because of the big range chosen for sleeve X , in some simulations sleeve X was bigger than the target ring. In the second phase, the range was reduced to overcome the interference problems and therefore it did not surpass the height of the target ring. Presumably it caused the decrease of the influence of parameter sleeve X .



(a)



(b)



(c)

Figure 9.5: Results from Minitab of the second phase of the DoE, using the results of a full factorial analysis (see appendix F.3), (a) sleeveB X vs. target ring Z (coil spacing = 0.5), (b) sleeveB X vs. coil spacing (target ring Z = 0.5), (c) target ring Z vs. coil spacing (sleeveB X = 0.5).

Assembly & Test of Prototype Bottom Bracket

A prototype according to the design presented in chapter 7 was fabricated. The goal of this prototype was to function as a proof-of-concept. So it should be fully functioning, but the actual performance was less important. The fabrication of the parts, both metal and plastic parts, was done by a third party. The assembly was done in-house, as described in section 10.1. The sensor concept was tested outside of the assembly to evaluate its performance in section 10.2. Unfortunately, there was no time to perform dynamic tests before the print deadline of this thesis, but tests are planned in the near future.

10.1 Assembly of Prototype

A prototype of the torque sensing bottom bracket was built to function as a proof-of-concept. The results of the first test on this prototype would be used to judge the validity of the chosen sensor concept and will be a basis for further development.

As described in section 7.1.1, the intermediate piece would be made using a mold. This mold is shown, with the molded part, in figure 10.1. The material used for the molding was Macromelt OM 678, a thermoplastic molding compound based on polyamide that is normally used as an over-molding material.

The coils were wound by hand, with copper wire with a diameter of 0.2 mm. The coils have sixty turns each and an inductance of around 210 μH .

The complete assembly of the internal components and of the finished prototype is shown in figure 10.2.

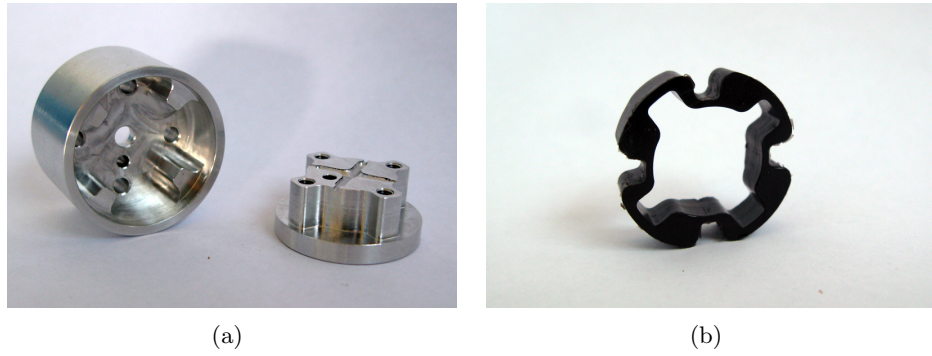


Figure 10.1: Mold for fabricating the intermediate part between the spindle and the chain wheel bracket. (a) Mold, (b) intermediate part.

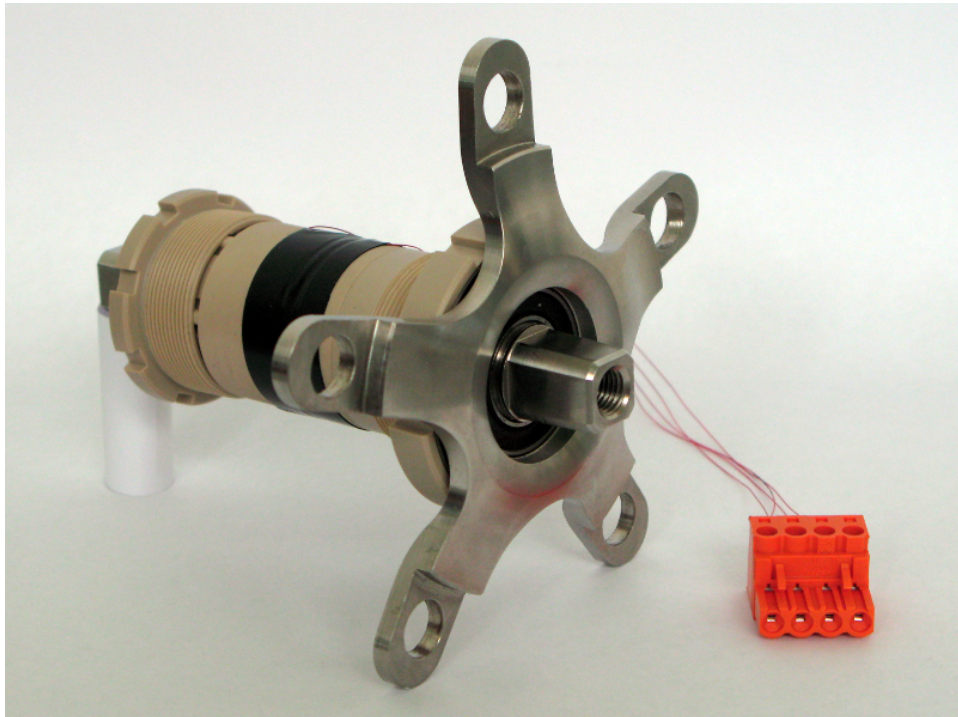


Figure 10.2: Complete assembled prototype.

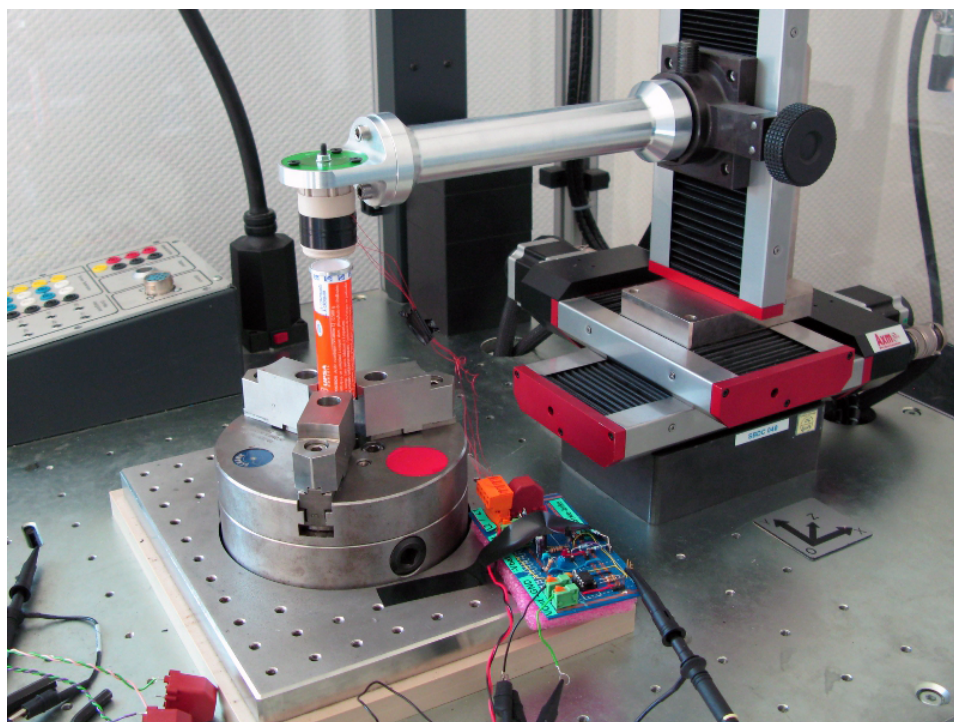


Figure 10.3: Test set-up for static test of measurement principle.

10.2 Test of Measurement Principle

The goal of these tests was to obtain the relationship between the displacement of the target ring and the output of the sensor. This was tested without the complete assembly.

10.2.1 Test Set-Up

The sensor body containing the two coils was fixed on a aluminium bar which is attached to an arm that can be moved in x,y and z-direction with a precision of $\pm 10\mu m$. The target ring was fixed on a plastic tube which was clamped onto the axis of rotation. The body was lowered over the target ring. In the neighborhood of the coils, the output of the sensor was measured as a function of the position. The output of the sensor was measured with an oscilloscope. The set-up is shown in figure 10.3. With these measurements, conclusions can be drawn about the theoretical sensitivity, the linearity and the correlation with the Maxwell simulations. A Maxwell model with only the target ring and the two coils gave a sensitivity of 560 mV/mm.

10.2.2 Test Results

During the test the overall sensitivity of the sensor was measured and the influence of eccentricity and mounting of the target ring was investigated.

Sensitivity

To measure the sensitivity, first the target ring was placed in the center of the tube by moving the tube in the x and y plane until the ring was positioned in the center of the opening of the tube. After the target ring was centered, the tube was lowered over the target ring. Empirically, the central position of the ring between the two coils was found by slowly lowering the tube over the ring until the maximum output voltage was found. This position on the z axis was set as relative zero point. Thereafter, the output of the sensor was observed within a region of ± 3 mm with a resolution of 0.1 mm. The results of the measurements are plotted in figure 10.4.

The results shows an output that is not symmetric around the relative zero point. This is caused by the influence of the aluminium arm that is used to connect the tube to the xyz-table. The left half of the plot, between -3 mm and 0 mm, represents the measurements that are not (or at least less) influenced by the arm. In that region a linear output of the sensor is visible. The sensitivity in that region is 120 mV/mm.

The measurements were repeated with a rotating target ring with a speed of 5 rpm and 50 rmp. For both rotational speeds, the output and thus the sensitivity remained the same.

Oscillation

During the measurement of the output of the sensor with a rotating target ring, some oscillation in the output signal was noticed. Presumably, this was caused by skewed assembly of the target ring on the plastic tube. To investigate this oscillation, the target ring was fitted extremely askew on purpose, and the output voltage was measured again on a specific position. The average output remained the same as with a straight target ring. The amplitude of oscillation however rose significantly to an amplitude of almost four times greater than a straight target ring, as can be seen in table 10.1.

Target ring	Amplitude [mV]
Straight	6.5
Skewed	23

Table 10.1: Oscillation of measurement signal caused by mounting of target ring.

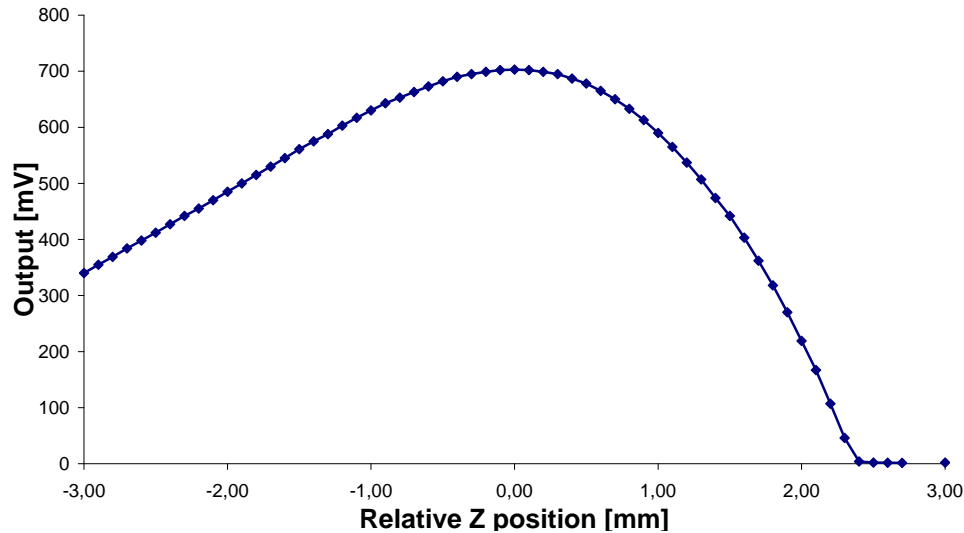


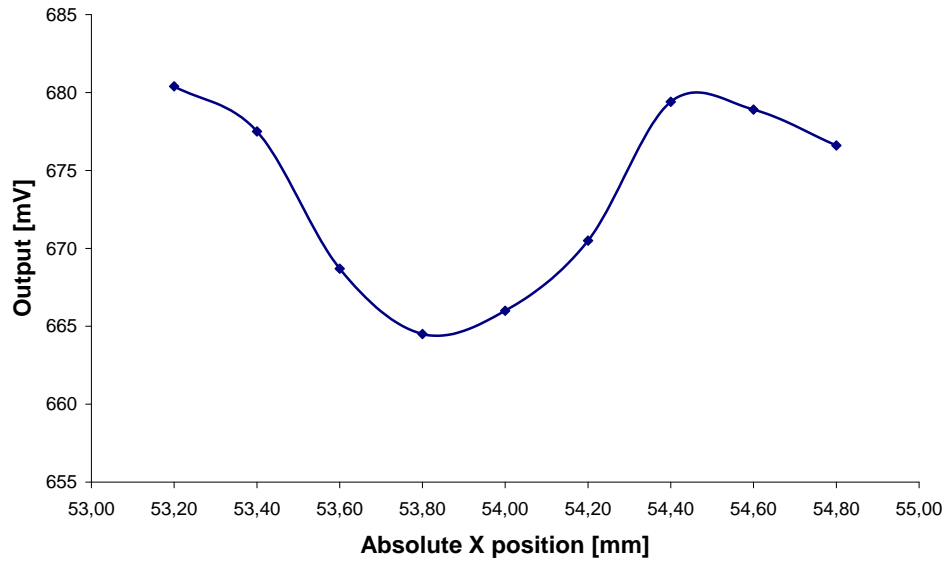
Figure 10.4: Output of sensor when moved ± 3 mm around the center between the coils. The plot shows a linear relation between the displacement and the output between -3 mm and the center. The other side of the plot is influenced by the aluminium arm of the test set-up.

Eccentricity

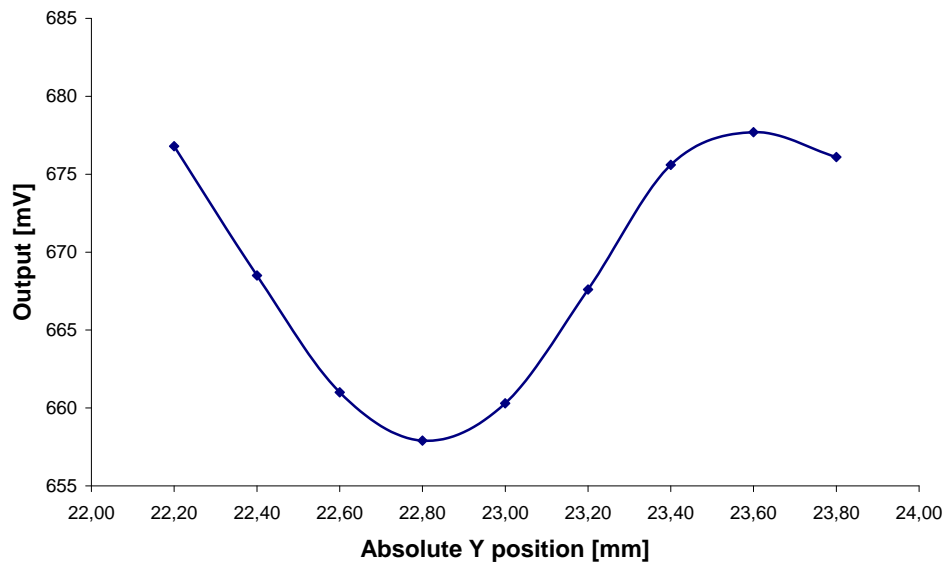
Another influence on the output of the sensor can be the position of the target ring in the plane of the coils. The eccentricity from the axis of the spindle and the coils that can occur during assembly can cause a change in the output voltage. To investigate this influence, the target ring was moved ± 0.8 mm in both x and y direction. The results of these measurements are plotted in figure 10.5. The initial x position of the target ring was 54 mm, the initial y position was 23 mm. Both plots show roughly the same shape. The increase of output voltage due to the eccentricity can be up to 3%.

10.3 Static Tests

The goal of the static test was to analyze whether the prototype was functioning. The spindle of the prototype was clamped in a workbench clamp. The chain wheel bracket was rotated by hand. The output of the sensor was measured with an oscilloscope. The output is shown in figure 10.6. The prototype suffered from a lot of play in the connection between the spindle and chain wheel bracket. After the initial play, it was hard to move the chain wheel bracket by hand. The output varied between 200 mV and 350 mV. The measurements show that the sensor concept works and has a sensitivity of at least 150 mV/mm.



(a)



(b)

Figure 10.5: Influence of eccentricity of the target ring on the output voltage (a) varying the absolute X position, (b) varying the absolute Y position.

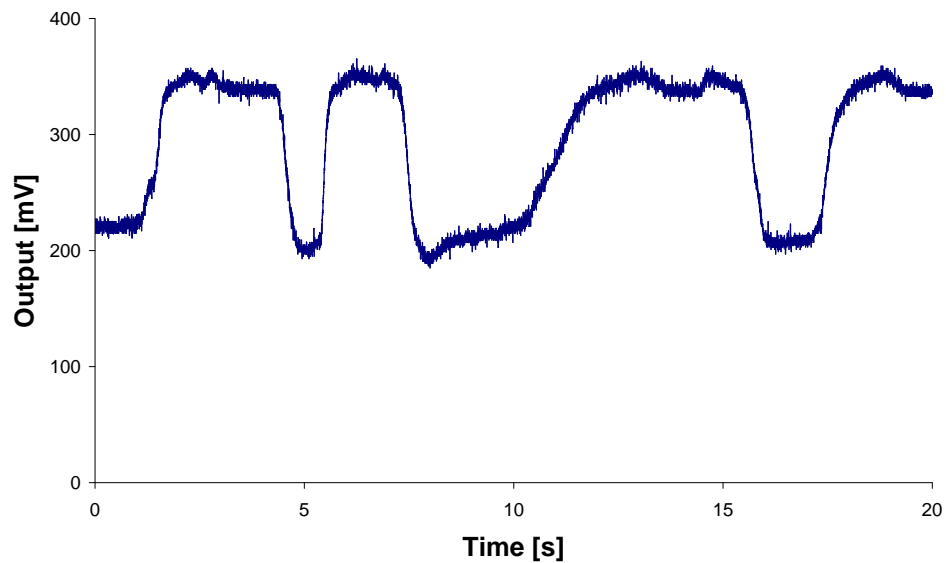


Figure 10.6: Output of the sensor during manipulation of the prototype which was clamped to a work bench.

10.4 Conclusions

The test of the measurement principle showed that the output has a linear relation to the displacement, as was expected. The sensitivity was lower than simulated. The oscillation and eccentricity tests showed that the sensor is sensitive to assembly errors. This is against the expectations. The reason for the choice of this measurement concept was that the full circumferential coils would eliminate these errors, because it would integrate the effect of the full circumference of the target ring. A possible explanation is that hand winding of the coils caused unevenly wound coils and therefore a not fully homogeneous magnetic field.

Conclusions and Discussion

The objective of this thesis was to investigate the possibilities for developing a torque sensing for SKF. This report showed which technologies already exists, what the functions of the sensor should be and how this could be realized.

11.1 Conclusions

The benchmarking phase showed that there are several existing technologies that are used to measure torque in either a power steering or e-bike application. The two most prevailing technologies are magnetic field measurement and magnetic phase shift measurement. The former makes use of the magnetostrictive effect and measures the stress applied to the sensing element directly by measuring the properties of the magnetic field. The latter measures a relative rotational displacement between two shafts which are connected through a torsion bar.

A structured analysis of the requirements was made to investigate the relative importance of all the functions of the product. By using the quality function deployment (QFD) method, needs and functions were rated against each other to find out which needs and functions are the most important. By focusing on these topics first, a design can be made that will quickly satisfy the customer. The analysis showed that that, next to torque measurement, price and safety are the most important functions. These results gave a good insight in the priorities for the design, although some functions are not yet realized in the prototype that was presented. Because this first design and prototype had as goal to function as a proof-of-concept, less attention was paid to the price for example. Although it has to be said that the chosen

sensor concept, which consists only of a simple aluminium ring, two coils and simple electronics, will probably be less expensive than other systems that use Hall effect sensors and magnetized rings or shafts.

The design phase showed a structured approach to developing a sensing concept. After answering the questions *where*, *what* and *how*, a sensor concept was chosen. It will be placed in the bicycle bottom bracket. It will measure a torsion angle. And it will measure that angle by sensing a displacement proportional to that torsion angle using an aluminium target ring and two coils. This measurement concept was mainly chosen because of its integrative properties. Because it is placed around the complete circumference of the spindle, harmonics were supposed to be eliminated. By choosing for a highly conductive target ring, the leading physical principle in the sensor would be the influence of induced eddy currents on the coils.

Finite element electromagnetic field simulations were made to analyze the influence of varying design parameters. In the initial tests, the parameters were varied one by one on a simplified model. The results of this analysis were used to design the torque sensing bottom bracket. In a second analysis, a design of experiment (DoE) was set up to make a more structured analysis, and to find interactions between several parameters. To speed up the analyses and the variation of parameters, an interface was made using MATLAB and modified Visual Basic scripts. The DoE was performed in two phases. The first phase had as goal to find the most influential parameters, the second to optimize the geometry. The DoE showed that the initial design was already close to the optimal geometry. It also showed a clear connection between the width of the target ring and the spacing between the coils.

At the end of the project, a fully functional prototype was made. The initial test on the measurement principle and the prototype showed promising results. The measurement principle shows a linear relation between the displacement of the target ring and the electronic output. Static tests on the prototype indicate that the sensor concept is working. But the lack of dynamic testing, due to lead time and test bench availability issues, a final decision on the validity of the concept still has to be made.

11.2 Discussion

This thesis ends with a proof-of-concept prototype. But the product is far from finished. To continue the project, several recommendations are given. At the end, a small discussion is given on the usability of the concept for other applications.

11.2.1 Torque Sensing for E-bike Applications

As said at the end of the conclusion, performing the dynamic tests is of the utmost importance to continue with the project. The dynamic tests will give an insight in the dynamic behavior of the sensor. With the results of these tests, the conclusions already drawn from the static test can be supported. If the overall conclusion is that the chosen measurement concept is a suitable concept, a start can be made with optimizing the design towards a product that can be produced and sold to customers. The next phase should focus on:

- **Design of intermediate part.** The plastic intermediate part that transfers the torque from the spindle to the chain wheel, and deforms under load, is at the moment not yet functioning as it should. A study should be done to find a suitable material that will fulfill a number of criteria. It should:
 - deform linear over the defined range of applied torque;
 - remain in the domain of elastic deformation;
 - sustain constant varying deformation.

The development of this piece will require extensive knowledge of plastics and rubbers and therefore will be a job for an expert, either in-house or from a third party. It might even be interesting to investigate the possibility of eliminating the piece completely and use the spring to define the relation between the applied torque the torsion angle. However, this might introduce harmonics into the system because the spring system will not have the damping properties of the plastic part.

- **Simplify mechanical assembly.** Although the sensor concept is elegantly simple, the mechanical assembly is quite complex. The assembly consists of more than ten parts and some of them are quite complicated. To simplify the assembly, it will be wise to review the current design and look for improvement.
- **Reduce costs.** As already mentioned in the previous point, the complicated assembly will also contribute to the cost price. To cut the cost, each part should be reviewed to cut cost. The current design uses three ball bearing, as opposed to two in a traditional bottom bracket. One of the ball bearings will only rotate up to six degrees, so its main function is to support the vertical loading of the spindle. If this ball bearing can be replaced by another part, considerable costs could be saved.

- **Sensation to the cyclist.** One aspect that has not yet been discussed is the sensation to the cyclist. The relative rotation between the spindle and the chain wheel might give a weak sensation or the sensation of power loss to the cyclist. At the moment, a maximum rotation of six degrees was chosen, but this choice is not yet supported by any research. More research should be done into the sensation of the cyclist, and the way the cyclist applies the torque to the bike.
- **Integration of electronics.** The electronics have to be integrated in to the bottom bracket assembly. This is not expected to be a problem, but it will need attention for the next version.

11.2.2 Torque Sensing Concept for Other Applications

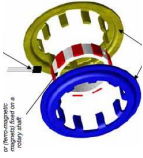


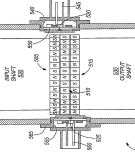
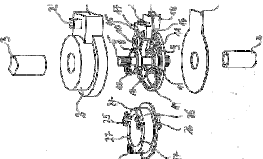
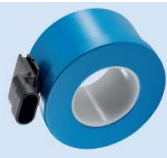

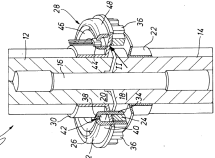
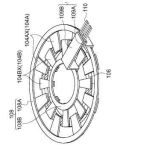
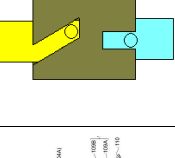
At the start of this thesis, it was not yet clear for what application the torque sensor should be designed. After the market research and competitor analysis was done, it was decided to design a sensor for e-bike applications. But now that a promising sensor concept is developed, it is time to look again at other possible markets. The two most interesting markets are electronic power steering (EPS) and drive train torque measurement. The latter one involves the measurement of torque on drive shafts and gearboxes. The presented sensor concept will be also suitable for these applications. The design would even be simpler. The problem that occurred in the e-bike sensor, measurement of two inputs (two pedals), does not exist in these applications. Therefore, the intermediate piece could be replaced by a torsion bar or a spring. However, care should be taken not to breach existing patents.

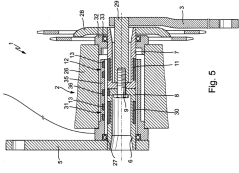

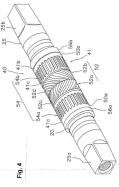
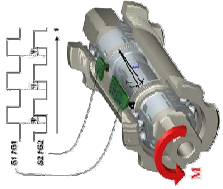
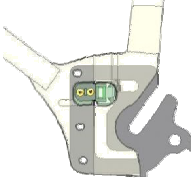

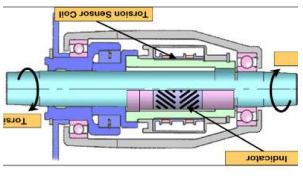


Part IV

Appendices

APPENDIX A

Competitor Analysis Matrix

Field Company	EPS MMT	Bosch	Continental	Bourns	Bourns	Bourns	Siemens VDO	ABB	NTCE	Valeo	NSK	"Honda Accord"
Picture												
Status of product	Licensing technology	Announced	Unknown	Production?	Unknown	Production?	Production?	Production?	Licensing technology, Production?			Production
Measurement principle	Magnetic Rotor-Stator Phase Shift Measurement	Magnetic Rotor-Stator Phase Shift Measurement	Magnetic Rotor-Stator Phase Shift Measurement	Magnetic Rings Phase Shift Measurement	Mechanical Phase Shift Measurement	Magnetic Field Measurement	Magnetic Field Measurement	Magnetic Field Measurement	Magnetic Field Measurement	Magnetic Rotor-Stator Phase Shift Measurement	Magnetic Rotor-Stator Phase Shift Measurement	Magnetic Translation Measurement
Technical data												
Range	$\pm 1^\circ$ to $\pm 8^\circ$	$\pm 4^\circ$	∞	$\pm 4^\circ$ to $\pm 10^\circ$	-	Costumer defined	10Nm to 5000Nm	Depends on design	-	-	-	-
Resolution	-	0.002°	-	2.5Nm to 4 Nm	-	-0.1%	-	0.01% FS	-	-	-	-
Accuracy	-	-	-	0.0083°	-	-	-	-	-	-	-	-
Hysteresis	$\pm 0.3\%$ to $\pm 0.05\%$ FS	-	-	1% FS	-	<0.1%	-	-	-	-	-	-
Non-linearity	$\pm 0.2\%$ FS	-	-	0.5%	-	<0.1%	-	-	-	-	-	-
Temperature range	-	-40°C to +120°C	-	-	-	-40°C to +150°C	-40°C to +200°C 250°C peak	-	-	-	-	-
Angular range	∞	∞	∞	∞	?	∞	∞	∞	∞	∞	∞	∞
Other specs	Stability No torque $\pm 0.03\%$ Max torque $\pm 0.3\%$	-	-	Total error $\pm 0.066^\circ$	-	Total error: $\pm 1\%$	Measuring error <2%, Repeatability error <0.1%	Repeatability: 0.05% FS	No specs; patent for production method			
Patents												
Number	US2004011138A1	DE102005031086A1 EP2006650A2	US2010139419A1, WO2008068334A1 WO2010007068A1	US7339370B2	DE102009011352B3	US2007034004A1	US2002189372A1	US2008115591A1	US2008105541A1	EP1424541A2	WO2008105541A1	
Status	Granted	Granted, Application (12/2008)	Appl. (06-2010) Appl. (06-2008) Appl. (01-2010)	Granted	Granted	Granted	Granted	Granted	Granted	Appl. (11-2003)	Appl (09-2008)	
Document	Espacenet.com	Espacenet.com Espacenet.com	Espacenet.com Espacenet.com Espacenet.com	Espacenet.com	Espacenet.com	Espacenet.com	Espacenet.com	Espacenet.com	Espacenet.com	Espacenet.com	Espacenet.com	
Conclusions												
Advantage	High precision	High precision	High precision	Compact construction	Proven sensor tech	Noncontacting No torsion bar	Noncontacting No torsion bar	Noncontacting No torsion bar	Noncontacting No torsion bar	High precision	High precision	Simple method No signal post processing
Disadvantage	Torsion bar Magnetic ring	Torsion bar Magnetic ring	Torsion bar Magnetic ring	Torsion bar Magnetic rings	Contacting method Mech. components Torsion bar	Needs magnetized shaft	Needs magnetized shaft	Needs magnetized shaft	Needs magnetized shaft	Torsion bar Magnetic ring	Torsion bar Magnetic ring	Mechanical components

Field Company	E-bike Schaeffer/FAG	Thun	Shimano	Ergomo	IDbike	Bosch	Panasonic	Chinese product	Chinese product
Picture									
Status of product	Announced	Production	Unknown	Production	Production	Announced	Production	Production	Production
Measurement principle	Magnetic Field Measurement	Magnetic Field Measurement	Magnetic Field Measurement	Optical Phase Shift Measurement	Displacement of Rear Drop-Out	-	Magnetic Field Measurement	Chain wheel torque (?) sensor	Torque sensor integrated in hub-motor
Technical data									
Range	0-90Nm (300Nm optional)	X-Cell RT ±200Nm	-	0 Nm to 450 Nm	TMM 0.3mm	eBike	-	-	-
Resolution	-	-	-	0.0025°	-	-	-	-	-
Accuracy	Up to 1%	2.5%	-	±0.5%	-	-	-	-	-
Hysteresis	-	-	-	-	-	-	-	-	-
Non-linearity	-	-	-	-	-	-	-	-	-
Temperature range	-	-	-	-	-10°C to +40°C	-	-	-	-
Other specs	-	Speed measurement	-	-	10 mV/µm ± 10 %	-	-	-	-
Patents									
Number	WO2009079980A1	-	EP1978343A2	US6356847B1	WO2006091089A2	-	-	-	-
Status	Appl. 07-2009	-	granted	Granted	Granted	-	-	-	-
Document	Espacenet.com	-	Espacenet.com	Espacenet.com	Espacenet.com	-	-	-	-
Price	-	€102 (sample)	-	\$700 + \$500 for MC	-	-	-	\$23	\$316
Comments									
Remarks	2 pedal separate torque measurement	Purchased, to be analyzed (test bench) and disassembled		Purchased, to be analyzed (test bench) and disassembled	Used mainly on Dutch e-bikes.	Complete system of motor, sensor, battery and controller, uses Schaeffer system	Used on several American bikes, like Kalkhoff and Giant	Purchased, to be analyzed and disassembled	Purchased, to be analyzed and disassembled
Advantages	Noncontacting No torsion bar	Noncontacting No torsion bar	Noncontacting No torsion bar	Cheap components	Simple method	Noncontacting No torsion bar	Noncontacting No torsion bar	Compact construction Integrated in motor	Compact construction Integrated in motor
Disadvantages	Needs magnetized shaft	Needs magnetized shaft	Needs magnetized shaft	High mounting precision Requires calculation with microprocessor	Needs modification of frame	Needs magnetized shaft	Needs magnetized shaft	Not a torque sensor	Magnetic rings Integrated in motor

APPENDIX B

Thun Bottom Bracket Sensor Data Sheet

Sensory BB-Cartridges X-CELL R and X-CELL RT

Specifications	X-CELL R	X-CELL RT	Remarks
Performance 1	Cadence: rotation/min.	Cadence: rotation/min.	
Performance 2	Rotational direction	Rotational direction	
Performance 3	-	Torque [Nm]	
Length of spindles	120K; 120L; 128K; 128L; 136L	120K; 120L; 128K; 128L; 136L	See drawing
Certification: EN 14764 (City-Trekking)	Yes	Yes	
Certification: EN 14766 (MTB)	Yes	TBC	
Cup threads	BS 1.375x24	BS 1.375x24	
Right-hand cup	Low profile	Low profile	
Material of cups	PA 6.6 Gf 30 %	PA 6.6 Gf 30 %	
Material of sensor shell	Macromelt	Macromelt	
Ball Bearings	2 x 61902 2RS	2 x 61902 2RS	
Square	12.73 mm	12.73 mm	
Surface of spindles	A2B	A2B	
Assembly tool	Shimano® compatible	Shimano® compatible	
Sensory system	2 x Hall-sensors	2 x Hall-sensors, PCME-sensor	
Impulse transmitter 1	Poled ring - 32 impulses/rotation	Poled ring - 32 impulses/rotation	
Impulse transmitter 2	-	Magnetized spindle	
Voltage feed	Analogue: +7...16 V DC, Digital: +4...16 V DC	+7...+16 V DC	For lower voltage feed please contact technical support.
White cable (input)	Power supply	Power supply	
Brown cable (output)	Sine signal	Sine signal	
Blue cable (output)	Cosine signal	Cosine signal	
Black cable (ground-connection)	Ground	Ground	
Grey cable (output)	No connection	Torque signal	
Length of cable	1100 mm	1100 mm	Different lengths optional: surcharge applies
Signal output: sine	Analogue or digital (open collector)	Analogue or digital (open collector)	Analogue: offset +2.5 V Amplitude max. 4.5 V _{SS} Digital: 0 V/Open collector
Signal output: cosine	Analogue or digital (open collector)	Analogue or digital (open collector)	Analogue: offset +2.5 V Amplitude max. 4.5 V _{SS} Digital: 0 V/Open collector
Signal output torque: attribute 1	-	Offset +2500 mV at 0 Nm	
Signal output torque: attribute 2	-	Analogue: ±10 mV/Nm	
Signal output torque: attribute 3	-	Bandwidth: 250 Hz at -3 dB	
Accuracy of signals: sine/cosine	± 3° (± 0,8 %)	± 3° (± 0,8 %)	Per turn of crank (360°)
Accuracy of signals: torque	-	Effective range ± 200 Nm	
Accuracy of signals: torque	-	± 2.5 %	Of effective range
IP level	IP 56 as per EN 60529	IP 56 as per EN 60529	

Technical Support: Dipl.-Ing. Toni Valente
0049-2333-836-170
valente@thun.de

Dipl.-Ing. Tareq Higlieh
0049-2333-836-115
higlieh@thun.de

WIRING DIAGRAM X-CELL R AND X-CELL RT



X-CELL RT Digital (open collector)

Wire color	Description	Signal	Signal range	Remark
White	Power supply	+7...16 V DC	max. 20 mA	-
Black	Ground	0 V	-	-
Blue	Output	Cosine	0 V/Open collector	16 Impulses/Rotation
Brown	Output	Sine	0 V/Open collector	16 Impulses/Rotation
Grey	Output	Torque	Offset +2,5 V bei 0 Nm	+/- 10 mV/Nm

X-CELL R Digital (open collector)

Wire color	Description	Signal	Signal range	Remark
White	Power supply	+4...16 V DC	max. 10 mA	-
Black	Ground	0 V	-	-
Blue	Output	Cosine	0 V/Open collector	16 Impulses/Rotation
Brown	Output	Sine	0 V/Open collector	16 Impulses/Rotation
Grey	No connection	-	-	-

X-CELL RT Analogue

Wire color	Description	Signal	Signal range	Remark
White	Power supply	+7...16 V DC	max. 20 mA	-
Black	Ground	0 V	-	-
Blue	Output	Cosine	Offset +2,5 V amplitude max. 4,5 Vss	16 Impulses/Rotation
Brown	Output	Sine	Offset +2,5 V amplitude max. 4,5 Vss	16 Impulses/Rotation
Grey	Output	Torque	Offset +2,5 V bei 0 Nm	+/- 10 mV/Nm

X-CELL R Analogue

Wire color	Description	Signal	Signal range	Remark
White	Power supply	+7...16 V DC	max. 15 mA	-
Black	Ground	0 V	-	-
Blue	Output	Cosine	Offset +2,5 V amplitude max. 4,5 Vss	16 Impulses/Rotation
Brown	Output	Sine	Offset +2,5 V amplitude max. 4,5 Vss	16 Impulses/Rotation
Grey	No connection	-	-	-

SIGNAL CHARACTERISTICS OF X-CELL R AND X-CELL RT

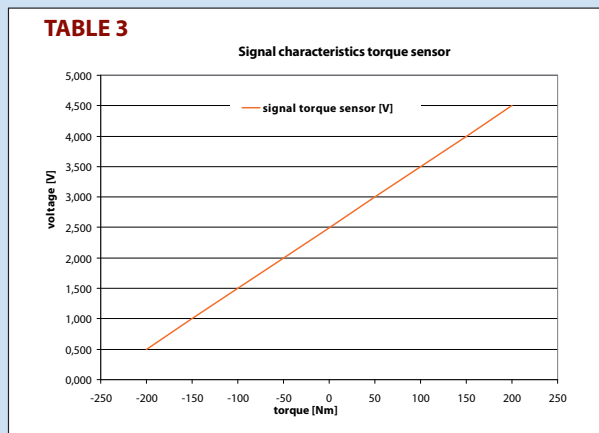
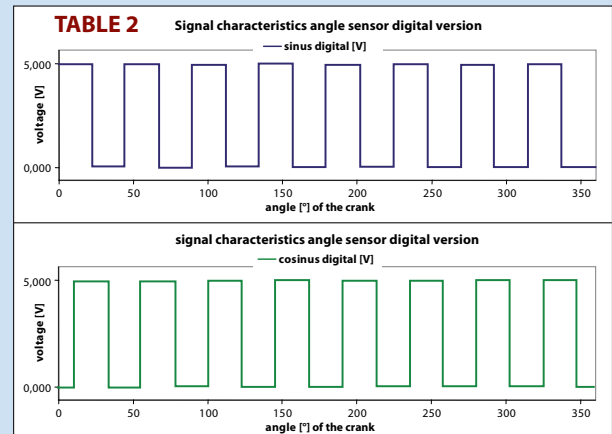
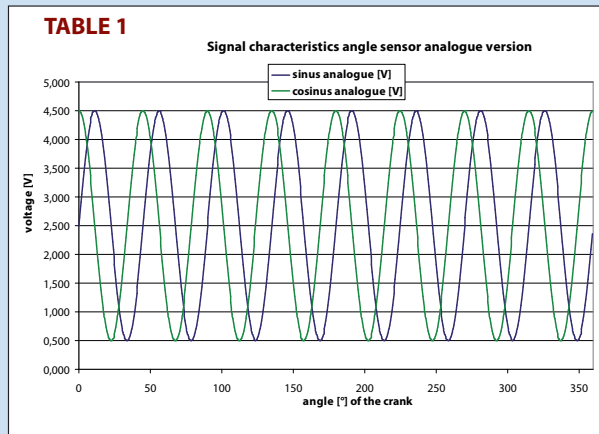
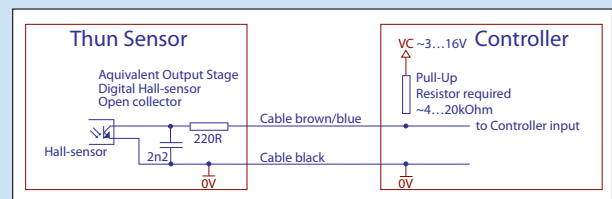


TABLE 1: X-CELL R and RT analogue version

TABLE 2: X-CELL R and RT digital version


TABLE 3: X-CELL RT torque



APPENDIX C

Paired Comparison Matrix

E-bike, Torque

Reading direction


1, 4, 7, 10

	Measure Torque	Measure Position	Measure Speed	Mechanically integrated in cust. Appl.	Communicate with cust. Appl.	Give no perception of presence	Be safe	Be maintainable	Be reliable	Withstand disturbances	Of reasonable cost	Total	Normalized weight
Measure Torque	1	10	4	4	4	7	4	7	4	4	7	56	18%
Measure Position	0,1	1	0,143	0,143	0,1	0,143	0,143	0,143	0,1	0,143	0,1	2,257	1%
Measure Speed	0,25	7	1	4	1	4	1	7	0,25	1	1	27,5	9%
Mechanically integrated in cust. Appl.	0,25	7	0,25	1	0,25	1	0,25	7	0,25	1	4	22,25	7%
Communicate with cust. Appl.	0,25	10	1	4	1	4	1	7	4	7	4	43,25	14%
Give no perception of presence	0,143	7	0,25	1	0,25	1	0,25	7	0,25	1	4	22,14	7%
Be safe	0,25	7	1	4	1	4	1	10	4	7	4	43,25	14%
Be maintainable	0,143	7	0,143	0,143	0,143	0,143	0,1	1	0,143	0,143	0,1	9,2	3%
Be reliable	0,25	10	4	4	0,25	4	0,25	7	1	4	4	38,75	13%
Withstand disturbances	0,25	7	1	1	0,143	1	0,143	7	0,25	1	1	19,79	6%
Of reasonable cost	0,143	10	1	0,25	0,25	0,25	0,25	10	0,25	1	1	24,39	8%

APPENDIX D

House of Quality #1

APPENDIX E

SVP BoB SimControl

Simulation Verification/Validation Plan & Report				Revision: 1	Date : 18-04-2011			
Simulated Application :		Matlab interface for BB testing in Maxwell		Quality Engineer :				
		Mechatronic Engineer : Mr. Marien van Ditten		Project Manager :				
				MANAGER:				
Test #	Assessment	References Test Name/Purpose	Acceptance Criteria	Test Responsible	Initial Tests			
					Initial Testing	Test Scheduled	Test completion Date	Tests results Report #
Block Simulations Verification								
TITLE: Maxwell_interface_GUI.m								
11-1	OK	Change value in GUI and observe if the value in the workspace is changed to make variables visible in workspace, use GetVarsInWS.m	Launch Maxwell_interface_GUI by typing Maxwell_Interface_GUI	MvD	18/04/2011	18/04/2011	18/04/2011	SVP_BoB_11.doc
11-2	OK		Change variable SpindleZ, observe change in workspace	MvD	18/04/2011	18/04/2011	18/04/2011	SVP_BoB_11.doc
11-3	OK		SpindleX	MvD	18/04/2011	18/04/2011	18/04/2011	SVP_BoB_11.doc
11-4	OK		SleeveAZ	MvD	18/04/2011	18/04/2011	18/04/2011	SVP_BoB_11.doc
11-5	OK		SleeveAX	MvD	18/04/2011	18/04/2011	18/04/2011	SVP_BoB_11.doc
11-6	OK		SleeveBX	MvD	18/04/2011	18/04/2011	18/04/2011	SVP_BoB_11.doc
11-7	OK		SleeveCZ	MvD	18/04/2011	18/04/2011	18/04/2011	SVP_BoB_11.doc
11-8	OK		SleeveCX	MvD	18/04/2011	18/04/2011	18/04/2011	SVP_BoB_11.doc
11-9	OK		TargetRingZ	MvD	18/04/2011	18/04/2011	18/04/2011	SVP_BoB_11.doc
11-10	OK		TargetRingX	MvD	18/04/2011	18/04/2011	18/04/2011	SVP_BoB_11.doc
11-11	OK		CoilZ	MvD	18/04/2011	18/04/2011	18/04/2011	SVP_BoB_11.doc
11-12	OK		CoilX	MvD	18/04/2011	18/04/2011	18/04/2011	SVP_BoB_11.doc
11-13	OK		CoilSpacing	MvD	18/04/2011	18/04/2011	18/04/2011	SVP_BoB_11.doc
11-14	OK		Airgap	MvD	18/04/2011	18/04/2011	18/04/2011	SVP_BoB_11.doc
11-15	OK		Offset	MvD	18/04/2011	18/04/2011	18/04/2011	SVP_BoB_11.doc
11-16	OK		Mesh Coils	MvD	18/04/2011	18/04/2011	18/04/2011	SVP_BoB_11.doc
11-17	OK		Mesh Target Ring	MvD	18/04/2011	18/04/2011	18/04/2011	SVP_BoB_11.doc
11-18	OK		Mesh Sleeve	MvD	18/04/2011	18/04/2011	18/04/2011	SVP_BoB_11.doc
11-19	OK		Number of Turns	MvD	18/04/2011	18/04/2011	18/04/2011	SVP_BoB_11.doc
11-20	OK		Circuit Voltage	MvD	18/04/2011	18/04/2011	18/04/2011	SVP_BoB_11.doc
11-21	OK		Circuit Frequency	MvD	18/04/2011	18/04/2011	18/04/2011	SVP_BoB_11.doc
11-22	OK		File Name	MvD	18/04/2011	18/04/2011	18/04/2011	SVP_BoB_11.doc
11-23	OK		Reads DefaultValuesModel.m	Push 'Return to Default', all values in GUI should return to their default value	MvD	18/04/2011	18/04/2011	18/04/2011
TITLE: GUI_AnalysisSettings.m								
12-1	OK	Change value in GUI and observe if the value in the workspace is changed	Push Analysis Settings: open Analysis Settings GUI	MvD	18/04/2011	18/04/2011	18/04/2011	SVP_BoB_12.doc
12-2	OK		Change Simulation Time, push save: Value in workspace changes	MvD	18/04/2011	18/04/2011	18/04/2011	SVP_BoB_12.doc
12-3	OK		Analysis Step	MvD	18/04/2011	18/04/2011	18/04/2011	SVP_BoB_12.doc
12-4	OK		Results Save start	MvD	18/04/2011	18/04/2011	18/04/2011	SVP_BoB_12.doc
12-5	OK		Results Save stop	MvD	18/04/2011	18/04/2011	18/04/2011	SVP_BoB_12.doc
12-6	OK		Results Save step	MvD	18/04/2011	18/04/2011	18/04/2011	SVP_BoB_12.doc
TITLE: WriteNewVBScript.m								
13-1	OK		New VB file is written to build model	MvD	18/04/2011	18/04/2011	18/04/2011	SVP_BoB_13.doc
13-2	OK		New VB file is written for the external circuit	MvD	18/04/2011	18/04/2011	18/04/2011	SVP_BoB_13.doc
13-3	OK		New VB file is written for the analysis	MvD	18/04/2011	18/04/2011	18/04/2011	SVP_BoB_13.doc

Simulation Verification/Validation Plan & Report				Revision: 1	Date : 18-04-2011						
Simulated Application :				Matlab interface for BB testing in Maxwell				Quality Engineer :			
				Mechatronic Engineer : Mr. Marien van Ditten				Project Manager :			
								MANAGER:			
Test #	Assessment	References Test Name/Purpose	Acceptance Criteria	Test Responsible	Initial Tests						
					Initial Testing	Test Scheduled	Test completion Date	Tests results Report #			
13-4	OK	Change parameters and run WriteNewVBScript.m	Change dimensions in GUI, observe change in script	MvD	18/04/2011	18/04/2011	18/04/2011	SVP_BoB_13.doc			
13-5	OK		Change mesh parameters in GUI, observe change in script	MvD	18/04/2011	18/04/2011	18/04/2011	SVP_BoB_13.doc			
13-6	OK		Change electrical parameters in GUI, observe change in script	MvD	18/04/2011	18/04/2011	18/04/2011	SVP_BoB_13.doc			
13-7	OK		Change analysis parameters in GUI, observe change in script	MvD	18/04/2011	18/04/2011	18/04/2011	SVP_BoB_13.doc			
13-8	OK										
TITLE: RunScriptInMaxwell.m											
14-1	OK	When RunScriptInMaxwell.m is run, all the parameters controlled by the program should be in the Maxwell simulation	Run RunScriptInMaxwell.m, Maxwell should open and execute the script	MvD	19/04/2011	19/04/2011	19/04/2011	SVP_BoB_14.doc			
14-2	OK		The script VB_BuildModel.VBS should build the model	MvD	19/04/2011	19/04/2011	19/04/2011	SVP_BoB_14.doc			
14-3	OK		All model parameters should correspond with inputted values in the WS	MvD	19/04/2011	19/04/2011	19/04/2011	SVP_BoB_14.doc			
14-4	OK		All mesh parameters should correspond with inputted values in the WS	MvD	19/04/2011	19/04/2011	19/04/2011	SVP_BoB_14.doc			
14-5	OK		All analysis parameters should correspond with inputted values in the WS	MvD	19/04/2011	19/04/2011	19/04/2011	SVP_BoB_14.doc			
14-6	OK		The script VB_Analysis.VBS Should launch the analysis, and plot the output of the measurement of the voltmeter	MvD	19/04/2011	19/04/2011	19/04/2011	SVP_BoB_14.doc			
TITLE: RetrieveParameters.m											
15-1	OK	Check calculations after parameter change in RetrieveParameters.m, by using calculation in excel-sheet SVP_BoB_15.xls	Compare parameters in WS to results in excel sheet	MvD	19/04/2011	19/04/2011	19/04/2011	SVP_BoB_15.doc			
TITLE: GUI_BatchSettings.m											
16-1	OK	When either Run batch - 1 parameter of Run batch - 2 Parameters is pushed, the information in the GUI is put in to the appropriate variables	Create vector <i>OffsetBatch</i> , with values in corresponding boxes	MvD	20/04/2011	20/04/2011	20/04/2011	SVP_BoB_16.doc			
16-2	OK		Create vector <i>Parameters</i> , filled with ones	MvD	20/04/2011	20/04/2011	20/04/2011	SVP_BoB_16.doc			
16-3	OK		Modify <i>Parameters</i> , insert the length of <i>OffsetBatch</i> as the first element		20/04/2011	20/04/2011	20/04/2011				
16-4	OK		Change value <i>BatchVar1</i> corresponding to chosen parameter in first pull down menu	MvD	20/04/2011	20/04/2011	20/04/2011	SVP_BoB_16.doc			
16-5	OK		Create <i>BatchVar1Vecotr</i> , with values in corresponding boxes	MvD	20/04/2011	20/04/2011	20/04/2011	SVP_BoB_16.doc			
16-6	OK		Modify <i>Parameters</i> for the chosen parameter	MvD	20/04/2011	20/04/2011	20/04/2011	SVP_BoB_16.doc			
16-7	OK		Change value <i>BatchVar2</i> corresponding to chosen parameter in second pull down menu	MvD	20/04/2011	20/04/2011	20/04/2011	SVP_BoB_16.doc			
16-8	OK		Create <i>BatchVar2Vecotr</i> , with values in corresponding boxes	MvD	20/04/2011	20/04/2011	20/04/2011	SVP_BoB_16.doc			
16-9	OK		Modify <i>Parameters</i> for the chosen parameter	MvD	20/04/2011	20/04/2011	20/04/2011	SVP_BoB_16.doc			
TITLE: RunBatchScript2Para.m											
17-1	OK	In GUI_BatchSettings, the parameters for the offset are chosen and 2 parameters are selected. The button Run Batch -2 parameters is pushed, and the batch of simulations is launched	Create new *_BatchInfo.txt file	MvD	21/04/2011	21/04/2011	21/04/2011	SVP_BoB_17.doc			
17-2	OK		Create <i>BatchIteration</i> parameter	MvD	21/04/2011	21/04/2011	21/04/2011	SVP_BoB_17.doc			
17-3	OK		For each batch iteration: Increase <i>BatchIteration</i> parameter, update <i>FileName</i> , change chosen parameter for batch, write new line in <i>ParameterVector</i>	MvD	21/04/2011	21/04/2011	21/04/2011	SVP_BoB_17.doc			
17-4	OK		Save output voltmeter in Maxwell sim as .csv file	MvD	21/04/2011	21/04/2011	21/04/2011	SVP_BoB_17.doc			
17-5	OK		Calculate Output of voltmeter	MvD	21/04/2011	21/04/2011	21/04/2011	SVP_BoB_17.doc			
17-6	OK		write <i>ParametersString</i>	MvD	21/04/2011	21/04/2011	21/04/2011	SVP_BoB_17.doc			
17-7	OK		Save vectors: <i>ParameterVector</i> , <i>Result</i> , <i>Parameters</i> and <i>ParametersString</i>	MvD	21/04/2011	21/04/2011	21/04/2011	SVP_BoB_17.doc			
17-8	OK		Calculate sensitivity of each configuration, plot and save the results as .fig and .png, and save in <i>Sensitivity</i> parameter	MvD	21/04/2011	21/04/2011	21/04/2011	SVP_BoB_17.doc			
17-9	OK		Save vectors: <i>Sensitivity</i> , <i>BatchVar1Vector</i> , <i>BatchVar2Vector</i>	MvD	21/04/2011	21/04/2011	21/04/2011	SVP_BoB_17.doc			
17-10	OK		Make surface and contour plot of results (<i>Sensitivity</i>) with the right parameters on the X and Y axis.	MvD	21/04/2011	21/04/2011	21/04/2011	SVP_BoB_17.doc			

Simulation Verification/Validation Plan & Report		Revision: 1		Date : 18-04-2011				
Simulated Application :		Matlab interface for BB testing in Maxwell		Quality Engineer :				
		Mechatronic Engineer : Mr. Marien van Ditten		Project Manager:				
				MANAGER:				
Test #	Assessment	References Test Name/Purpose	Acceptance Criteria	Test Responsible	Initial Tests			
					Initial Testing	Test Scheduled	Test completion Date	Tests results Report #
17-11	OK		save vector: SensMatrix	MvD	21/04/2011	21/04/2011	21/04/2011	SVP_BoB_17.doc
17-12	OK		Save surface and 3D plot as .fig and .png	MvD	21/04/2011	21/04/2011	21/04/2011	SVP_BoB_17.doc
17-13	OK		If chosen batch variables are switched in GUI, plots will change accordingly	MvD	21/04/2011	21/04/2011	21/04/2011	SVP_BoB_17.doc
TITLE: RunBatchScript1Para.m								
18-1	OK	In GUI_BatchSettings, the parameters for the offset are chosen and 1 parameters are selected. The button Run Batch -1 parameters is pushed, and the batch of simulations is launched	Create new *_BatchInfo.txt file	MvD	21/04/2011	21/04/2011	21/04/2011	SVP_BoB_17.doc
18-2	OK		Create BatchIteration parameter	MvD	21/04/2011	21/04/2011	21/04/2011	SVP_BoB_18.doc
18-3	OK		For each batch iteration: Increase <i>BatchIteration</i> parameter, update <i>FileName</i> , change chosen parameter for batch, write new line in <i>ParameterVector</i>	MvD	21/04/2011	21/04/2011	21/04/2011	SVP_BoB_18.doc
18-4	OK		Save output voltmeter in Maxwell sim as .csv file	MvD	21/04/2011	21/04/2011	21/04/2011	SVP_BoB_18.doc
18-5	OK		Calculate Output of voltmeter	MvD	21/04/2011	21/04/2011	21/04/2011	SVP_BoB_18.doc
18-6	OK		write <i>ParametersString</i>	MvD	21/04/2011	21/04/2011	21/04/2011	SVP_BoB_18.doc
18-7	OK		Save vectors: <i>ParameterVector</i> , <i>Result</i> , <i>Parameters</i> and <i>ParametersString</i>	MvD	21/04/2011	21/04/2011	21/04/2011	SVP_BoB_18.doc
18-8	OK		Calculate sensitivity of each configuration, plot and save the results as .fig and .png, and save in <i>Sensitivity</i> parameter	MvD	21/04/2011	21/04/2011	21/04/2011	SVP_BoB_18.doc
18-9	OK		Save vectors: <i>Sensitivity</i> , <i>BatchVar1Vector</i> , <i>BatchVar2Vector</i>	MvD	21/04/2011	21/04/2011	21/04/2011	SVP_BoB_18.doc
18-10	OK		Make plot of results (<i>Sensitivity</i>) with the right parameters on the X.	MvD	21/04/2011	21/04/2011	21/04/2011	SVP_BoB_18.doc
18-11	OK		Save plot as .fig and .png	MvD	21/04/2011	21/04/2011	21/04/2011	SVP_BoB_18.doc
TITLE: WriteBatchInfoFile.m								
19-1	OK	While running a batch, a file is written which contains all values of the	Write new line for each iteration containing all parameters that can be used in a batch	MvD	20/04/2011	20/04/2011	20/04/2011	SVP_BoB_19.doc
TITLE: CalcOutput.m								
20-1	OK	CalcOutput will calculate the average between the minimum and maximum of the second half of the graph of the output of the voltmeter.	Calculate the output	MvD	21/04/2011	21/04/2011	21/04/2011	SVP_BoB_20.doc

APPENDIX F

Design of Experiment

F.1 DoE Screening 1

StdOrder	RunOrder	CenterPt	Blocks	Air Gap	Coil Spacing	Spindle X	Sleeve AX	Sleeve A Z	Sleeve B X	Target Ring X	Target Ring Z	Coil X	Coil Z	Number of Turns	Supply Voltage	Supply Frequency	VOLTAGE
14	1	1	1	5	0,5	10	5	15	0,5	5	0,5	0,5	0,5	500	10	10000	196
8	2	1	1	5	10	10	1	35	0,5	0,5	0,5	0,5	5	500	1	1000000	11,5
1	3	1	1	0,5	0,5	5	1	15	0,5	0,5	0,5	2	2	500	10	1000000	716
12	4	1	1	5	10	5	5	15	3,5	0,5	0,5	0,5	5	10	10	10000	79
5	5	1	1	0,5	0,5	10	1	35	0,5	5	10	0,5	5	10	10	10000	278
10	6	1	1	5	0,5	5	5	35	0,5	0,5	10	2	0,5	10	10	1000000	14
6	7	1	1	5	0,5	10	1	15	5	0,5	10	2	0,5	500	1	10000	1,78
7	8	1	1	0,5	10	10	1	15	3,5	5	0,5	2	0,5	10	10	1000000	900
16	9	1	1	5	10	10	5	35	5	5	10	2	5	500	10	1000000	265
2	10	1	1	5	0,5	5	1	35	5	5	0,5	0,5	0,5	10	1	1000000	6
15	11	1	1	0,5	10	10	5	15	0,5	0,5	10	0,5	0,5	10	1	1000000	47
13	12	1	1	0,5	0,5	10	5	35	0,5	0,5	0,5	2	5	10	1	10000	10,4
4	13	1	1	5	10	5	1	15	0,5	5	10	2	5	10	1	10000	3,5
11	14	1	1	0,5	10	5	5	35	0,5	5	0,5	2	0,5	500	1	10000	3,6
9	15	1	1	0,5	0,5	5	5	15	5	5	10	0,5	5	500	1	1000000	10,5
3	16	1	1	0,5	6	5	1	35	5	0,5	10	0,5	0,5	500	10	10000	34

F.2 DoE Screening 2

StdOrder	RunOrder	CenterPt	Blocks	Supply Voltage	Air Gap	Coil Spacing	Target Ring X	Target Ring Z	Supply Frequency	Number of Turns	Sleeve B X	Output Voltage
14	1	1	1	10	0,5	10	5	0,5	1000000	10	0,5	69
16	2	1	1	10	5	10	5	10	1000000	500	5	114
4	3	1	1	10	5	0,5	0,5	10	1000000	10	0,5	6
12	4	1	1	10	5	0,5	5	0,5	10000	10	5	102
9	5	1	1	1	5	0,5	5	10	1000000	10	5	0,7
7	6	1	1	1	5	10	0,5	0,5	1000000	10	5	143
8	7	1	1	10	5	10	0,5	0,5	10000	500	0,5	14
5	8	1	1	1	0,5	10	0,5	10	1000000	500	0,5	11
2	9	1	1	10	0,5	0,5	0,5	0,5	1000000	500	0,9	600
3	10	1	1	1	5	0,5	0,5	10	10000	500	5	148
11	11	1	1	1	5	0,5	5	0,5	1000000	500	0,5	5
10	12	1	1	10	0,5	0,5	5	10	10000	500	0,5	14
1	13	1	1	1	0,5	0,5	0,5	0,5	10000	10	0,5	14
13	14	1	1	1	0,5	10	5	0,5	10000	500	5	41
15	15	1	1	1	5	10	5	10	10000	10	0,5	7
6	16	1	1	10	0,5	3,5	0,5	10	10000	10	5	218

F.3 DoE Full Factorial

SleeveBX	TargetRingZ	CoilSpacing	Sensitivity
0,5	0,5	0,5	124,4
0,5	0,5	2,5	101,2
0,5	0,5	4,5	69,4
0,5	0,5	6,5	13,7
0,5	0,5	8,5	11,8
0,5	2,5	0,5	183,4
0,5	2,5	2,5	162,9
0,5	2,5	4,5	124,9
0,5	2,5	6,5	84,0
0,5	2,5	8,5	34,3
0,5	4,5	0,5	149,5
0,5	4,5	2,5	159,0
0,5	4,5	4,5	155,2
0,5	4,5	6,5	124,6
0,5	4,5	8,5	84,8
0,5	6,5	0,5	85,1
0,5	6,5	2,5	117,2
0,5	6,5	4,5	145,4
0,5	6,5	6,5	147,7
0,5	6,5	8,5	121,2
0,5	8,5	0,5	42,6
0,5	8,5	2,5	67,5
0,5	8,5	4,5	105,2
0,5	8,5	6,5	138,7
0,5	8,5	8,5	142,7
1,0	0,5	0,5	117,4
1,0	0,5	2,5	72,0
1,0	0,5	4,5	7,6
1,0	0,5	6,5	27,5
1,0	0,5	8,5	20,3
1,0	2,5	0,5	175,9
1,0	2,5	2,5	151,4
1,0	2,5	4,5	108,4
1,0	2,5	6,5	33,6
1,0	2,5	8,5	9,9
1,0	4,5	0,5	138,5
1,0	4,5	2,5	151,1
1,0	4,5	4,5	143,9

SleeveBX	TargetRingZ	CoilSpacing	Sensitivity
1,0	4,5	6,5	106,3
1,0	4,5	8,5	32,9
1,0	6,5	0,5	81,1
1,0	6,5	2,5	110,3
1,0	6,5	4,5	138,1
1,0	6,5	6,5	137,3
1,0	6,5	8,5	102,9
1,0	8,5	0,5	41,9
1,0	8,5	2,5	64,9
1,0	8,5	4,5	100,8
1,0	8,5	6,5	130,8
1,0	8,5	8,5	129,9
1,5	0,5	0,5	64,2
1,5	0,5	2,5	20,6
1,5	0,5	4,5	41,7
1,5	0,5	6,5	32,5
1,5	0,5	8,5	20,5
1,5	2,5	0,5	161,7
1,5	2,5	2,5	130,0
1,5	2,5	4,5	48,8
1,5	2,5	6,5	13,8
1,5	2,5	8,5	21,6
1,5	4,5	0,5	130,5
1,5	4,5	2,5	142,2
1,5	4,5	4,5	124,6
1,5	4,5	6,5	50,0
1,5	4,5	8,5	11,1
1,5	6,5	0,5	77,3
1,5	6,5	2,5	106,6
1,5	6,5	4,5	130,8
1,5	6,5	6,5	115,8
1,5	6,5	8,5	47,2
1,5	8,5	0,5	37,4
1,5	8,5	2,5	60,7
1,5	8,5	4,5	96,2
1,5	8,5	6,5	122,9
1,5	8,5	8,5	110,0

Bibliography

- [1] C.-J. Yang 2010 *Launching strategy for electric vehicles: Lessons from China and Taiwan*, Technological Forecasting & Social Change 77, p.831-834
- [2] Bike Europe 2010 *In Holland One out of Eight Bikes Is Electric*, <http://www.bike-eu.com/news/4030/in-holland-one-out-of-eight-bikes-is-electric.html> (15-12-2010)
- [3] <http://road.cc/content/news/18907-shimano-announce-steps-e-bike-groupset>, (12-05-2011)
- [4] <http://www.bosch-ebike.de>
- [5] EBSC *Manuel de service version 4.0*, E-bike service manual for Ion-Technology E-bikes
- [6] Schaeffler (UK) Ltd. 2010 *Precision bearings make electric bikes more reliable and energy efficient*, Press release 000-002-672 GB-EN, 30-11-2010, Sutton Coldfield U.K.
- [7] Akira Noguchi et al. 2004, *Development of a Steering Angle and Torque Sensor of Contact-type*, Furukawa Review, No.25
- [8] Moving Magnet Technologies 2004 *Position sensor, designed in particular for detecting a steering column torsion*, patent US7,028,545
- [9] SSI Technologies Inc. 2007 *Position and torque sensor*, patent application WO2007/067196 A1
- [10] Bourns Inc 2010 *Torsion angle sensor*, patent application US2010/0224011 A1

-
- [11] Schaeffler KG 2009 *Tretlager mit Drehmomentsensorik*, patent application WO2009/079980A1
- [12] <http://www.ncte.de/ncte/cms/upload/downloads/motorsport/Handout.pdf> , (12-05-2011)
- [13] Loïc La Pierre *Honda Accord EPAS Systems*, Application note, SKF ACD-SI
- [14] <http://www.ergomousa.com/index.cfm/ergomo-products/?event=store.item&itemGUID=b2ca8fbb-8bf8-4e7c-a953-1b7f4dd0ed23>, (12-05-2011)
- [15] <http://www.idbike.com/tmm-powermanagement.htm>, (12-05-2011)
- [16] Shimano Inc 2010 *Bicycle bottom bracket force sensor*, patent application US2010/0282001 A1
- [17] NTCEngineering GmbH 2008 *Torque Sensor*, patent application US2008/0115591 A1
- [18] http://www.thun.de/thun_eng/sensor_technology_video.html, (14-04-2011)
- [19] Dr. Yoji Akao 1994 *QFD: The Customer Driven Approach to Quality Planning and Deployment*, Asian Productivity Organization, Tokyo, Japan
- [20] <http://www.lionprecision.com/tech-library/technotes/tech-pdfs/article-0011-cve.pdf>, (12-05-2011)
- [21] John P. Bentley 2005 *Principles of Measurement Systems*, 4th edition, Pearson Education Limited, Essex, England
- [22] *Introduction to Scripting in Maxwell*, 5th edition September 2010, ANSYS Inc., Canonsburg, Pennsylvania, USA
- [23] <http://www.minitab.com>
- [24] *Design of Experiments Basics*, Six Sigma Black Belt training, SKF

